Modeling and control of a wing at low Reynolds number with high amplitude aeroelastic oscillations

Fabien Niel

THÈSE

En vue de l'obtention du

DOCTORAT DE L'UNIVERSITÉ DE TOULOUSE

Délivré par :

Institut Supérieur de l'Aéronautique et de l'Espace

Présentée et soutenue par :
Fabien NIEL

le vendredi 26 janvier 2018

Titre :

Modélisation et contrôle d'une aile en présence d'oscillations Aéroélastiques de grande amplitude et à faible nombre de Reynolds

Modeling and control of a wing at low Reynolds number with high amplitude aeroelastic oscillations

---

École doctorale et discipline ou spécialité :
EDSYS : Automatique 4200046

Unité de recherche :
Laboratoire d'Analyse et d'Architecture des Système - CNRS

Directeur/trice(s) de Thèse :

M. Luca ZACCARIAN et M. Alexandre SEURET

Jury :
Mme Isabelle QUEINNEC - Président du Jury
M. Marc JUNGERS - Rapporteur
M. Marco LOVERA - Rapporteur
M. Charles POUSSOT-VASSAL - Membre du Jury
M. Giorgio VALMORBIDA - Membre du Jury
M. Luca ZACCARIAN - Directeur de thèse

"Il n'y a peut-être rien de si fou que de croire avoir toujours raison."

Voltaire

Extrait du *Dictionnaire philosophique*

Acknowledgements

First of all, I want to thank my supervisors Dr. Luca Zaccarian and Dr. Alexandre Seuret who followed me in this adventure providing much more than supervision, but also support, advice and confidence. This PhD has been realized in unconventional conditions. Indeed, as a French Air Force Officer I had the privilege to move in the United States of America at the Unites States Air Force Academy (Colorado, United States). However, considering the distance and my new position as a teacher in the Department of Aeronautical Engineering, the topic I was covering at this time was not suitable anymore, and also difficult to bring to its conclusion. Especially all along these years, I always worked on my own time on this personal project. Far from giving up facing such a situation, my directors supported me in a complete change of subject, much more in line with the contents of my instruction. After two years, I realize that this incredible change of direction was a unique opportunity that they offered me, and required probably more understanding of the situation than I could expect. I realize the scale of this incredible chance I had. I want also to thank them particularly for their high availability using emails, video-conferences, sometimes in the worst connectivity conditions. I also would like to thank Prof. Marco Lovera and Dr. Marc Jungers for having accepted to review my manuscript as well as the members of my jury: Dr. Isabelle Queinnec, Dr. Charles Poussot-Vassal and Dr. Giorgio Valmorbida. I want to thank my team MAC at LAAS-CNRS in Toulouse and especially Dr. Denis Arzelier to have introduced me and welcomed me into the team.

I want to express all my gratitude to the Department of Aeronautics (DFAN) of the United States Air Force Academy (USAFA) and the head of department, Colonel Cinnamon, for having let me share my passion and work with my cadets during classes and projects. Especially, I thank the Laboratory, and its director Dr. Tom McLaughlin, to have permitted me to work on the subsonic wind tunnel on these projects. Particularly, I want to thank Dr. Casey Fagley who allowed me to start this new adventure at the Academy, and for his incredible help and advice.

I also want to thank Dr. François Bateman, my former teacher and colleague, for the passion, example, and rigor he always represented to me and for his support, Dr. Caroline Bérard to have developed my taste for control and to have helped me to get started in research, Colonel Angela Suplisson for her kind words and unconditional support, Dr. Mehdi Ghoreyshi for the too numerous coffees we shared and Matt Satchell for his support and friendship. A huge thanks to my family for being so supportive and comprehensive during all these years, but a real special thanks to Anne-Charlotte for always reveling my absent-mindedness in my papers.

Finally, I want to thank my kids Emma and Hadrien who always considered as normal to see me working during the evenings, week-ends and vacations. And most of anything else, I want to thank my wife for the faith she always had in me, for her help in the best and worst moments, for enduring all the sacrifices, for understanding and accepting all my absences, and for having made possible this PhD.

Abstract

Modeling and control of a wing at low Reynolds number with high amplitude aeroelastic oscillations

by Fabien Niel

At high angles of attack or low Reynolds number, aircraft wings or blades of helicopters or even wind turbines may encounter separation of the flow which can eventually lead to aeroelastic couplings such as flutter. These instabilities can be particularly destructive and are limiting for numerous applications. This thesis aims at considering the aeroelastic modeling and control of a pitching wing in flutter conditions and at providing a general approach to tackle this problem. First, an aeroelastic model is developed based on previous works. This model provides an extension of the model proposed by Goman-Khrabrov, and modified by Williams, using the ONERA BH model. If the first component of the model captures the hysteresis of the aerodynamic load of a pitching wing, the second one allows us to capture the vortex shedding and dynamic stall model which can be observed. This second component is particularly challenging to predict, while it plays an important role in the dynamics of the wing. The aerodynamic model is then trained and successfully compared to experimental data for a NACA 0018 rigid wing undergoing pitch oscillations at low Reynolds number. This model, like many aeroelastic or aerodynamic models, suffers from its inherent complexity and nonlinearities which make its analysis and control highly complicated with respect to the automatic control point of view. For this reason, the set of equations is conveniently manipulated to encapsulate the nonlinearities in a polytopic formulation with unknown parameters. Then, control strategies dedicated to linear time invariant systems are derived to account for this polytopic formulation. In addition, rate and magnitudes saturations are a major and recurrent issue in flight control and are also considered as an additional constraint in the control loop. Based on linear quadratic regulation theory, several theorems are developed using framework of linear matrix inequalities and allow not only to synthesize a stabilizing controller but also to define the region of attraction. The theorems are then applied to solve the problem of stall flutter and successfully stabilize the closed-loop system in presence of rate and magnitude saturations, which demonstrate the potential of the contributions developed within this PhD approach.

Abstract (French)

A fort angles d'attaque ou à faible nombre de Reynolds, l'écoulement sur les ailes d'avion ou les pales d'hélicoptères ou d'éoliennes peut se séparer, ce qui peut éventuellement mener à des couplages aéroélastiques tels que le phénomène de flottement (flutter). Ces instabilités peuvent être particulièrement limitantes pour de nombreuses applications, voire destructrices. L'objectif de cette thèse est de s'intéresser à la modélisation et au contrôle d'une aile oscillant dans des conditions de flutter ainsi que de fournir une approche générale pour aborder ce problème. Tout d'abord, un modèle aéroélastique est développé en s'appuyant sur de précédents travaux. Le modèle est une extension de celui proposé par Goman-Khrabrov, et modifié par Williams, par l'utilisation du modèle ONERA BH. Si la première composante de ce modèle permet de rendre compte du phénomène d'hystérésis des charges aérodynamiques d'une aile en oscillation, la seconde permet d'inclure le détachement des tourbillons ainsi que le phénomène de décrochage dynamique qui peut être observé. Cette seconde composante est particulièrement délicate à prédire alors qu'elle joue un rôle important dans la dynamique de l'aile. Le modèle aérodynamique est alors entraîné et comparé avec succès aux résultats expérimentaux obtenus pour une aile rigide de type NACA 0018 oscillant autour de son axe de tangage. Ce modèle, comme de nombreux modèles aéroélastiques ou aérodynamiques, souffre d'une complexité inhérente et de non-linéarités qui rendent son analyse et son contrôle particulièrement compliqués du point de vue de l'automatique. Pour cette raison, l'ensemble d'équations a été modifié afin d'inclure les non-linéarités dans une formulation polytopique dont les paramètres sont incertains. Des stratégies dédiées aux systèmes à temps invariant sont alors étendues aux systèmes polytopiques. De plus, les saturations en vitesse ou en position qui sont un problème majeur et récurent de la dynamique du vol, sont considérées comme une contrainte supplémentaire dans la boucle d'asservissement. S'appuyant sur la théorie de la commande linéaire quadratique, plusieurs théorèmes sont alors développés en utilisant une formulation à partir des inégalités des matrices linéaires, afin de permettre non seulement de synthétiser un correcteur stabilisant mais aussi de définir une région d'attraction. Les théorèmes sont alors appliqués avec succès au cas du flottement de décrochage (stall flutter), stabilisant le système en boucle fermée en présence de saturations en position et en vitesse, ce qui montre le potentiel des contributions développées dans ce travail de thèse.

Short Abstract

This thesis aims at providing a general approach for aeroelastic control. First, an aeroelastic model of an oscillating wing is developed to capture the phenomena of hysteresis of aerodynamic load and dynamic stall which can be observed at low Reynolds number or large angles of attack. The model is then trained and successfully compared to experimental data for a NACA 0018 wing. This model, like many aeroelastic models, suffers from its inherent complexity and nonlinearities which make its analysis and control challenging. Consequently, the set of equations is conveniently manipulated to encapsulate the nonlinearities in a polytopic formulation with unknown parameters. Then, based on linear quadratic regulation theory and using framework of linear matrix inequalities, several theorems are developed considering saturations which are a major and recurrent issue in flight control. The theorems are then successfully applied to solve the problem of stall flutter in presence of rate and magnitude saturations.

Short Abstract (in French)

L'objectif de cette thèse est de fournir une approche générale permettant d'aborder les problèmes de contrôle aéroélastique. Tout d'abord, un modèle d'aile oscillante est développé afin de rendre compte des phénomènes d'hystérésis des charges aérodynamiques et de décrochage dynamique qui peut être observé, particulièrement à fort angles d'attaque ou à faible nombre de Reynolds. Le modèle est alors entraîné et comparé avec succès aux résultats expérimentaux obtenus pour une aile NACA 0018. Ce modèle, comme de nombreux modèles aérodynamiques, souffre d'une complexité inhérente et de non-linéarités qui rendent son analyse et son contrôle complexes. Par conséquent, le modèle a été modifié afin d'inclure les non-linéarités dans une formulation polytopique aux paramètres incertains. S'appuyant sur la théorie de la commande linéaire quadratique et utilisant les inégalités des matrices linéaires, plusieurs théorèmes sont développés, considérant les saturations qui sont un problème majeur et récurent de la dynamique du vol. Les théorèmes sont alors appliqués avec succès au cas du stall flutter en présence de saturations en position et en vitesse.

Contents

List of Figures

List of Tables

Abbreviations

AFC	**A**ctive **F**low **C**ontrol
CFD	**C**omputational **F**luid **D**ynamics
CNRS	**C**entre **N**ational de la **R**echerche **S**cientifique
DMD	**D**ynamic **M**ode **D**ecomposition
DNS	**D**irect **N**avier **S**tokes equations
GK	**G**oman **K**hrabrov model
GKO	**G**oman **K**hrabrov **O**NERA model
ICE	**I**nnovative **C**ontrol **E**ffectors
LAAS	**L**aboratoire d'**A**nalyse et d'**A**rchitecture des **S**ystèmes
LCO	**L**imit **C**ycle **O**scillation
LDI	**L**inear **D**ifferential **I**nclusion
LMI	**L**inear **M**atrix **I**nequality
LPV	**L**inear **P**arameter **V**arying
LQR	**L**inear **Q**uadratic **R**egulator
LTI	**L**inear **T**ime **I**nvariant
MAC	**M**éthodes et **A**lgorithmes de **C**ommande
NACA	**N**ational **A**dvisory **C**ommittee for **A**eronautics
NASA	**N**ational **A**eronautics and **S**pace **A**dministration
ONERA	**O**ffice **N**ational d'**E**tudes et de **R**echerches **A**érospatiales
ONERA BH	**ONERA B**ifurcation de **H**opf model (French)
PID	**P**roportional **I**ntegral **D**erivative
PIO	**P**ilot **I**nduced **O**scillations
PLDI	**P**olytopic **L**inear **D**ifferential **I**nclusion
POD	**P**roper **O**rthogonal **D**ecomposition
PWM	**P**ulse **W**idth **M**odulation

RCS	**R**adar **C**ross **S**ection
ROM	**R**educed **O**rder **M**odels
USAFA	**U**nited **S**tates **A**ir **F**orce **A**cademy
UCAV	**U**nmanned **C**ombat **A**erial **V**ehicle

Symbols

AERODYNAMICAL NOMENCLATURE

ρ	Density	$kg.m^3$
μ	Viscosity	$kg.m^{-1}.s^{-1}$
a	Speed of sound	$m.s^{-1}$
M	Mach number	$none$
f	Pitching frequency	s^{-1}
ω	Pitching angular frequency	$rad.s^{-1}$
k	Reduced frequency	$none$
t_{conv}	Convective time	s
t^+	Normalized time	$none$
$C_{M,\frac{1}{2}}$	Pitching moment coefficient at mid chord	$none$
$C_{M,\frac{1}{4}}$	Pitching moment coefficient at quarter chord	$none$
C_L	Lift coefficient	$none$
b	Span	m
c	Chord	m
α	Angle of attack at tip	^{o}
β	Angle of deflection of the flap	^{o}
U	Freestream velocity	$m.s^{-1}$
Re	Reynolds number	$none$
Re_c	Chord based Reynolds number	$none$
q	Dynamic pressure	$N.m^{-2}$
S	Planform area	m^2

x_s	Separation point location	*none*
$x_{s,0}$	Static separation point location	*none*
τ	Time constant	s
$\eta_1 = A$	Coefficient of moment slope for fully detached flow	*none*
$\eta_2 = A + B$	Coefficient of moment slope for fully attached flow	*none*
λ	Duty cycle	*none*

MATHEMATICS AND CONTROL THEORY NOMENCLATURE

$\mathbb{R}$	Set of real numbers	*none*
$\mathbb{C}$	Set of complex numbers	*none*
$\mathbb{Z}$	Set of integer numbers	*none*
s	Laplace variable	*none*
$\dot{x}(t) = \frac{dx}{dt}$	Derivative of x with respect to the time	N/A
$\left[\begin{array}{c\|c} A & B \\ \hline C & D \end{array}\right]$	State space representation	*none*
J	Cost function	*none*
$sat(.)$	Saturation (magnitude and/or rate)	N/A
$\Phi(.)$	Dead zone	N/A
$dim(A)$	Dimension of the matrix A	*none*
$rank(A)$	Rank of the matrix A	*none*
A^T	Transpose of the matrix A	N/A
$\mathbb{I}$	Identity matrix	*none*
$*$	Symmetric entry of a symmetric matrix	*none*

To my wife and my children, who missed me so many times...

Introduction

Context and Motivation

If modern fighter or bomber aircraft tend to have more performance in terms of payload, range, ceiling, efficiency and maneuverability, one of the most important characteristics for the future combat remains *stealthiness*. *Stealthiness* is defined by the capability of a vehicle to reduce its radar, acoustic, Infra Red, electromagnetic or visible signature to make it undetectable or "low observable". Benefiting from stealthy geometries and materials, the Lockheed Martin F-117A Nighthawk, Lockheed Martin F-22 Raptor or F-35 Lightning II, Northrop Grumman X-47B, Dassault nEUROn, the experimental Unmanned Combat Aerial Vehicle (UCAV) inspired from the Northrop B-2 Spirit, are remarkable examples of the effort produced by manufacturers to obtain this essential feature [3, 4].

Indeed, despite the exceptional maneuverability of the new fighter aircraft, a close air-to-air dogfight seems to be less and less likely nowadays, considering the highly advanced avionics systems to detect and/or target any aircraft from long range. Radar, as well as missiles, have increased their range and efficiency so intensively that the strikes and potential combats are engaged before having a visual contact.

Consequently, one of the keys to success is undoubtedly to become as invisible as possible, i.e as stealthy as possible. Radar Cross Section (RCS) is one of the measures of the aircraft's stealthiness. Reducing an aircraft's RCS is a combination of choice of materials, shapes and strategies whose flight control system is undoubtedly part of. Indeed, the actuation of the flap or rudder will create a change in the shape of the aircraft that can be at the origin of the reflection of potential radar signals. Thus, the control associated to an aircraft, while maintaining its required level of performances, remains extremely critical. If accurate data could not be found in the literature, it is known that saturation of the actuators in terms of magnitude or rate helps to maintain the desired level of stealthiness by reducing the exposed surface and the reflections.

Classical control surfaces like flaps, ailerons, slats and rudders, are used to ensure the controllability of the aircraft. However, *active flow control*, using blowing actuators could be an advantageous application for such considerations. Indeed, this type of actuation relies on jets, or synthetic jets, blowing or pulsing air, which modify the flow around the aircraft in such way that the desired effect in terms of moment and force is obtained. These techniques clearly avoid movable surfaces on the aircraft. Active flow control is not new, considering that air has been blown or sucked onto the wings of fighter aircraft for many years now, especially to increase the performances during takeoff and landing on aircraft carriers. Indeed, due to the limited length of the runways, it proved to be necessary to increase the efficiency of the wing of these aircraft in such situations. However, the drawbacks of such a technology, especially in terms of weight and mass flow extracted from the engine, had been very limiting and the efforts made in terms of aerodynamics have reduced the interest of active flow control.

If this technology does not seem to be adapted anymore to increase the lift produced by a wing, especially due to the improvements in terms of thrust or structure, active flow control can find a renewed interest to provide flight control authority. Indeed, projects like Innovative Control Effectors (ICE) [5], aim at replacing all the control surfaces by powerful blowing actuators for stealth considerations. However, hybrid solutions can also be considered to enhance flight control in such conditions. Flight control is a challenging problem and includes many individual problems in terms of performances, efficiencies, Pilot Induced Oscillations (PIO) [6], high maneuverability, high angle of attack [7] or aeroelastic instabilities among others. All these interesting problems remain diverse and particularly challenging, especially on a whole aircraft.

To obtain a better understanding of the complex dynamics involved in flow control, the general problem is often reduced to the study of an oscillating wing. This apparently much simpler problem remains particularly relevant and challenging due to the non-linear dynamics of the flow, whose complexity is increased by the introduction of the flow control. Moreover, a wing is the place of aeroelastic instabilities, resulting from a coupling between the structure and the flow around the wing, which remains a major issue in flight control. For this reason, many works have been published on aeroelastic instabilities for an oscillating wing. While most of these studies concern control surfaces, many of them consider the use of active flow control [8, 9].

Active Flow Control Overview

Active flow control (AFC) defines the action of actively modifying the flow around an object to obtain a certain desired effect. This definition includes movable control

surfaces, like flaps or rudders, and blowing or sucking actuation. Contrary to AFC, passive flow control can also be defined, where the actuator or material, does not involve energy addition such as dissipative material or passive oscillators as in [10], or even fixed modification of the geometry, such as vortex generators. However, in this work, passive flow control will not be considered and we will restrict the use of AFC to the specific case of blowing or sucking actuation only.

Many actuators have been developed and investigated for this purpose. These studies permit us to understand their operating principles to assess the expected performances, to optimize their uses in terms of mass flow rate or frequency, and ultimately to be able to model their dynamics [11]. The most prominent ones are certainly discrete pulsed actuation [12], plasma actuators [13–15], synthetic jet actuators [16], or blowing actuators [17].

Blowing actuators have found some increasing interest, as seen in the recent work conducted by Williams [8], Greenblatt [18] and Muller-Vahl groups [19, 20]. Their studies demonstrate the effects of steady blowing on the lift coefficient and propose an extended modeling of the Goman-Khrabrov (GK) model. In a continuously blowing technique, the coefficient of momentum, *i.e.* the quantity of air injected relatively to the freestream over the wing, can be adapted by varying the velocity of the actuator jet. A larger momentum coefficient has larger effects on the flow while a small momentum coefficient proves to be particularly inefficient or even decreases the performance of the wing.

The efficiency of periodic excitation to excite the boundary layer and obtain some control over the flow has also been demonstrated and widely experimented using various actuation types [21]. An interesting review can be found in Greenblatt & Wygnanski's work [22] and Collis' work [23].

Despite the many works published in this field, the modeling and understanding of the AFC remain extremely challenging. Recent studies have been performed in this direction, especially using blowing actuation [24–28]. The quantity of air blown is possibly varied and used as the command input.

In [29], a Pulse width modulation technique (PWM) on a constant pressure blowing AFC is used. The objective is to obtain a control input based on the duty cycle. While the beneficial effects are observed in the stall region, the small amount of air used in the experiment did not enable yet the development of an advanced model of the actuator.

However, in all the different cases, the control considered in such studies suffers from the high complexity of the model, which limits the development of advanced controllers. Specifically, the leading edge blowing actuators tend to interact with the leading edge vortex that can be produced.

The modeling and the control of the vorticity, leading edge or trailing edge, remain extremely challenging. Because of the low energy and because of its property to emphazise separation, low Reynolds number flows are of particular interest to illustrate this complex phenomenon and have attracted much research [30–32].

Modeling and Control for Aerodynamics System

Thus, the understanding and modeling of the flow is still a fertile field of research.

Many different techniques and strategies have been used to tackle this problem of modeling, trying to capture the maximum amount of energy [33] or the main modes of the flow dynamics. However, the methods can suffer from a lack of physical meaning of the states, usually in large number. On the other hand, more meaningful or physical models with a lower number of states can be limited by their apparent simplicity. If a more accurate model seems to be logically more attractive, its complexity and number of states can quickly become an issue for its control. Indeed, in control theory, a controller is developed to calculate the command to obtain the desired output. Continuous blowing or suction over a wing to increase lift or to control the boundary layer is an example of application where the constant control input is computed *a priori* to provide the desired effect. The command is not re-evaluated based on a feedback measuring the desired effect. This type of command corresponds to some open-loop control. On the contrary, closed-loop control uses the information of the states, or outputs, to calculate at each instant the appropriate command. The closed-loop control allows us to be much more robust to external disturbances, i.e. it allows us to keep the desired performance in spite of unpredicted variations of the states (gusts of wind, initial conditions,...). Nevertheless, the performances of the closed-loop system highly depend on the nature of the disturbances or uncertainties and the controller itself. Control theory allows us to synthesize controllers for a wide range of systems, perturbations, uncertainties and desired performances. The complexity of the controllers depends on all of these parameters. Most importantly, control theory requires a synthesis model (except for specific constructions) which can possibly be different from the complex governing equations. Indeed, in order to be able to apply classical control theory and obtain a simple controller (avoiding unnecessary computation resources), the synthesis model has to be as simple as possible as long as the closed-loop system allows us to satisfy the desired performances. We can thus understand the difficult trade-off between:

- a *too complex model* which permits us to accurately reproduce the states of the system. However, it will suffer from a high order and less flexibility to control it.

- and a *too simple model* which allows us to apply control theory but may fail to reproduce the expected behavior of the system.

This is especially true with flow control, which proves to be particularly challenging since the system governing the equations can be highly complex. For this reason, reduced order modeling (ROM) for flow control has become a major axis of research to be able to apply advanced control theory, where the trade off between complexity and fidelity is obtained [34–36].

Nonlinearities, which are often present in the system equations is one of these complexities. Several works addressed this problem [9, 37]. Feedback linearization has been extensively used in this context. In this method, the nonlinearity is encapsulated in the output command by inverting the system dynamics. The resulting system is a linear system whose control is particularly well covered by the theory. However, feedback linearization may not be suitable for singular systems and is not robust to uncertainties or unknown varying parameters [38]. In [39], a robust controller is developed using mixed norm $\mathcal{H}_2/\mathcal{H}_\infty$ control theory to account for speed variation. In [40], an $\mathcal{H}_\infty$-based gain scheduling approach is developed. Linear Quadratic control has also been widely considered as in [33, 37, 41, 42] or in [43] where nonlinear torsional stiffness and freestream velocity variations are considered. In [44], leading edge and trailing edge control is addressed. An interesting review is provided in [45, 46].

Most of these works address the problem using adaptive control, that is to say that the system is considered as depending on known varying parameters. Such systems are known as linear parameter varying systems (LPV). The controller is thus also dependent on these parameters providing robustness to the closed-loop system. This approach can be motivated by the Takagi-Sugeno theorem [47] stating that every system can be represented by an LPV or polytopic system. However, the parameters are not necessarily known in general and the previous methods are then no longer suitable.

Thesis Contributions

The objective of this work is to control a rigid wing undergoing high pitch oscillations at low Reynolds number. Although the problem is addressed using a conventional trailing edge flap, this work aims at being ultimately extended to active flow control. Indeed, due to its overall complexity, the problem of active flow control needs to be broken down into several steps, which are mainly proposing a model allowing for an understanding of the phenomena of separation and vortex shedding, demonstrating the capacity of control such a system, and extending the results to active flow control by proposing a

model of the actuator and applying the previous control strategies. While the model of the blowing actuation has not been completed in this work, the contributions of this thesis remain three-fold. First, a new aerodynamic model including dynamic stall is developed at low Reynolds number to emphasize the separation and vortex shedding. Second, linear quadratic results in presence of saturation are presented and extended to polytopic systems. Finally, the last contribution consists of interesting formulation of the proposed model into an uncertain polytopic system to solve the problem of stall flutter on a fixed wing.

To ultimately develop a model of the wing equipped with a leading edge blowing actuator, it is first necessary to have a good understanding of the flow over a wing without actuation. For this reason, the first objective of this thesis is to provide a reduced order model of a rigid wing undergoing forced oscillations. This model is initially based on Dr. Williams' model [8] derived form a Goman and Khrabrov study [2]. The model is then developed and enhanced to predict leading edge vortex shedding relying on previous work realized by Truong [48]. The aerodynamic model is validated using a NACA 0018 wing in a low Reynolds number flow. The NACA 0018 has been selected for its symmetry and properties to exhibit deep stall. The equations are primarily developed for pitch oscillations but are extended to pitch and plunge oscillations coupled with structural dynamics.

The objective of this work is to provide theoretical and practical methods for aeroelastic control. The second contribution is then to provide an interesting and practical approach to tackle the complexity due to the aeroelastic formulation. The problem of stall flutter is considered due to the capacity of this aeroelastic instability to be excited only using the pitch axis while classical flutter for instance requires pitch and plunge axis. This one degree of movement allows us to isolate the phenomena to obtain a better understanding of the physical phenomenon. However, despite the single degree of freedom considered, the model remains extremely challenging to control due to the nonlinear nature of the aeroelastic system. The model is then conveniently written as a multi-affine system where some parameters are considered as uncertain. This formulation allows us in particular to integrate representative nonlinearities, like saturations, which are inherent to the actuation systems, conventional or blowing actuators. To the knowledge of the author, the approach consisting in modeling the nonlinear aeroelastic system as an uncertain polytopic system undergoing input saturation has not been considered.

The final contribution concerns the controller design methods which are developed and extended to the previous model. In particular, a Linear Quadratic approach is considered and detailed in the cases of magnitude and rate actuator's saturation. Regions of attraction are introduced to provide guarantees on the cost function. The theorems are

derived for the case of uncertain polytopic systems. The controllers are then evaluated using the simulation model computed with MATLAB.

Thesis Outline

Following these objectives, this dissertation is organized in three chapters as follows.

Chapter 1 presents a new reduced order model of an oscillating wing based on previous works from Dr. Williams' team and Dr. Truong. The proposed parameter varying system permits us to consider the vortex shedding on an oscillating wing. The parameters of this model are identified for a NACA 0018 pitching wing using experimental data. The results of the computation for the moment coefficient are then compared to the experimental data to validate the model. The set of equations can consequently be used for the system analysis and control.

Chapter 2 presents several theoretical results dedicated to the analysis and control of linear and multi-affine systems under various saturation constraints for optimal control. The theorems detailed are formulated using the Linear Matrix Inequalities framework. Numerical academic examples are provided using the mass and spring system.

Chapter 3 exposes the main contribution of this thesis which consists of the application of the theorems detailed in Chapter 2 to the specific problem of Stall Flutter. The application is limited to a one degree of freedom pitching airfoil in the presence of potential saturation. This chapter aims at providing some practical techniques to apply control theory to a nonlinear aeroelastic system. In particular, the uncertainties and nonlinearities such as switched dynamics, unknown varying parameters or saturations are encapsulated in a multi-affine polytopic formulation. Numerical simulation results are provided, and remarks are formulated concerning the region of attraction, conservatism and limitations of the methods.

Finally, after presenting some concluding remarks, future perspectives are provided to extend the application domain of this work.

Publications

- [49] Fabien Niel, Alexandre Seuret, Luca Zaccarian and Casey Fagley. Robust LQR control for stall flutter suppression: a polytopic approach. In *IFAC-PapersOnLine*, 2017
- [29] Fabien Niel, Casey Fagley , Jürgen Seidel and Thomas McLaughlin. Modeling of transient blowing actuation using Pulse Width Modulation on a dynamically pitching NACA 0018 Airfoil. In *35th AIAA Applied Aerodynamics Conference*, 2017
- [50] Fabien Niel, Casey Fagley, Jürgen Seidel and Thomas McLaughlin. Reduced order modeling of a dynamically pitching NACA 0018 Airfoil. In *55th AIAA Aerospace Sciences Meeting*, 2017
- [51] Fabien Niel, Yann Ameho, Jean-Marc Biannic, François Defaÿ and Caroline Bérard. A novel parameter varying controller synthesis method for quadrotor control. In *Proceedings of the AIAA Guidance, Navigation, and Control Conference*, 2013
- [52] Yann Ameho, Fabien Niel, Jean-Marc Biannic, François Defaÿ and Caroline Bérard. Adaptive control for quadrotors. In *Robotics and Automation (ICRA), 2013 IEEE International Conference*, 2013

Chapter 1

Aeroelastic Modeling

1.1 Introduction

Many applications such as wind turbines, unmanned aerial vehicles, helicopters, and fighter or other agile aircraft look for improving their performances by increasing their operating envelope and/or modifying their structure. Such modifications are limited by the interactions between the aerodynamic modes and the structural modes which can lead to aeroelastic instabilities. These aeroelastic instabilities can develop quickly and be particularly destructive as The Helios prototype, a solar powered flying wing, experienced developing unforeseen and catastrophic excitations [53].

Modeling accurately those limiting phenomena occurring in the system {Wing-Flow} and developing a robust control strategy are the key for future developments and improvements.

However, developing a too complex model may be limiting to compute suitable controllers. A trade-off is often necessary between a complex model, reproducing closely the reality of the system but often non-usable from a control point of view, and a more simplistic model which permits us to apply control theory tools but which may fail to reproduce higher order dynamics of the considered system. The aeroelastic models used to describe the flow around a wing correspond perfectly to the situation where a full description of the flow predicted by the non-linear equations of Navier-Stokes at every point of fluid would be completely useless from an automation perspective. On the other hand, a too simplistic model would not be representative of the flow physics.

This chapter aims at developing an accurate model capable of predicting the lift and moment on an oscillating airfoil including the vortex shedding which occurs and varies consequently the load. First, a general aeroelastic model is presented. The aerodynamic

load is then detailed and a new model based on previous works from Dr. Williams and Dr. Truong is proposed for the pitching coefficient of lift and moment. This model provides the necessary accuracy while keeping a low number of parameters in view of later on facilitates its control. Using static and dynamic motion data, the aerodynamic model is trained and successfully compared to experimental results.

1.2 Aeroelastic Model

This work aims at developing an adapted modeling of the flow around an oscillating wing in the view of developing and computing controllers using classical and advanced control theory. Particularly, the model has to be able to represent the structural dynamics as well as the aerodynamic load over the airfoil including the vortex shedding while maintaining the ability of being controlled in presence of nonlinearities such as saturation.

For this purpose, an oscillating and plunging rigid wing section is considered as depicted in Fig. 1.1. The wing is placed in a flow with a freestream velocity U. The flow generates some aerodynamic loads, forces, known as lift, L, and drag, D, and moment, $\mathcal{M}$. In order to tackle later on the phenomenon of flutter, the angle of attack, α, and the plunge, h, will be studied.

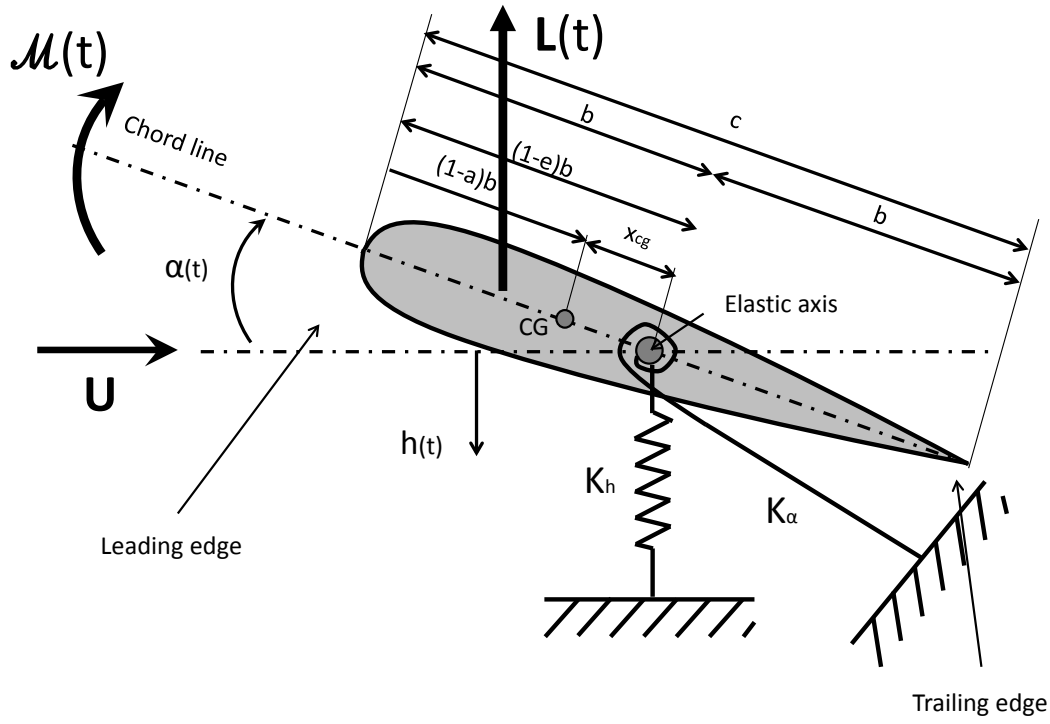

FIGURE 1.1: Model of the pitching and plunging airfoil

Using the Fig. 1.1, the commonly adopted linearized equations for a wing section under aerodynamic loads are given by:

$$\begin{bmatrix} m & mx_{CG} \\ mx_{CG} & I_\alpha \end{bmatrix} \begin{bmatrix} \ddot{h} \\ \ddot{\alpha} \end{bmatrix} + \begin{bmatrix} C_h & 0 \\ 0 & C_\alpha \end{bmatrix} \begin{bmatrix} \dot{h} \\ \dot{\alpha} \end{bmatrix} + \begin{bmatrix} K_h & 0 \\ 0 & K_\alpha \end{bmatrix} \begin{bmatrix} h \\ \alpha \end{bmatrix} = \begin{bmatrix} -L_{tot} \\ \mathcal{M}_{tot} \end{bmatrix} \tag{1.1}$$

where

- c is the chord representing the segment length between the leading edge and the trailing edge,
- b represents the semi-chord, $(b = c/2)$,
- e is the distance between the middle of the chord and the elastic axis normalized by b. The elastic axis is defined as the line on the wing composed of the points where no twist or torsion will be generated if we apply a force at this location or likewise where there is no plunging applying a torque, In our case, the axis of rotation corresponds to the elastic axis and $e = 0$,
- a is the distance between the middle of the chord and the center of mass normalized by b,
- $x_{CG} = (a - e)b$ corresponding to the distance between the elastic axis and the center of mass,
- K_h, K_α are respectively the plunging and torsional stiffness,
- I_α the inertia around the y axis,
- m the mass of the wing section,
- C_h, C_α are the damping coefficients,
- L_{tot} and $\mathcal{M}_{tot}$ are respectively the lift and the moment corresponding to the aerodynamic load undergone by the wing,
- h is the plunge displacement,
- α is the torsional deflection between the freestream velocity and the chord line of the wing or angle of attack.

Note that in the model proposed here, no structural nonlinearities are considered in order to focus the study on the aerodynamic aspect. However, nonlinear stiffness, for example, could be easily introduced as in [37].

The lift and moment result from the aerodynamic load generated by the flow around the wing. These aerodynamic components highly depend on the geometry of the wing and the properties of the flow.

Lift, or pitching moment, is a complex interaction of the flow, the wing, and possibly of the actuator deflection and/or the flow modification. For the sake of clarity in the modeling, these contributions, represented as scalar values, are split into two independent components. The first one, $\{L,\ \mathcal{M}\}$, is the resultant of the flow and the wing geometry interaction without actuation. The second one $\{L_{act},\ \mathcal{M}_{act}\}$ is the negative or positive increment of lift and moment generated by the actuator which will be detailed in 1.2.2. The sum of those two components forms the total aerodynamic resultant expressed as follows:

$$\begin{bmatrix} L_{tot} \\ \mathcal{M}_{tot} \end{bmatrix} = \begin{bmatrix} L + L_{act} \\ \mathcal{M} + \mathcal{M}_{act} \end{bmatrix} \tag{1.2}$$

The following generic lift and moment coefficients are also defined:

$$C_{\mathcal{L}ift} = \frac{\mathcal{L}ift}{\rho b U^2 l} \quad \text{and} \quad C_{\mathcal{M}oment} = \frac{\mathcal{M}oment}{2\rho b^2 U^2 l}, \tag{1.3}$$

where $\mathcal{L}ift$ can be any lift or lift increment and $\mathcal{M}oment$ can be any moment or moment increment.

These coefficients, used for aeronautical notation consistency, permit to normalize the former values by the dynamic pressure, $q = \frac{1}{2}\rho U^2$ and the surface area $2bl = S$, where b is equal to half of the chord length and l is the span.

Using the previous notation, the lift and moment take the following form:

$$\begin{bmatrix} L_{tot} \\ \mathcal{M}_{tot} \end{bmatrix} = \begin{bmatrix} qS\left[C_L(t, x(t)) + C_{L,act}(t, x(t), u(t))\right] \\ qSc\left[C_{\mathcal{M}}(t, x(t)) + C_{\mathcal{M},act}(t, x(t), u(t))\right] \end{bmatrix} \tag{1.4}$$

where $x(t)$ represents the state vector, i.e. the state of the wing and flow, $C_L(t, x(t))$ and $C_{\mathcal{M}}(t, x(t))$ are respectively the coefficients of lift and moment resulting from the flow and $C_{L,act}(t, x(t), u(t))$ and $C_{\mathcal{M},act}(t, x(t), u(t))$ respectively the coefficients of lift and moment resulting from the actuation.

Eq. (1.1) becomes:

$$\begin{bmatrix} m & mx_{CG} \\ mx_{CG} & I_\alpha \end{bmatrix} \begin{bmatrix} \ddot{h} \\ \ddot{\alpha} \end{bmatrix} + \begin{bmatrix} C_h & 0 \\ 0 & C_\alpha \end{bmatrix} \begin{bmatrix} \dot{h} \\ \dot{\alpha} \end{bmatrix} + \begin{bmatrix} K_h & 0 \\ 0 & K_\alpha \end{bmatrix} \begin{bmatrix} h \\ \alpha \end{bmatrix} = \begin{bmatrix} -qS\left[C_L(t,x(t)) + C_{L,act}(t,x(t),u(t))\right] \\ qSc\left[C_{\mathcal{M}}(t,x(t)) + C_{\mathcal{M},act}(t,x(t),u(t))\right] \end{bmatrix} \tag{1.5}$$

If the left side of Eq. 1.5 is commonly adopted, the choice of the aerodynamic models used to define C_L, $C_{L,act}$ or $C_{\mathcal{M}}$, $C_{\mathcal{M},act}$ prove to be particularly critical.

1.2.1 Aerodynamic Model

1.2.1.1 State of the Art

Numerous of models have been proposed over the past eighty years. If the use of the Direct Navier Stokes equations (DNS) is clearly unrealistic considering the infinite number of states involved, the selected model has to be accurate enough to capture the non-linearities and unsteadinesses encountered during a pitch and plunge motion. Many different approaches and techniques have actually been employed to obtain Reduced Order Models (ROM), like Proper Orthogonal Decomposition (POD) [33], or Dynamic Mode Decomposition (DMD). A detailed description can be found in [45]. Nevertheless, in order to keep a certain level of physical meaning necessary to extend the model to active flow actuator, only the techniques based on the flow description will be considered in the sequel.

One of the first well-known works can be attributed to Theodorsen [54], where many assumptions like incompressible, inviscid and potential flow are necessary to obtain an unsteady model of the forces and moments around a thin airfoil. This model is decomposed into added mass and quasi-steady components using a weight function modulating the amplitude and phases due to the wake vorticity such as presented by Brunton & Rowley [34]. Due to the physical significance of each component, this model proves to be widely used. Especially, the weighting function, known as the Theodorsen function and described by a Hankel function, has been approximated in multiple articles to obtain a set of equations that is easier to compute, which has allowed researchers to derive numerous models. An interesting review of the various approximations, and state space representations, has been made by Brunton & Rowley [34].

Nevertheless, since Theodorsen's model is only formulated for attached flow, it likely fails to capture the highly nonlinear and unsteady effects due to flow separation. Indeed,

high angles of attack or rapid maneuvers can lead to full or partial separation of the flow over the airfoil. The separation and fast changes in the flow are responsible for the flow hysteresis and dynamic stall which have been observed experimentally. Especially, during the pitch cycle of an oscillating wing, the flow alternately separates and reattaches over the airfoil as described by McCroskey et al. [1]. The lags observed in the lift force and moments in such situations can result in dynamic stall or stall flutter where the structural modes of the flexible wing are excited by these aerodynamic oscillations.

Dynamic stall deserves a particular attention as it is involved in many aerodynamic systems and proves to be particularly limiting for many applications. Especially, helicopters blades or wind turbines are very sensitive to this phenomenon which can generate vibrations, fatigue, and loss of performances. For this reason, many researches about this subject have been initiated [55, 56].

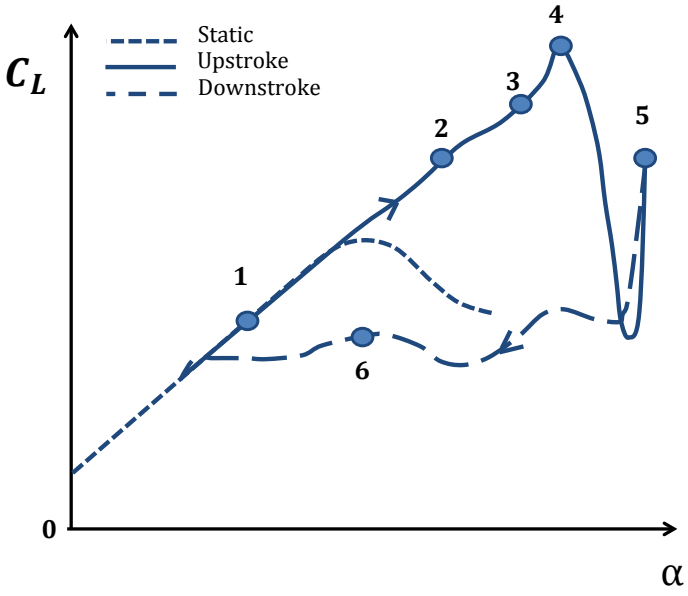

FIGURE 1.2: Lift evolution and dynamic stall from [1]

Fig. 1.2, from [1], provides an illustration of lift evolution for a pitching wing. As detailed in the original paper, until point 1, the flow remains attached and the dynamic evolution follows the static one. At point 2, the flow remains attached longer due to the upstroke of the wing. Then, the flow starts to reverse at the trailing edge and a leading edge vortex starts to form. Between point 3 and 4, the leading edge vortex grows until shed along the wing providing more lift. When the vortex is completely passed along the wing and the separation reaching the all upper surface, the lift drops abruptly. However, a

second leading edge vortex starts to grow providing a new increase of lift at point 5. The second vortex sheds in turn, generating oscillations on the down-stroke. The flow remains detached until it reattaches completely for a lower angle of attack than the static case.

Many works have been carried out for over 50 years, mostly on pitching airfoil, and have allowed us to collect many data and observations. In particular, it is known that dynamic stall is influenced by the geometry of the airfoil, the pitching frequency or reduced frequency which will be introduced later, the amplitude and mean angle and the Mach number, corresponding to the ratio of the velocity and the speed of sound.

Many models have been developed to account for this phenomenon, especially for helicopter or wind turbine blades where low Reynolds number or large angles of attacks are commonly encountered and are particularly inclined to demonstrate dynamic stall. The complexity of the phenomena involved in flow separation has been included in the development of models using empirical or semi-empirical techniques. A comparison of various models was made by Johnson, Bierbooms and Beaudet [56–58]. Among them, the ONERA model (Office national d'études et de recherches aérospatiales), where the coefficients of lift and moment are described using second order differential equations [59], has been widely used [39, 55]. In particular, this method has been used in a "unified model", which gave good agreement with experimental results in [60]. The ONERA model has been modified using Tobak's work on the Hopf Bifurcation [61] which has been represented by a Van der Pol equation [48]. This model, denoted as ONERA BH for Hopf Bifurcation in French, requires a relatively low number of parameters [62]. Another interesting model has been developed by Leishman and Beddoes [63, 64]. These models have seen many uses and adaptations, such as by Sheng et al. [30], who are accounting for low Reynolds number. The popularity of this model can be attributed to the step-by-step methodology used to describe increasingly complex physical observations.

Using a different approach based on cavitation theory, Goman and Khrabrov relate the separation point location to the lift coefficient [2]. This model, like other models cited above, introduces some hysteresis in the flow description to obtain a simplified model in terms of equations. Inspired by this work, Williams derived an interesting approach with the goal of achieving a linearized model [8] for the pitching oscillation. Williams' formulation, combined with the ONERA BH equations, will be used to develop a new model used in this study. The details of this work can be found below.

1.2.1.2 Aerodynamic Model Development

As mentioned previously, one of the first models of the aerodynamic loads for a pitching and plunging wing has been proposed by Theodorsen [54] using thin airfoil theory for attached flow.

In this model, the coefficients C_L and C_M at quarter chord are given in [65] by:

$$C_L = \frac{L}{\rho b U^2 l} = C_{L,\alpha} C(k)(\alpha + \frac{\dot{h}}{U} + (\frac{1}{2} - a)\frac{b\dot{\alpha}}{U}) + \pi(\frac{b\dot{\alpha}}{U} + \frac{b}{U^2}\ddot{h} - \frac{ab^2}{U^2}\ddot{\alpha}) \tag{1.6}$$

$$C_M = \frac{M}{2\rho b^2 U^2 l} = C_{M,\alpha} C(k)(\alpha + \frac{\dot{h}}{U} + (\frac{1}{2} - a)\frac{b\dot{\alpha}}{U}) + \frac{\pi}{2}(\frac{b\dot{\alpha}}{U}(a - \frac{1}{2}) + \frac{ab}{U^2}\ddot{h} - \frac{b^2}{U^2}(\frac{1}{8} + a^2)\ddot{\alpha}) \tag{1.7}$$

where $C_{L,\alpha}$ and $C_{M,\alpha}$ are the static lift and moment coefficient, $k = \frac{2\pi b}{fU}$ is the *reduced frequency* with f the pitching frequency and $C(k)$ the so-called Theodorsen's function. The Theodorsen's function can be written by incorporating Hankel functions. This function is well defined for purely sinusoidal movement depending on k. Many approximations of this function have been studied. An interesting list of these approximations is given in [34].

The formulation proposed by Theodorsen has been widely adopted for the prediction of aeroelastic instabilities such as *divergence* or *"classical" flutter*. Unfortunately, this extensively used model assumed attached flow and therefore does not take into account phenomenon like the separation of the flow. That proves to be limiting for many applications, especially involving high angle of attack or low speed where separation can occur.

Among many models, the interesting and promising work made by Williams team as well as Greenblatt and Müller-Vahl offers an attractive approach for modeling, analyzing and consequently controlling a wing with blowing actuator. The concept behind this approach is detailed in the sequel.

1.2.1.3 Nonlinear GK Williams Model

Based on the work of Goman and Khrabrov [2], a model of the lift coefficient for a pitching airfoil is derived by Williams [8]. This model proves to be very interesting due to its ability to capture the hysteresis of the lift coefficient but also for its small number of empirical parameters.

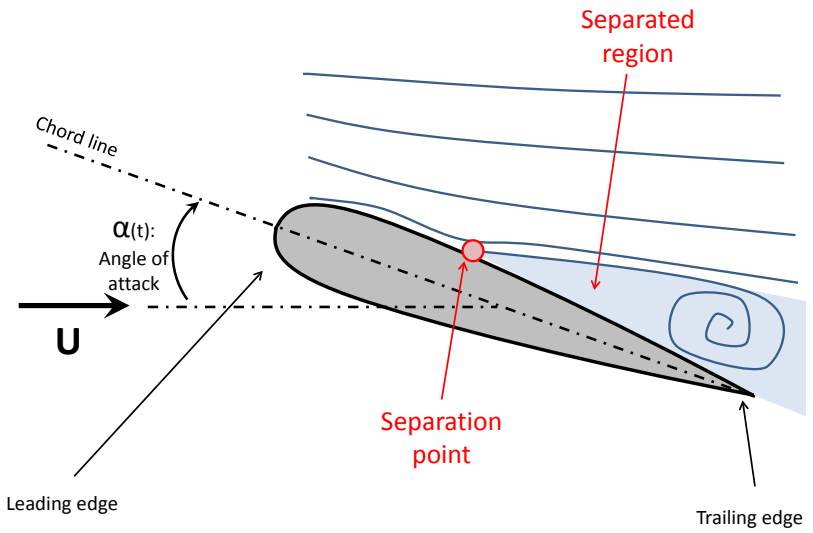

FIGURE 1.3: Separated flow

As described earlier, the separation point location, as represented on Fig. 1.3, modifies the pressure distribution on the flow and consequently the lift and moment values. For a static or quasi-static motion, the separation point location, x_0, is represented in function of α by a solid line on Fig. 1.4. The separation point location is the distance between the leading edge and the separation point location normalized by the chord length. Thus, this continuous function, x_0, is bounded between 0, when the flow is fully separated, and 1, when the flow is completely attached.

If the airfoil is driven by a pitching motion, then a lag will appear on the position of the separation. This shift is function of the velocity of the pitch and is thus function of the first time derivative of α, $\dot{\alpha}$ and a time constant τ_2. This shift is illustrated on Fig. 1.4 by the dot line. A hysteresis phenomena is clearly observed in such sinusoidal motion.

The work of Goman and Khrabrov was to relate the separation point location to the lift coefficient in [2] as it can be observed on Fig. 1.4 and 1.5.

The lift coefficient is predicted by:

$$C_L(\alpha, x_s(t)) = \frac{\pi}{2} sin(\alpha(1 + \sqrt{x_s})^2). \tag{1.8}$$

Hence, Fig. 1.4 allows us to state that the lift coefficient follows a first slope for a complete attached flow, $x_s = 1$, and another different slope for a detached flow $x_s \simeq 0$. The slope of these lines just depends on the degree of attachment of the flow and not on

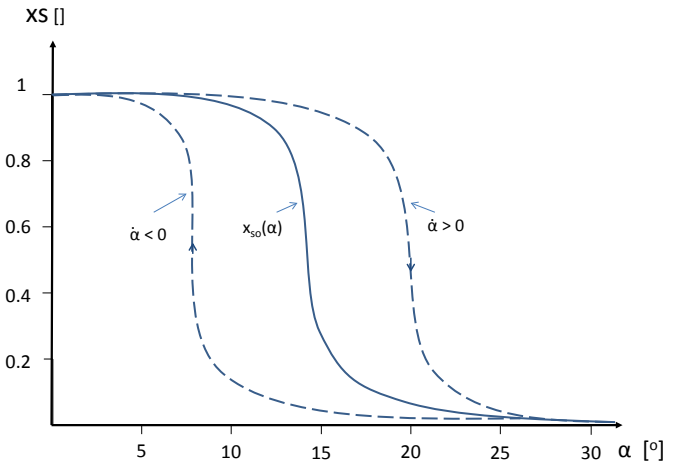

FIGURE 1.4: Evolution of the normalized separated point location in function of α adapted from [2].

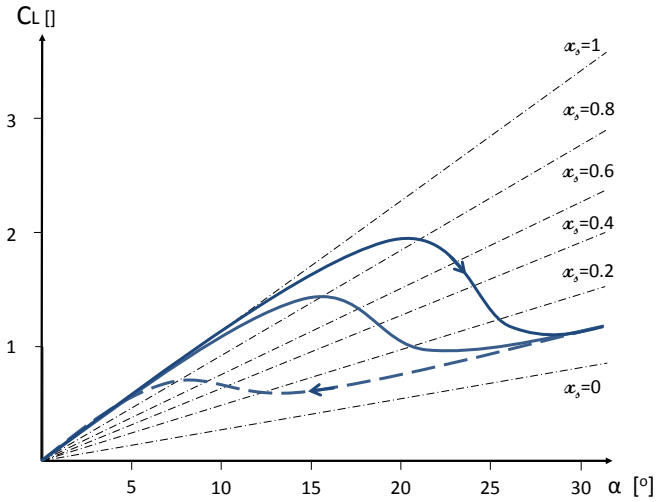

FIGURE 1.5: Evolution of C_L in function of α adapted from [2].

the motion itself. The values of these slopes can thus be estimated by static, or quasi-static, information. The variation of the flow between these two bounds is function of the hysteresis of the separation point location.

Using this observation, Williams' group expresses the lift coefficient as a function of this position of the separation point, x_s, the angle of attack and only three other parameters:

$$C_L(\alpha, x_s(t)) = 2\pi\alpha(t)(A_L + B_L x_s(t)) + C_{L\text{offset}}, \tag{1.9}$$

where $2\pi A_L$ and $2\pi\left(A_L + B_L\right)$ are scalar value, using notations in [8] and represent the lift coefficient curve slopes, respectively, for a fully separated flow ($x_s = 0$) and fully attached flow ($x_s = 1$). A_L can be easily identified on a static lift curve for a sufficiently

large range of angles of attack. Note that for a small angle of attack, corresponding to a fully attached flow, the slope $2\pi\left(A_L + B_L\right)$ must be close to 2π, predicted by the thin airfoil theory, leading to $A_L + B_L = 1$.

Once those two parameters are identified, the curve of the separation point location can be also deduced from the same static lift or moment curve and Eq. (1.9). $C_{L\text{offset}}$ represents the lift for an angle of attack equal to zero. These values will be considered equal to zero for a symmetric airfoil, and will be omitted in the sequel.

The dynamic position of the separation point is following a first order dynamic where the input is the shifted static position,

$$\tau_1 \dot{x}_s + x_s = x_{s,0}(\alpha - \tau_2 \dot{\alpha}). \tag{1.10}$$

where $x_{s,0}(\alpha)$ is the static position of the separation point as a function of α, and τ_1 and τ_2 are respectively the time constant for the separated flow to reach its static position and the time constant of the flow related to the pitch rate of the wing $\dot{\alpha}$. τ_1 and τ_2 can then be obtained from a fit to computational fluid dynamics (CFD) results or experimental dynamic data.

Note that in this formulation, the shifting is not constant but depends on the angular velocity $\dot{\alpha}$.

Assuming that the coefficient of moment at mid chord is $C_{M,\frac{1}{2}}(\alpha, x_s(t)) = C_{M,\frac{1}{4}}(\alpha, x_s(t)) + 0.25cC_L(\alpha, X(t))$ and that $C_{M,\frac{1}{4}}$, the coefficient of moment at quarter chord is depending on the separation point as well, a similar formulation is proposed here:

$$C_{M,\frac{1}{2}}(\alpha, x_s, t) = 2\pi\alpha(t)(A_M + B_M x_s(t)) + C_{M\text{offset}}. \tag{1.11}$$

As it can be seen on the comparison between experimental values and Williams' model prediction of the coefficient of moment as a function of α during a pitch oscillation Fig. 1.6, this model captures the dynamic hysteresis.

However, in spite of these interesting results, the model fails at reproducing the oscillatory behavior that can be experienced due to the vortex shedding [24]. For this reason, the ONERA approach is also explored to enhance the previous model.

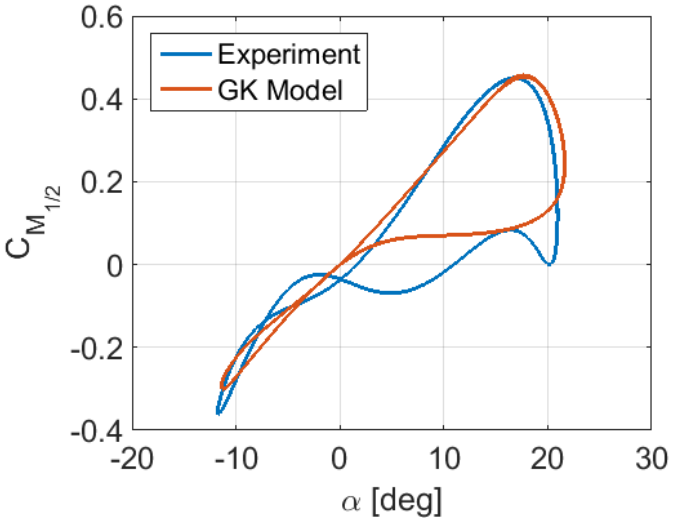

FIGURE 1.6: Comparison between experimental values of the coefficient of moment and Williams' model prediction

1.2.1.4 ONERA Hopf Bifurcation Model

The ONERA BH (Bifurcation de Hopf) method breaks down the expression of the lift coefficient into a steady and an unsteady components:

$$C_L = C_{L_s} + C_{L_u}. \tag{1.12}$$

The Hopf Bifurcation model (ONERA BH) [48, 66, 67] is an enhanced version of the original ONERA method [59] and aims at describing more accurately the vortex shedding dynamics using Tobak's work on Hopf bifurcation [61]. The steady component is based on a first order dynamic model with a time constant τ_s following a similar approach than Leishman-Beddoes method [30, 56, 64]. An adapted formulation [57] is presented here:

$$\dot{C}_{L_s} + \frac{1}{\tau_s} C_{L_s} = \frac{1}{\tau_s} C_{L_s}^{equil}. \tag{1.13}$$

$C_{L_s}^{equil}$ is calculated based on Kirchoff's equation, such as:

$$C_{L_s}^{equil} = C_L^{\alpha} \left(\frac{1 + \sqrt{x_s}}{2} \right)^2 \alpha, \tag{1.14}$$

where x_s is given by a piecewise function [64].

Nevertheless, comparing to Leishman-Beddoes method, the lag effects of the separation point location, x_s are modeled by one shifted angle of attack ($\alpha(t) \rightarrow \alpha(t - \tau)$) and one

first order dynamic equation:

$$\dot{x}'_s + \frac{1}{\tau_f} x'_s = \frac{1}{\tau_f} x_s. \tag{1.15}$$

Concerning the unsteady component, a Van der Pol-like equation is used:

$$\ddot{C}_{L_u} - w_S(\beta_L^{\pm} - \gamma_L^{\pm} C_{L_u}^2)\dot{C}_{L_u} + w_S^2 C_{L_u}(1 - \eta_L^{\pm} C_{L_u}^2 - a_{2,L}^{\pm} C_{L_u}) = -E_L^{\pm} w_S \dot{\alpha} - D_L^{\pm} w_S \ddot{\alpha}. \tag{1.16}$$

where w_S, $\beta_L^{\pm}$, $\gamma_L^{\pm}$, $\eta_L^{\pm}$, $a_{2,L}^{\pm}$, $E_L^{\pm}$, $D_L^{\pm}$ are two sets of constants. The set of constants to use depends on the regime defined by $\alpha > \alpha_s$ which corresponds to the decay regime (noted X^-) and $\alpha < \alpha_s$ for the growth regime (noted X^+).

Indeed, during the decay regime,

$$\beta_L^- \neq \beta_L^+,\ \gamma_L^- = 0,\ \eta_L^- = 0,\ a_{2,L}^- = 0,\ E_L^- = 0,\ D_L^- = 0.$$

Note that during this regime, Eq. (1.16) becomes a damped harmonic oscillator equation.

In the sequel, we will denote these parameters in function of x, such as $\beta_L(x)$, $\gamma_L(x)$, $\eta_L(x)$, $a_{2,L}(x)$, $E_L(x)$, $D_L(x)$.

1.2.1.5 New Aerodynamic Model: GKO Model

Based on the two previous models, a new model is proposed.

Indeed, as mentioned previously, the GK model is not adapted to predict the oscillatory behavior due to the secondary vortex shedding [24]. On the other hand, the ONERA BH method suffers from its complexity due to the number of parameters and their empirical determination. Thus, both models are combined and adapted to develop the Goman-Khrabrov-ONERA (*GKO*) model whose details are provided hereafter.

First of all, the *GKO* model follows the overall structure of the ONERA BH model where:

$$C_L = C_{L_s} + C_{L_u}. \tag{1.17}$$

However, the model proposed by Williams is preferred to predict the steady component, C_{L_s}.

After trial and error, this model has been slightly adapted.

In particular, the two regimes have been adjusted and renamed. Instead of using the angle of attack to determine the regime during the downstroke, the separation point location is preferred. The first regime, called *excited* regime, corresponds to the part

where the flow is mainly separated. This regime begins for a sufficient angle of attack, $\alpha > \alpha_s$, until it reattaches, $0 < x_s < x_{s,c}$, where α_s and $x_{s,c}$ are the critical angle of attack and critical separation point location to determine. The angle of attack for $x_s = x_{s,c}$, during the downstroke is denoted $\alpha_{d\ x_s=x_{s,c}}$. The remaining part of the motion envelope is named the *non-excited* regime. Illustration of these regimes is provided in Fig.1.7.

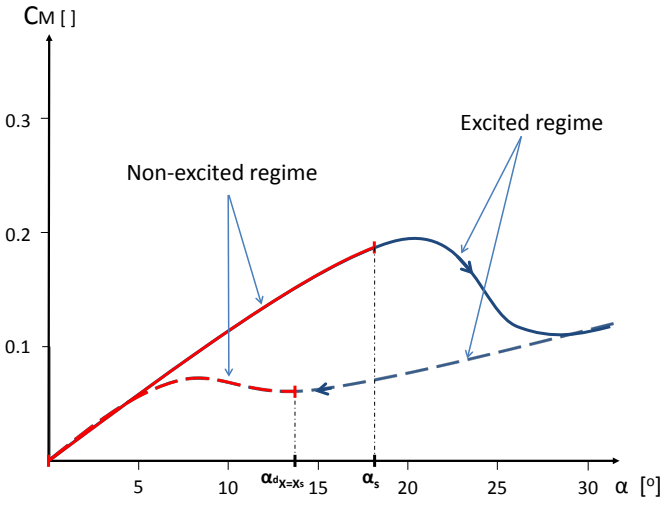

FIGURE 1.7: Description of the two regimes governing the unsteady set of equations

The resulting model for a non-actuated system is thus a combination of the Williams' model and the ONERA BH model. This model will be referred as Goman-Khrabrov-ONERA model, or *GKO* model. It aims at using the efficiency of Williams' model to predict the hysteresis of the pitching moment and the capability of the ONERA BH model to reproduce the oscillatory behavior.

The equations for the resulting model of the lift and moment coefficients are given by:

$$C_L(t) = C_{L,\alpha}C(k)\frac{\dot{h}(t)}{U} + \pi\frac{b}{U^2}\ddot{h}(t) + 2\pi\alpha(t)(A_L + B_L x_s(t)) + C_{L\text{offset}} + C_{L_u}(t) \quad (1.18)$$

$$C_{M,\frac{1}{4}}(t) = C_{M,\alpha}C(k)\frac{\dot{h}(t)}{U} + \frac{\pi}{2}\frac{ab}{U^2}\ddot{h}(t) + 2\pi\alpha(t)(A_M + B_M x_s(t)) + C_{M\text{offset}} + C_{\mathcal{M}_u}(t) \quad (1.19)$$

with

$$\begin{cases} \tau_1 \dot{x_s} + x_s & = & x_{s,0}(\alpha - \tau_2 \frac{d\alpha}{dt}), \\ \ddot{C}_{M_u} + D_M(x) w_S \ddot{\alpha}\,(t) & = & w_S(\beta_M(x) - \gamma_M(x) C_{M_u}^2)\dot{C}_{M_u} - w_S^2 C_{M_u}(1 - \eta_M(x) C_{M_u}^2 \\ & & -a_{2,M}(x) C_{M_u}) - E_M(x) w_S \dot{\alpha}\,(t)\,, \\ \ddot{C}_{L_u} + D_L(x) w_S \ddot{\alpha}\,(t) & = & w_S(\beta_L(x) - \gamma_L(x) C_{L_u}^2)\dot{C}_{L_u} - w_S^2 C_{L_u}(1 - \eta_L(x) C_{L_u}^2 \\ & & -a_{2,L}(x) C_{L_u}) - E_L(x) w_S \dot{\alpha}\,(t)\,. \end{cases} \tag{1.20}$$

where C_{M_u} and C_{L_u} are the unsteady coefficients of moment and lift as defined in [48], $C_{L,\alpha}$, $C_{M,\alpha}$, $C_{L\text{offset}}$, $C_{M\text{offset}}$, A_L, B_L, A_M and B_M are constant, ρ is the density, U the flow velocity, $C(k)$ is the Theodorsen's function, only well defined for pure oscillations, depending on the reduced frequency k. Approximations can be found in [34].

Note that $\beta_M(x)$, $\gamma_M(x)$, $\eta_M(x)$, $a_{2,M}(x)$, $E_M(x)$, $D_M(x)$ and $\beta_L(x)$, $\gamma_L(x)$, $\eta_L(x)$, $a_{2,L}(x)$, $E_L(x)$, $D_L(x)$ are two sets of parameters depending on x_s. Each varying parameter can only switch between two values, possibly zero.

Consequently, Eq. 1.20 is a piece-wise set of equations and represents a challenging control problem.

1.2.2 Actuator Model

In this section, a model is proposed for the actuator model.

Two different methods of actuation can be considered:

- a trailing edge flap,
  Trailing edge control surfaces have been widely studied and used. Numerous of models are available in the literature such as in [39, 54, 68]. The flap aims at modifying the geometry of the wing by increasing or decreasing the curvature of the wing. The position of the flap is given by the angle between the chord line of the wing and the chord line of the flap and is denoted $\beta(t)$. The position of the flap can possibly have its own dynamics depending on the type of actuator used to move the flap, generally an electric motor. The angle of deflection is also limited in amplitude, and the control signal is consequently saturated.

- an AFC actuator,
  As described earlier, AFC actuator aims at sucking or blowing air to control the boundary layer. The air can be blown in relatively high quantity over the wing comparing to the flow, or dynamic pressure over the wing. This technique has

been particularly used to enhance the overall lift. When smaller quantities of air are used, the effect sought is an interaction with the boundary layer, to attach or separate the flow and eventually control the vorticity over the wing. The level of complexity of the physics is extremely important and modeling the resulting effect proves to be challenging [29, 69].

In both cases, the actuator aims at modifying the flow properties over the airfoil and thus at modifying the lift and moment. A general control input $u(t)$ is defined and will respectively correspond to $\beta(t)$ or $\lambda(t)$ accordingly to the actuation technique used [29].

However, this work aims at considering a generic model in order to make possible some potential future similarities with AFC actuation. Such similarities have been done in previous work [70] for synthetic jet actuator and denoted *virtual surface deflection*, i.e. the effect of the AFC actuator is equivalent to the deflection of a virtual surface.

Thus, we consider that the lift and moment produced by the trailing flap, or virtual surface, are simply defined by

$$\begin{aligned} \mathcal{L}_\beta &= \tfrac{1}{2}\rho U^2 S C_{L,\beta}\beta, \\ \mathcal{M}_\beta &= \tfrac{1}{2}\rho U^2 S c C_{M,\beta}\beta, \end{aligned} \tag{1.21}$$

where

- $C_{L,\beta} = \dfrac{\partial C_L}{\partial \beta}$ is the change of lift per unit of change of flap deflection and is known constant,
- $C_{M,\beta} = \dfrac{\partial C_M}{\partial \beta}$ is the change of wing moment per unit of change of flap deflection and is known constant,
- β is the flap deflection.

The deflection, or virtual deflection, can eventually be the resulting state of the actuator system dynamics. Although different models, generally a first order or second order dynamic, are also described in the literature, the dynamic is commonly not considered. Indeed, the dynamic of the actuator is often considered as much faster than the dynamic of the wing itself. Moreover, in order to keep a generic formulation, especially in view of being extended to the AFC actuator, introducing a second order dynamic would certainly be irrelevant comparing to the nonlinear dynamic of the latest [29, 69].

1.2.3 Complete Aeroelastic Equation Set

As presented in Fig. 1.8, the resulting model is a combination of a *GK* model and a modified ONERA BH which form the aerodynamic *GKO* model and an elastic model.

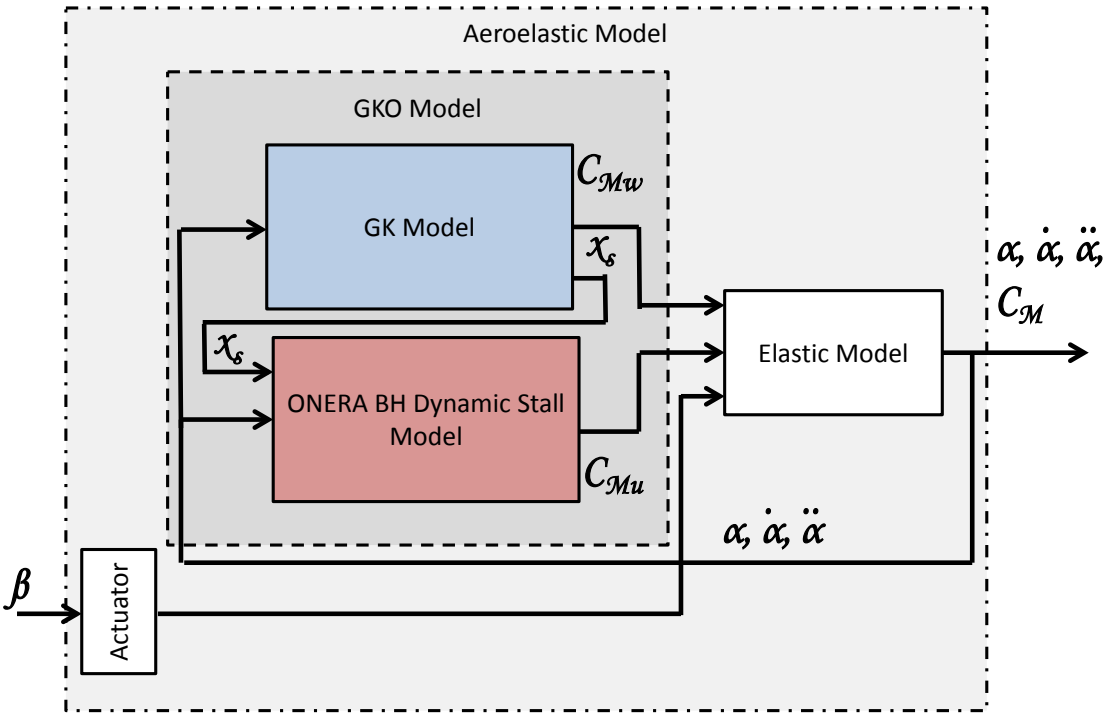

FIGURE 1.8: Architecture of the aeroelastic system.

The set of equations can now be used to predict the aeroelastic behavior of an oscillating wing and is gathered herein:

$$\begin{bmatrix} m & mx_{CG} \\ mx_{CG} & I_\alpha \end{bmatrix} \begin{bmatrix} \ddot{h} \\ \ddot{\alpha} \end{bmatrix} + \begin{bmatrix} C_h & 0 \\ 0 & C_\alpha \end{bmatrix} \begin{bmatrix} \dot{h} \\ \dot{\alpha} \end{bmatrix} + \begin{bmatrix} K_h & 0 \\ 0 & K_\alpha \end{bmatrix} \begin{bmatrix} h \\ \alpha \end{bmatrix} = \begin{bmatrix} -qS\left[C_L(t,x(t)) + C_{L,act}(t,x(t),u(t))\right] \\ qSc\left[C_{\mathcal{M}}(t,x(t)) + C_{\mathcal{M},act}(t,x(t),u(t))\right] \end{bmatrix} \tag{1.22}$$

$$\begin{cases} C_L(t) = C_{L,\alpha} C(k) \frac{\dot{h}(t)}{U} + \pi \frac{b}{U^2} \ddot{h}(t) + 2\pi\alpha(t)(A_L + B_L x_s(t)) + C_{L\text{offset}} + C_{L_u}(t) \\ C_M(t) = C_{M,\alpha} C(k) \frac{\dot{h}(t)}{U} + \frac{\pi}{2} \frac{ab}{U^2} \ddot{h}(t) + 2\pi\alpha(t)(A_M + B_M x_s(t)) + C_{M\text{offset}} + C_{M_u}(t) \end{cases} \tag{1.23}$$

with

$$\begin{cases} \tau_1 \dot{x_s} + x_s & = & x_{s,0}(\alpha - \tau_2 \frac{d\alpha}{dt}), \\ \ddot{C}_{M_u} + D_M(x) w_S \ddot{\alpha}\,(t) & = & w_S(\beta_M(x) - \gamma_M(x) C_{M_u}^2)\dot{C}_{M_u} - w_S^2 C_{M_u}(1 - \eta_M(x) C_{M_u}^2 \\ & & -a_{2,M}(x) C_{M_u}) - E_M(x) w_S \dot{\alpha}\,(t)\,, \\ \ddot{C}_{L_u} + D_L(x) w_S \ddot{\alpha}\,(t) & = & w_S(\beta_L(x) - \gamma_L(x) C_{L_u}^2)\dot{C}_{L_u} - w_S^2 C_{L_u}(1 - \eta_L(x) C_{L_u}^2 \\ & & -a_{2,L}(x) C_{L_u}) - E_L(x) w_S \dot{\alpha}\,(t)\,. \end{cases} \tag{1.24}$$

$$\begin{cases} L_\beta & = & \frac{1}{2}\rho U^2 S C_{L,\beta}\beta, \\ \mathcal{M}_\beta & = & \frac{1}{2}\rho U^2 S c C_{M,\beta}\beta. \end{cases} \tag{1.25}$$

The resulting set of equations is consequently strongly nonlinear due to coupling between the pitch and plunge, the switching parameters, the bilinear states and the shift in the separation point location dynamic.

These equations will be used for the simulation model to test the theorem and practical control techniques developed later on. To provide more visibility to the different signals and provide more flexibility for potential augmentations, especially with the introduction of different types of saturation, a MATLAB Simulink model has been implemented.

1.3 Experimental Results and Aerodynamic Model Validation

In this section, the parameters of the previous model will be identified for a NACA 0018 wing undergoing forced pitching oscillations. Experiments have been performed for static and dynamic pitch variations for various reduced frequencies and amplitudes or mean angles of attacks. Moments and moment coefficients about the mid chord collected from [71] are used. In particular, parameters are identified using these experimental results. Once the model trained using an identification algorithm, simulations will be computed and compared to experimental data to validate the *GKO* model.

1.3.1 Set up and Facility

The experiments were conducted in the Subsonic wind tunnel in the Aeronautics Laboratory at the United States Air Force Academy. The wind tunnel is a recirculating tunnel, designed and built by FluiDyne Engineering. It has a 0.91 m by 0.91 m by

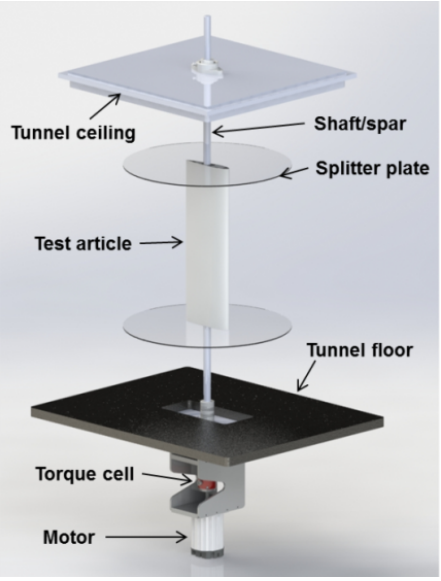

FIGURE 1.9: Illustration of the experimental model for dynamic pitching.

1.83 m test section and a maximum achievable velocity of M = 0.6. The wind tunnel velocity is based on total temperature and pressure and the dynamic pressure measured between a static ring at the entrance of the test section and the total pressure in the stilling chamber.

1.3.1.1 NACA 0018 Wing Description

As previously mentioned, the test article is a rectangular, finite span wing with a chord of $c = 0.15$ m and a span of $l = 0.45$ m. The airfoil profile selected is a NACA 0018 which provides a smooth transition into flutter [72]. The wing is fabricated by a stereolithography process, and is designed to minimize the amount of mass internally to the wing to reduce the inertial loads. As shown in Fig. 1.9, the wing section oscillates about the mid chord by a circular spar. The spar is attached to a Teknic NEMA 3441 DC brushless motor which dynamically pitches the wing section. The motor can be operated in position mode by the use of a Copley motor controller. The axis of rotation of the wing is located at $0.5c$. The torque on the wing spar is measured using a Futek FSH02818 transducer. The aerodynamic loads are dissociated from the structural loads by a rigorous analysis of the structural inertia and friction in the system.

1.3.1.2 Experimental Approach

The experiments were conducted at the United States Air Force Academy (USAFA) with an elevation of $7,000\ ft$. The freestream velocity was chosen at $U_\infty = 22.5\ m/s$. This relatively low value allows us to be slow enough to visualize the different aeroelastic

phenomena remaining in a low frequency range of oscillations relatively to the flow. This resulted in a Mach number of $M = 0.068$ and a low chord-based Reynolds number $Re_c = 190,000$. The convective time is defined by $t_{conv} = \frac{c}{U_\infty}$. We further normalize time with the convective time, $t^+ = \frac{t}{t_{conv}}$. For the simulations with pitch oscillations,

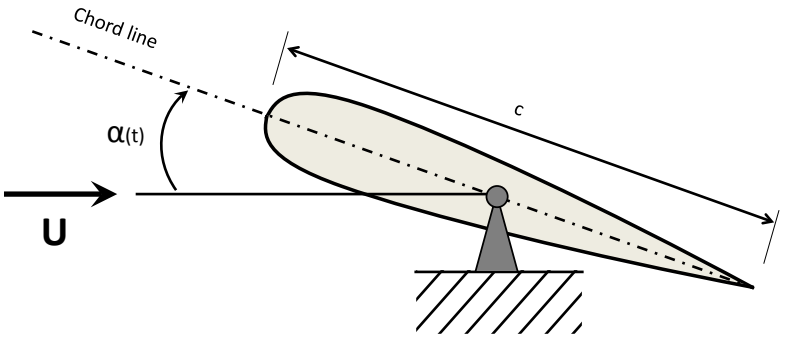

FIGURE 1.10: Model of the pitching airfoil

we define the reduced frequency as $k = \frac{2\pi f c}{U_\infty} = \frac{\omega c}{U_\infty}$ where $\omega = 2\pi f$ is the angular frequency. The resulting pitch oscillation is described as $\alpha = \alpha_0 + \alpha_1 sin(kt^+)$, following Fig. 1.10. To capture the phenomena of hysteresis and vortex shedding under various conditions, the experiments have been carried out at various reduced frequencies ($k = [0.01,\ 0.1,\ 0.15,\ 0.2]$), as well as various mean angles of attack ($\alpha_0 = [0°,\ 5°,\ 10°,\ 15°]$), and amplitudes ($\alpha_1 = [5°,\ 10°,\ 15°,\ 35°]$).

1.3.2 Static Experiments

As discussed above, the static case proves to be particularly interesting. Fig. 1.11 shows the static coefficient of moment curve $C_M(\alpha)$. Classical parameter identification such as the maximum coefficient of lift $C_{M_{max}}$, stall angle of attack α_{stall} or angle of attack for zero lift $\alpha_{M=0}$ can be easily performed.

The static curve has been scrutinized to identify the parameters A_M, B_M and x_0. First, the parameter A, corresponding to the slope of the moment coefficient for a fully detached flow has been calculated. The value $B_M = 0.2417$ is deduced from $A_M = 0.0303$ considering the slope of the attached flow. The separation point location curve $x_0(\alpha)$ is then calculated using Eq. (1.9) and the previous parameters. $x_0(\alpha)$ is represented in Fig. 1.12 by the dots. As predicted [69], as static hysteresis can clearly be identified between the downstroke and the upstroke of the quasi-static motion.

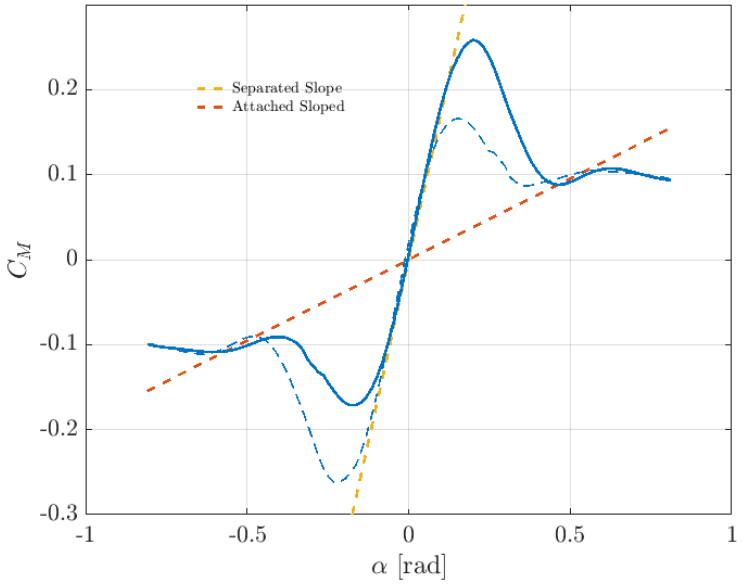

FIGURE 1.11: Static moment coefficient from experiments and slopes for attached and separated flow

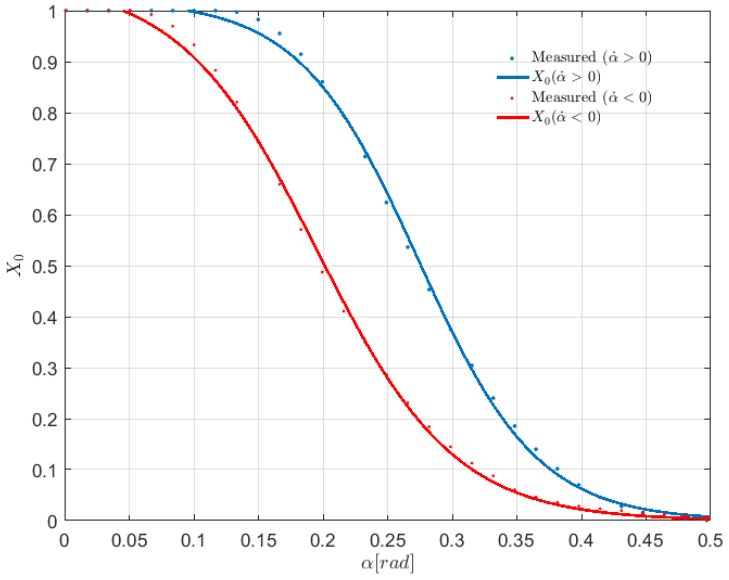

FIGURE 1.12: Static separation point location relative to the chord

The following set of equations using sigmoid-like functions is used to describe the static bifurcation of the separation point:

$$x_0(\alpha) = \begin{cases} \dfrac{1}{1+10^{-9.8260(0.2766-\alpha)}} & \text{for } \dot{\alpha} > 0 \\ \dfrac{1}{1+10^{-9.0781(0.2035-\alpha)}} & \text{for } \dot{\alpha} < 0 \end{cases} . \tag{1.26}$$

The results of this model are compared to the previous identification in Fig. 1.12 (plain lines).

1.3.3 Dynamic Experiments

Varying the amplitude, the average point or the reduced frequencies, several pitching oscillations have been performed on the NACA 0018 airfoil. Examples of the results are provided in Fig. 1.13. The static evolution (black plain line) is used as a reference line where we can clearly see the linear evolution for small angles of attack and the static hysteresis. The colored lines correspond to the dynamic experiments. The increase of moment coefficient can clearly be observed during the upstroke for each dynamic cases as well as a large hysteresis loop. For the large amplitude and fast motion, oscillations during the downstroke corresponding to the leading edge vortex shedding can easily be observed.

Some of the results are then used to train the model and identify the parameters. For this purpose, the *System identification toolbox* of MATLAB is used through the function `idnlgrey`[73]. However, the algorithm used required some initial values of the parameters.

Concerning the model developed by Williams, A_M, B_M have already been identified. However, these values will be adjusted by the identification process as well to obtain a better accuracy of the prediction. The time constants τ_1 and τ_2 from Eq. (1.8), can be identified by visually approximating data obtained from dynamic experimentation. The parameters for the ONERA BH model have been extracted from the literature [48]. However, the values of the parameters correspond to a NACA 0012 airfoil and have also been visually adjusted.

These values, as well as dynamical results, have then been used to train the proposed *GKO* model. The resulting parameters from the identification are provided in Table 1.1.

1.3.4 Validation of the GKO Model

Resulting parameters are then introduced to perform and compute various simulations using MATLAB. Fig. 1.14 shows the results from the experimentation (blue line), the prediction using Williams' GK model (yellow line) and the prediction of the *GKO* model (red line) for 6 different cases including 3 different reduced frequencies and different amplitudes and mean angles of attack. The values of the parameters used for each case are provided in Table 1.2.

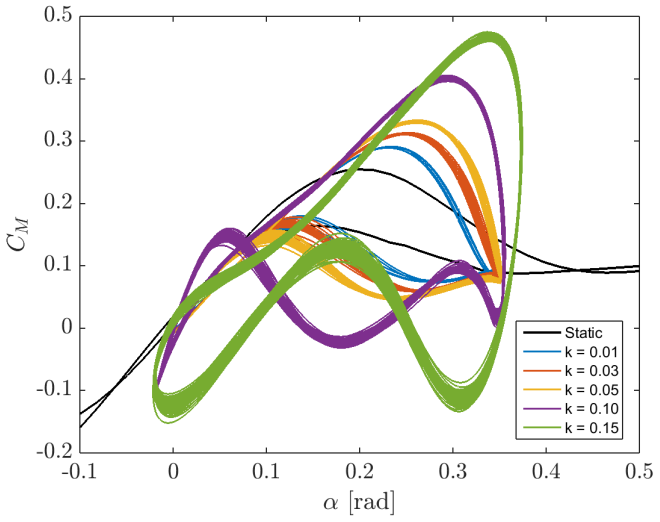

(a)

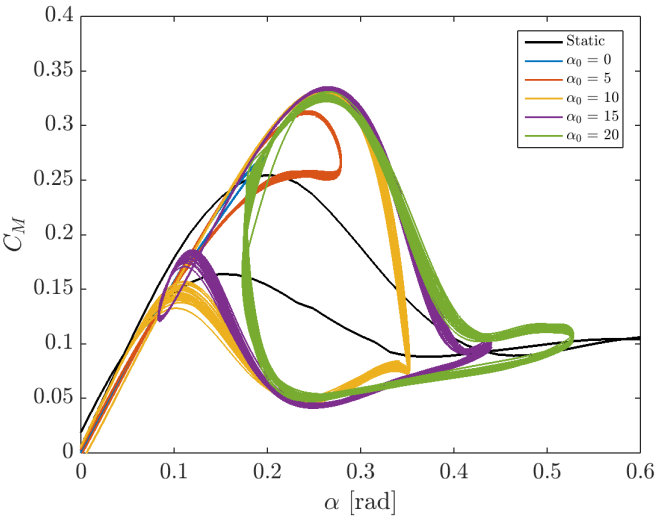

(b)

FIGURE 1.13: Dynamic pitch moment curves for variation of reduced frequency (a) and variation of base angle of attack (b).

In each case, both models permit us to capture the dynamic hysteresis for the simulated range of reduced frequencies and amplitudes. However, the *GKO* model, in red, successfully predicts the oscillatory behavior which is not present in the GK model's predictions. Especially, in case 1, 3, 4 and 5, it can be seen that the model captures the deep stall phenomenon produced by the leading edge vortex shedding. The frequency of the oscillation is also particularly well predicted for the various set of simulation parameters. In case 6, it is interesting to observe that the unsteady behavior due to the vortex shedding influences consequently the moment coefficient. The *GKO* model captures the main trend even remaining slightly inaccurate. Particularly the change of sign in the moment coefficient is not predicted at all for the *GK* model while the *GKO* model tends

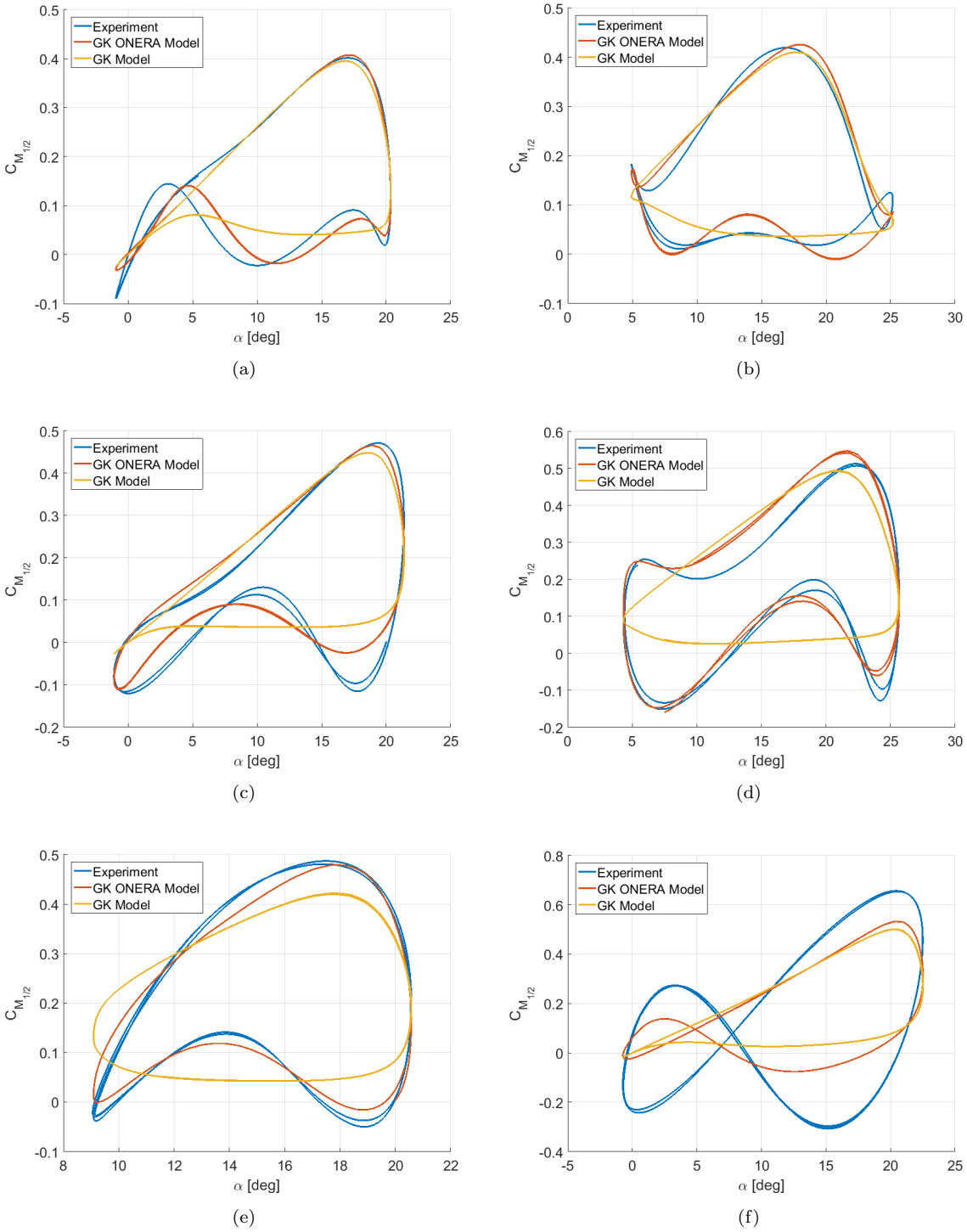

FIGURE 1.14: Moment coefficient predictions and measures for different sets of reduced frequencies, amplitudes and bias: **a** Case 1, **b** Case 2, **c** Case 3 , **d** Case 4, **e** Case 5 and **f** Case 6.

Parameter	Value
τ_1	0.0115
τ_2	0.0322
A_M	0.0159
B_M	0.2235
β_M^+	0.19
a_{2,M^+}	-0.3428
η_{M^+}	-0.246
γ_{M^+}	0.717
D_M^+	-0.3367
E_M^+	-0.2674
β_M^-	-0.8423

TABLE 1.1: Identified parameters for the *GKO* model.

Case	α_0	α_1	k
1	10°	11°	0.1
2	15°	10°	0.1
3	10°	11°	0.15
4	15°	12°	0.15
5	15°	6°	0.2
6	10°	12°	0.2

TABLE 1.2: Parameters of the dynamic cases.

to reproduce it. Thus, in the range of the studied reduced frequencies and amplitude, the *GKO* model and the identified parameters give some successful results.

Based on these results and analysis, we can validate the structure of the *GKO* model.

However, as experimental data are used, the parameter identification remains sensitive to the set of data selected to train the models. It is assumed that using a larger set of data, the model would be capable of extending the range of the studied reduced frequencies and amplitude.

1.4 Chapter Summary

This chapter has permitted us to establish the equations of the pitch and plunge motion of a wing. A new model for lift and moment prediction for pitch oscillation has been derived from the Goman and Khrabrov model on the one hand, and ONERA BH model on the other hand.

Experimental data has been collected on a dynamically pitching NACA 0018 airfoil in a subsonic wind tunnel. The static data has permitted us to identify the corresponding

parameters of the model and to estimate the coefficient of moment for the dynamic situations of the GK model. Coefficients values for the ONERA BH have been extracted from literature [48] and visually adapted. These initial values as well as dynamic experiments results have then been used to identify more accurately the values of the parameters using an identification algorithm.

Once the model was trained, the predictions are successfully compared to the experimental data. Especially, these results permit us to highlight the ability of the *GKO* model to capture the hysteresis as well as the oscillations of the moment coefficient due to the vortex shedding, which can thus be interestingly used to enhance the prediction especially during pitching oscillation. This prediction could be interestingly used especially in the case of AFC, where a control of the boundary and vorticity is sought.

The set of equations remains extremely nonlinear. However, this set of equations can be expressed under the following nonlinear form:

$$\begin{cases} \dot{x}(t) = f(t, x(t)) + g(t, x(t), u(t)), \\ y(t) = j(t, x(t)) + k(t, x(t), u(t)), \\ z(t) = [h(t) \quad \alpha(t)]^T, \end{cases} \tag{1.27}$$

where x is the state vector, y is the measured output signals, z is the desired controlled output, f, h, j and k are nonlinear functions. This formulation, which corresponds to a control theory approach, will allow us to apply the different tools developed in this field.

This model, including a small numbers of states, will be conveniently used in closed-loop control. Especially, the developed model will be manipulated and derived in a more convenient formulation allowing stability and control analysis including the use of flaps as well as blowing actuator.

Chapter 2

Robust Input Saturation Control using a Polytopic Approach

2.1 Introduction

Closed-loop system performances can be affected by the actuator limitations. Saturation typically refers to the fact that some static or dynamic nonlinearity limiting the amplitude or the rate of change of the input affects the requested control input and causes a mismatch between the controller output (controlled plant input) and the actual plant input.

If the control theory has developed many effective control solutions, many of them have trouble being transferred to industry exactly because of these limitations making the typical linearity assumptions hard to satisfy from a practical viewpoint.

Techniques like anti-windup have emerged to provide an interesting answer to the above problems. Handling saturation in a direct way may allow us to guarantee some performances to the closed-loop system also in a practical industrially relevant case. The drawback of such powerful methods can remain their relative complexity regarding the order of the open-loop system and the accuracy of the model developed.

In this chapter, Linear quadratic control is considered for Linear time invariant systems where stability is sought while optimizing a cost function. The results are extended to uncertain systems represented as multi-affine systems. The uncertain parameters are varying and bounded and allowed us to consider their variation inside a polytope. Magnitude saturations are then considered. Local and global stability are studied. In the case of local stability, a region of attraction is defined and is sought to be maximized while guaranteeing a minimum cost. The case of rate saturation is studied using an

augmented formulation of the initial system. Each theorem will be applied to a mass-spring system academic example.

2.2 Linear Quadratic Regulator

2.2.1 Linear Quadratic Regulator (LQR) Synthesis for LTI system

Consider the following LTI system:

$$\dot{x}(t) = Ax(t) + Bu(t) \tag{2.1}$$

where $x \in \mathbb{R}^n$ and $u \in \mathbb{R}^m$ represent the state and the input of the system, respectively, where n and m are positive integers. Matrices $A \in \mathbb{R}^{n\times n}$ and $B \in \mathbb{R}^{n\times m}$ are constant and known. The optimal control problem aims at finding a controller that stabilizes the plant while optimizing a cost function. The cost function results from the desire of maintaining a certain level of performances, on the regulated output for instance, and the limitation of the command input. Thus, let us define the following quadratic cost function:

$$J = \int_0^\infty \left(x(t)'Qx(t) + u(t)'Ru(t)\right) dt, \tag{2.2}$$

where $R \in \mathbb{R}^{m\times m}$ is a positive definite matrix and $Q \in \mathbb{R}^{n\times n}$ is a symmetric positive definite matrix that may be freely selected. Following the parallel approaches to those adopted in [74] and used in [49], the following theorem is proposed. Its proof is postponed because it will be shown to follow from a more general statement provided in Theorem 2.3. In particular, the proof of the following theorem is reported at the end of Section 2.3.2.

Theorem 2.1. *Given $Q = Q' > 0$ and $R > 0$, assume that there exists $W = W' > 0 \in \mathbb{R}^{n\times n}$, Y in $\mathbb{R}^{m\times n}$ and positive scalar ν satisfying the following inequalities:*

$$\begin{bmatrix} He(AW + BY) & W & Y' \\ * & -\nu Q^{-1} & 0 \\ * & * & -\nu R^{-1} \end{bmatrix} < 0. \tag{2.3}$$

Then, selecting $K = YW^{-1}$ ensures:

1. *global exponential stability of the origin of system (2.1) with $u = Kx$;*
2. *for any initial condition $x(0) \in \mathbb{R}^n$, the cost function J in (2.2) evaluated along the corresponding (unique) solution to (2.1), K satisfies $J \leq \mu x_0^T W^{-1} x_0$.*

2.2.2 LQR Synthesis for Polytopic System

The objective of this section is to extend the results of Theorem 2.1 to the case of polytopic system. This class of systems has been widely used in the literature to represent uncertain systems and will be useful to the overall objectives of manuscript to model in an appropriate manner the aerodynamic equations of the flutter. To proceed, let us first introduce the generic model of polytopic systems as follows

$$\dot{x} = \sum_{i=1}^{N} \mu_i(t) \left(A_i x + B_i u\right), \tag{2.4}$$

where matrices $A_i \in \mathbb{R}^{n\times n}$ and $B_i \in \mathbb{R}^{n\times m}$ are constant and known, for all $i = 1, .., N$, where N is a positive integer. The coefficients $\mu_i \in [0, 1]$ are such that their sum is equal to 1. The objective is now to find an optimal control input $u = Kx$ that addresses (suboptimally) the minimization of the cost function (2.2). The following Theorem is provided without proof because its proof follows from the results given later in Section 2.3.3

Theorem 2.2. *Given $Q = Q' > 0$ and $R > 0$, assume that there exists $W = W' > 0 \in \mathbb{R}^{n\times n}$, Y, X in $\mathbb{R}^{m\times n}$, a diagonal positive matrix $S > 0 \in \mathbb{R}^{m\times m}$ and positive scalar ν satisfying the following inequalities:*

$$\begin{bmatrix} He(A_i W + B_i Y) & W & Y' \\ * & -\nu Q^{-1} & 0 \\ * & * & -\nu R^{-1} \end{bmatrix} < 0, \quad \forall i = 1, \ldots, n \tag{2.5}$$

Then, selecting $K = YW^{-1}$ ensures:

1. *global exponential stability of the origin of system (2.4) with $u = Kx$;*
2. *for any initial condition $x(0) \in \mathbb{R}^n$, the cost function J in (2.2) evaluated along the corresponding (unique) solution to (2.4), K satisfies $J \leq \nu x_0^T W^{-1} x_0$.*

Remark 1. It is worth noting that the previous conditions include an inherent conservatism. While it is true that imposing the negative definiteness of the matrix in (2.5) for all $i = 1, \ldots, N$, solves the problem, the reverse is not true. Indeed, it suffices to consider the case where for one i the inequality does not hold and the associated weight satisfies $\mu_i = 0$ at all times.

2.2.3 Numerical Example

To illustrate this method, let us introduce the classical example of the mass spring system studied in [75, Example 7.2.6]. We consider the plant:

$$A = \begin{bmatrix} 0 & 1 \\ -k/m & -f/m \end{bmatrix}, \; B = \begin{bmatrix} 0 \\ 1/m \end{bmatrix}, \tag{2.6}$$

where $m = 0.1$ represents the mass of the body, $k = 1$ the spring's elastic constant, $f = -0.01$ the damping coefficient. The eigenvalues of state matrix A are $\lambda_{1,2} = 0.0500 \pm 3.1619i$. As the real part of the eigenvalues is positive, the open-loop system is unstable. We verify that the pair (A, B) is controllable as $rank([B \; A.B]) = 2$ using the Kalman criteria for controllability.

Using $Q = \left[\begin{smallmatrix} 100 & 0 \\ 0 & 1 \end{smallmatrix}\right]$ and $R = 1$, we obtain a stabilizing controller $K_{LQ} = [9.0499 \;,\; 1.6863]$ minimizing the cost J. Note that the MATLAB command `lqr` gives the same value with a negative sign using $u = -Kx$.

The relative weights of Q and R determine the relative importance to the performance of the system (states going to zero) or to the limitation of the control input. Using the same matrix Q but increasing the weight due to the control input to $R = 10$, more importance is given to the minimization of the control input. The resulting stabilizing controller is now given by $K_{LQ} = [2.3166 \;,\; 0.7606]$. This new gain is lightly smaller than previously providing a smaller control input. The price to pay is obviously that the state will converge to zero more slowly.

In order to illustrate the polytopic case, we will consider the same system where coefficients f and k are uncertain or time varying. Although the parameters are unknown, the values are bounded and define a polytope. We consider that the parameters may vary up to 10%, i.e. $f =\in [-0.011, -0.009]$ or $k =\in [0.9, 1.1]$. Using Theorem 2.2 and the same weights $Q = \left[\begin{smallmatrix} 100 & 0 \\ 0 & 1 \end{smallmatrix}\right]$ and $R = 1$, we obtain a stabilizing controller $K_{LQ} = [9.2007 \;,\; 1.6952]$ guaranteeing an optimal cost on the parameter variation range. Note that the previously computed controller may also provide good performances in the same conditions. However, no guarantees are provided outside of the values initially used for the controller synthesis.

2.3 Linear Quadratic Regulator (LQR) in presence of Magnitude Saturation

2.3.1 Problem Formulation

In the previous section, we have considered the problem of LQR optimal control design for linear (time invariant nominal or uncertain) systems. While these classes of systems allow us to represent a wide range of systems already, there exist phenomena that cannot be captured efficiently. Among those phenomena, we would like to point out the relevant problem of saturations, which appears frequently in practical applications. The reader is referred to [75–78] for some selected references on the topic.

Indeed saturations represent a particular class of nonlinearities, which affects many systems in practice. This nonlinearity corresponds to a difference between the control input computed by the controller and the effective command delivered by the actuators. If this issue is not taken into account while synthesizing the controller, it may affect the performance of the system up to the destruction of the system. This common nonlinearity is the origin of many problems in practical engineering. In aeronautics, saturation has been the cause of several plane crashes and is particularly well-known for inducing an instability known as Pilot Induced Oscillation (PIO).

In this section we consider that the actuators have limited magnitudes. This nonlinearity is designated as a magnitude saturation. Considering that all the saturation channels are independent from each other, they are considered as decentralized saturation.

We suppose that the function $s = sat(.)$ is a decentralized magnitude saturation with saturation bounds $u_0 = [u_{01}...u_{0m}]'$, namely $s = sat(u)$ corresponds to enforcing

$$s_i = max(-u_{0i}; min(u_{0i}; u_i)),$$

where s_i and u_i denote the i^{th} components of s and u, respectively, for all $i = 1, .., m$. Such a system is presented in Fig. 2.1 where $\mathcal{H}$ is the state-space representation.

Complementarily, one defines the deadzone nonlinearity. Let us define the deadzone function $\phi(u) \in \mathbb{R}^m$, as follows

$$\phi(u) = u - sat(u) \tag{2.7}$$

A typical way to represent saturation nonlinearities in otherwise linear closed-loops is the use of the global sector represented in Fig. 2.2. However, it has been long known that the stability conditions are conservative with this sector approach (dating back

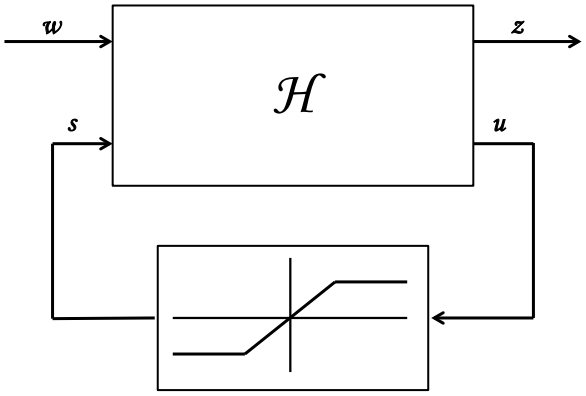

FIGURE 2.1: Closed-loop system with magnitude saturation.

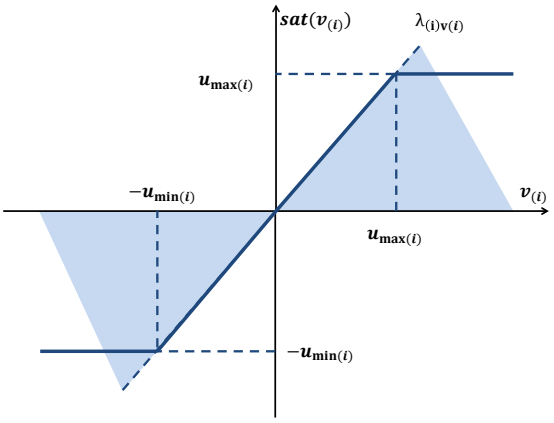

FIGURE 2.2: Saturation included in a global Sector.

to the absolute stability literature). The intuitive alternative is to simply narrow the sector hoping to be able to provide a bound on the magnitude of the saturation input (See Fig. 2.3). Unfortunately, this approach is not really effective because providing and guaranteeing the input bounds is challenging. More recently researchers have proposed the so-called generalized sector conditions that follow a more sophisticated approach summarized below. Let us define some generalized sector conditions relative to the deadzone functions. To this end, let us first define the following set:

$$S(v-w,u_{min},u_{max})=\{v\in\mathbb{R}^m;w\in\mathbb{R}^m;-u_{min}\leq v-w\leq u_{max}\} \tag{2.8}$$

Lemma 1. [79] If v and w are elements of $S(v-w,u_{min},u_{max})$, then the nonlinearity $\phi(v)$ satisfies the following inequality:

$$\phi(v)'T(\phi(v)+w)\geq 0 \tag{2.9}$$

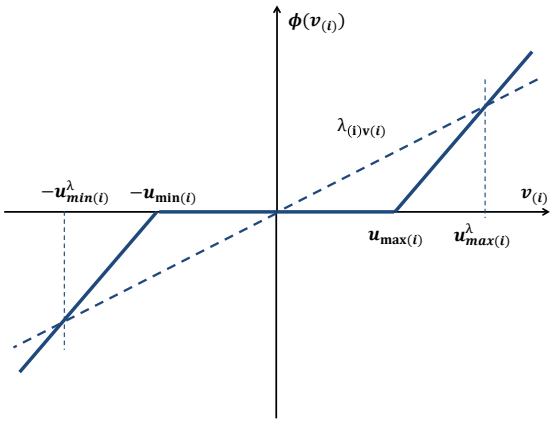

FIGURE 2.3: Deadzone treated with sector narrowing.

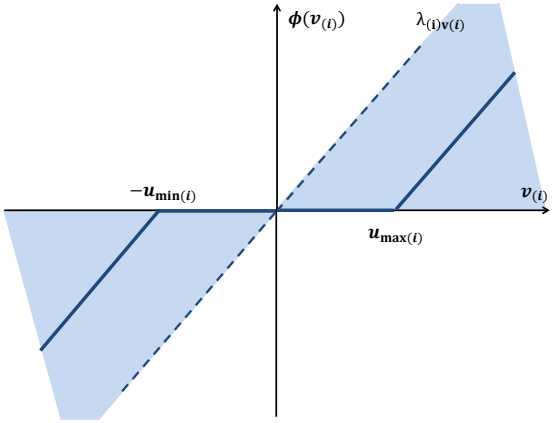

FIGURE 2.4: Deadzone in a global sector.

for any diagonal positive definite matrix $T \in \mathbb{R}^{m\times m}$.

Proof. The proof is taken from [79] but is recalled for consistency matters. Assume that v and w are elements of $S(v-w, u_{min}, u_{max})$, thus, $-u_{i,min} - v_i + w_i \leq 0$ and $u_{i,max} - v_i + w_i \geq 0$, $i = 1, .., m$. Three situations may then occur:

Case 1: Assume that $v_i > u_{i,max}$. Then $\phi(v_i) = v_i - sat(v_i) = v_i - u_{i,max} > 0$ and $\phi(v_i) + w = u_{i,max} - v_i + w_i \geq 0$ which gives $\phi(v_i)' T_{i,i}(\phi(v_i) + w) \geq 0$ since $T_{i,i} > 0$.

Case 2: Assume that $u_{i,min} \leq v_i \leq u_{i,max}$. Then $\phi(v_i) = v_i - sat(v_i) = 0$ which gives $\phi(v_i)' T_{i,i}(\phi(v_i) + w) = 0$, $\forall T_{i,i}$.

Case 3: Assume that $v_i < u_{i,min}$. Then $\phi(v_i) = v_i - sat(v_i) = v_i - u_{i,min} < 0$ and $\phi(v_i) + w = u_{i,in} - v_i + w_i \leq 0$ which gives $\phi(v_i)' T_{i,i}(\phi(v_i) + w) \geq 0$ since $T_{i,i} > 0$.

which concludes the proof. □

Lemma 2. [80] Consider a scalar saturation function. Then, for any row vector H it holds:

$$(sat(u) + Hx)(u - sat(u)) \geq 0, \quad \forall x \text{ s.t. } sat(Hx) = Hx \tag{2.10}$$

Proof. First, note that $\forall\ sat(Hx) = Hx \ \Rightarrow\ \|Hx\| \leq u_0$.

Consider two cases:

- $u = sat(u)$ then $(u - sat(u)) = 0$
- If $u \neq sat(u)$, then $sign(u - sat(u)) = sign(u)$. Then, two cases may occur:
  - If $u > 0$, then $sat(u) = u_0$.

$$-u_0 \leq Hx \leq u_0$$
$$0 \leq Hx + sat(u) \leq 2u_0$$

    Then, $sign(sat(u) + Hx) = sign(u)$ and $(sat(u) + Hx)(u - sat(u)) \geq 0$.
  - $u < 0$ then $sat(u) = -u_0$.

$$-u_0 \leq Hx \leq u_0$$
$$-2u_0 \leq Hx + sat(u) \leq 0$$

    Then $sign(sat(u) + Hx) = sign(u)$ and $(sat(u) + Hx)(u - sat(u)) \geq 0$.

□

Lemma 3. [80] Considering a decentralized saturation function as described in (2.7). Then, for all $u \in \mathbb{R}^m$ and any diagonal positive definite matrix $T \in \mathbb{R}^{m \times m}$ it holds:

$$\phi(w) = 0 \Rightarrow \phi(u)'T(u - \phi(u) + w) \geq 0. \tag{2.11}$$

Proof. The proof is straightforward considering Lemma 2, with $w = Hx$, $\phi(u) = u - sat(u)$ and noticing that $\phi(w) = 0 \Leftrightarrow sat(w) = w$. □

2.3.2 LQR Synthesis for LTI System with Magnitude Saturation

The objective of this section is the use of the previous lemmas in order to develop a constructive stabilization theorem for linear systems subject to magnitude input saturations. Let us first recall the definition of the control problem. Consider linear system given by:

$$\dot{x}(t) = Ax(t) + Bsat(u(t)) \tag{2.12}$$

where $x \in \mathbb{R}^n$ and $u \in \mathbb{R}^m$ represent the state and the input of the system, respectively, where n and m are positive integers. Matrices $A \in \mathbb{R}^{n\times n}$ and $B \in \mathbb{R}^{n\times m}$ are constant and known. The saturation function has been defined in the previous paragraph. The control input u results from a static state feedback control law given by:

$$u = Kx \tag{2.13}$$

Again, let us define the following quadratic cost function:

$$J = \int_0^\infty \left(x(t)'Qx(t) + u(t)'Ru(t)\right) dt, \tag{2.14}$$

where $R \in \mathbb{R}^{m\times m}$ is a positive definite matrix and $Q \in \mathbb{R}^{n\times n}$ is a symmetric positive definite matrix, which may be freely selected as long as (A, B) is stabilizable. The following theorem holds.

Theorem 2.3. *[81] Given $Q = Q' > 0$ and $R > 0$, assume that there exists $W = W' > 0 \in \mathbb{R}^{n\times n}$, Y, X in $\mathbb{R}^{m\times n}$, a diagonal positive matrix $S > 0 \in \mathbb{R}^{m\times m}$ and positive scalars α, ν satisfying the following inequalities:*

$$\begin{bmatrix} W & X_j' \\ X_j & u_{0,j}^2 \end{bmatrix} \geq 0, \ \forall j = 1, .., m, \tag{2.15}$$

$$\begin{bmatrix} I & \alpha I \\ \alpha I & W \end{bmatrix} \geq 0 \tag{2.16}$$

$$\begin{bmatrix} He(AW + BY) & (Y + X)' - BS & W & Y' \\ * & -2S & 0 & -S \\ * & * & -\nu Q^{-1} & 0 \\ * & * & * & -\nu R^{-1} \end{bmatrix} < 0, \tag{2.17}$$

where X_j denotes the j^{th} row of matrix X. Then, selecting:

$$K = YW^{-1} \tag{2.18}$$

ensures:

1. *local exponential stability of the origin of system (2.12), (2.13) with region of attraction* $\varepsilon(W^{-1}) = \{x \in \mathbb{R}^n : x'W^{-1}x \leq 1\}$ *which contains the* α*-ball* $\mathcal{B}(\alpha) := \{x \in \mathbb{R}^n \ : \ |x| \leq \alpha\}$*;*

2. *for any initial condition* $x(0) \in \varepsilon(W^{-1})$*, the cost function* J *in (2.14) evaluated along the corresponding (unique) solution to (2.12), (2.13) satisfies* $J \leq \nu x_0^T W^{-1} x_0$*;*

3. *global exponential stability of the origin of system (2.12), (2.13), if the solution to (2.15-2.17) is such that* $X = 0$*.*

Proof. Let us first rewrite the dynamics of system (2.12) using the deadzone formulation (2.7) and the state feedback control law (2.13). Indeed, we write

$$sat(u) = sat(Kx) = Kx - \phi(Kx).$$

Hence, system (2.12) becomes

$$\dot{x} = (Ax + BK)x - B\phi(Kx). \tag{2.19}$$

Consider now a quadratic Lyapunov function $V(x) = x'Px$ where P is a symmetric positive definite matrix. Differentiating it along the trajectories of (2.19), leads to

$$\begin{aligned} \dot{V}(x) &= \dot{x}'Px + x'P\dot{x} \\ &= (Ax + BKx - B\phi(Kx))'Px + x'P(Ax + BKx - B\phi(Kx)) \\ &= x'He(PA + PBK)x - 2\phi(Kx)'B'Px, \end{aligned}$$

where $\phi(Kx)$ is the deadzone nonlinearity verifying the conservative sector condition, for w such as:

$$\phi(w) = 0 \Rightarrow \phi(u)'T(u - \phi(u) + w) \geq 0. \tag{2.20}$$

where T is a diagonal positive matrix. To ensure the internal stability, it is sufficient to have the time derivative $\dot{V}$ negative except at the origin. However, including the sector condition due to the nonlinearity, the problem can be formulated such as if the sector condition holds, then the time derivative $\dot{V}$ is negative or

$$\begin{aligned} &\phi(Kx)'T(Kx - \phi(Kx) + w) \geq 0 \ (u, w) \neq 0 \Rightarrow \\ &\qquad \dot{V}(x) = x'(He(PA + PBK)x - \phi(Kx)'B'Px - x'PB\phi(Kx) \leq 0. \end{aligned} \tag{2.21}$$

In order to guarantee that the previous implication holds, we perform the selection $w = Hx$, and using the S-procedure, it is sufficient to check the following inequality:

$$\dot{V}(x) \leq \dot{V}(x) + 2\phi(Kx)'T(\phi(Kx) + Hx) \leq 0,\ \forall x \in \varepsilon(P) \tag{2.22}$$

Developing the right side of the previous equation, we obtain:

$$\dot{V}(x) \leq x'(He(PA+PBK))x - 2\phi(Kx)'B'Px + 2\phi(Kx)'T(Kx - \phi(Kx) + Hx),\ \forall x \in \varepsilon(P), \tag{2.23}$$

which can be rewritten in a quadratic form as follows

$$\dot{V}(x) \leq \begin{bmatrix} x \\ \phi(Kx) \end{bmatrix}' \begin{bmatrix} He(P(A+BK)) & -PB + (K+H)'T \\ * & -2T \end{bmatrix} \begin{bmatrix} x \\ \phi(Kx) \end{bmatrix},\ \forall x \in \varepsilon(P) \tag{2.24}$$

where the notation '$*$' refers to the symmetric entry of a symmetric matrix. In order to include the cost function (2.14) in this analysis, let us introduce the quadratic function $\psi(x)$ given by

$$\begin{aligned} \psi(x) &= \begin{bmatrix} x \\ sat(Kx) \end{bmatrix}' \begin{bmatrix} Q & 0 \\ 0 & R \end{bmatrix} \begin{bmatrix} x \\ sat(Kx) \end{bmatrix} \\ &= \begin{bmatrix} x \\ \phi(Kx) \end{bmatrix}' \begin{bmatrix} I & 0 \\ K & -I \end{bmatrix}' \begin{bmatrix} Q & 0 \\ 0 & R \end{bmatrix} \begin{bmatrix} I & 0 \\ K & -I \end{bmatrix} \begin{bmatrix} x \\ \phi(Kx) \end{bmatrix} \end{aligned} \tag{2.25}$$

where we recall that $Q = Q' > 0$ and $R > 0$. Therefore, this quadratic term is positive definite and, for any $\nu \geq 0$, we have

$$\begin{aligned} \dot{V}(x) &\leq \dot{V}(x) + 2\phi(Kx)'T(Kx - \phi(Kx) + Hx) + \tfrac{1}{\nu}\psi(x,s) \\ &= \begin{bmatrix} x \\ \phi(Kx) \end{bmatrix}' \Pi_0 \begin{bmatrix} x \\ \phi(Kx) \end{bmatrix},\ \forall x \in \varepsilon(P,1) \end{aligned} \tag{2.26}$$

where

$$\Pi_0 = \begin{bmatrix} He(P(A+PBK)) & -PB + (K+H)'T \\ * & -2T \end{bmatrix} + \begin{bmatrix} I & 0 \\ K & -I \end{bmatrix}' \begin{bmatrix} \frac{Q}{\nu} & 0 \\ 0 & \frac{R}{\nu} \end{bmatrix} \begin{bmatrix} I & 0 \\ K & -I \end{bmatrix}. \tag{2.27}$$

By pre and post multiplying matrix Π_0 by $\mathcal{T} = Diag(W, S)$, where $W = P^{-1}$ and $S = T^{-1}$, we get

$$\begin{aligned} \mathcal{T}'\Pi_0\mathcal{T} &= \begin{bmatrix} He(AW + BKW) & -BS + W(K + H)' \\ * & -2S \end{bmatrix} \\ &+ \begin{bmatrix} W & 0 \\ KW & -S \end{bmatrix}' \begin{bmatrix} \frac{Q}{\nu} & 0 \\ 0 & \frac{R}{\nu} \end{bmatrix} \begin{bmatrix} W & 0 \\ KW & -S \end{bmatrix} \end{aligned} \tag{2.28}$$

We note that the previous expression is nonlinear in the decision variables W, S and K. In order to obtain a linear formulation, let us introduce the new variable $Y = KP^{-1} = KW$ and $X = HP^{-1} = HW$. Then, the application of the Schur complement allows us to derive the following linear problem

$$\Pi_0 < 0 \quad \Leftrightarrow \quad \begin{bmatrix} He(AW + BY) & (Y + X)' - BS & W & Y' \\ * & -2S & 0 & -S \\ * & * & -\nu Q^{-1} & 0 \\ * & * & * & -\nu R^{-1} \end{bmatrix} < 0 \tag{2.29}$$

which corresponds exactly to the LMI given in (2.17). Therefore, if the LMI (2.17) is verified, matrix Π_0 is negative definite and equation (2.26) allows us to ensure that $\dot{V}(x)$ is negative definite for any x such that $\phi(Kx)'T(Kx - \phi(Kx) + Hx) > 0$.

Consider now LMI (2.15) and apply Schur complement to obtain $W - X_i' u_{0,i}^{-2} X_i \geq 0$. Then, Pre and post multiplying this equation by P yields $P \geq P X_i' u_{0,i}^{-2} X_i P$. Following the definition $X = HP^{-1}$, we straightforwardly have $X_i = H_i P^{-1}$ and $P \geq H_i' u_{0,i}^{-2} H_i$. Now Pre and post-multiplying respectively by x' and x, we obtain

$$x'Px \geq \left(\frac{\mid H_i x \mid}{u_{0,i}} \right)^2, \quad \forall i = 1...n, \tag{2.30}$$

Consider now any $x \in \varepsilon(P) = \{x \in \mathcal{R}^n, x'Px \leq 1\}$, then we have from (2.30) that $\mid H_i x \mid \leq u_{0,i}$, for all $i = 1, ..., n$ and $\phi(Hx) = 0$. Using Lemma 3 with $w = Hx$, we verify that $2\phi(Kx)'T(Kx - \phi(Kx) + Hx) \geq 0$ holds. Consequently, since $\psi(x, s) \geq 0$, inequality (2.26) implies that $\dot{V} \leq -\epsilon \|x\|^2$ for a small enough $\epsilon > 0$, i.e. that we proved local exponential stability with domain of attraction including $\varepsilon(P)$.

Consider now the LMI in (2.16). A Schur complement ensures that $\alpha^2 P \leq I$. Hence, for $x \in \mathcal{B}_\alpha$, we have

$$1 \geq \frac{x'x}{\alpha^2} \geq x'Px,$$

which means that $\mathcal{B}_\alpha \subset \varepsilon(P)$ and completes the proof for item 1.

Concerning item 3, if $X = 0$, then $H = XP = 0$ and in particular $\phi(Hx) = 0$. Consequently, the sector condition in Lemma 3 holds for all x, which gives global exponential stability.

To conclude the proof, we also note from (2.26) that $\dot{V}(x) + \frac{1}{\nu}\psi(x,s) < 0$. Integrating between 0 and any positive scalar $t > 0$, we have

$$\int_0^t \dot{V}(x)d\tau + \frac{1}{\nu}\int_0^t \psi(x,s)d\tau = V(x(t)) - V(x(0)) + \frac{1}{\nu}\int_0^t \psi(x,s)d\tau < 0 \qquad (2.31)$$

Letting $t \to \infty$, and keeping in mind that $V(x(t))$ tends to zero because of exponential stability, we have

$$J < \nu V(0) = \nu x(0)' P x(0) \leq \nu, \qquad (2.32)$$

which concludes the proof of item 2. □

It is worth noting that Theorem 2.3 has been developed to design stabilizing a state feedback control gain K such that the system (2.12) with input saturation is locally or globally asymptotic stable and such that the cost function (2.14) is minimized. This theorem can also cope with systems without saturations constraints, i.e. when the saturations bounds u_i tends to infinity and leading to the same problem as defined in Section 2.2. The corresponding theorem (Theorem 2.1) has been already introduced in Section 2.2.1 without any proof. The proof is reported below, and follows immediately from the above proof.

Proof. of Theorem 2.1. The proof only consists in noting that when the saturations bounds u_{0i} tend to infinity, LMI (2.15) is always verified and does not need to be considered anymore. To obtain LMI (2.3) for Theorem 2.3, it suffices to select $Y = X$ and $S = 0$ in (2.17). □

2.3.3 LQR Synthesis for Polytopic System with Magnitude Saturation

The objective of this section is to extend the result of Theorem 2.3 to the case of polytopic system.

To do this extension, let us introduce the generic model of polytopic systems with magnitude saturation as follows:

$$\dot{x} \quad = \quad \sum_{i=1}^{N} \mu_i \left(A_i x + B_i sat(u)\right), \qquad (2.33)$$

where matrices $A_i \in \mathbb{R}^{n\times n}$ and $B_i \in \mathbb{R}^{n\times m}$ are constant and known, for all $i = 1, .., N$, where N is a positive integer. The coefficients $\mu_i \in [0, 1]$ are such that their sum is equal

to 1. The control input u results from a static state feedback control law given by:

$$u = Kx. \tag{2.34}$$

Consider the polytopic open-loop system defined in Eq. (2.33) with (A_i, B_i) stabilizable for all i. The following theorem then generalizes the result in Theorem 2.3.

Theorem 2.4. *Given $Q = Q' > 0$ and $R > 0$, assume that there exists $W = W' > 0 \in \mathbb{R}^{n\times n}$, Y, X in $\mathbb{R}^{m\times n}$, a diagonal positive matrix $S > 0 \in \mathbb{R}^{m\times m}$ and positive scalars α, ν satisfying the following inequalities:*

$$\begin{bmatrix} W & X_j' \\ X_j & u_{0,j}^2 \end{bmatrix} \geq 0,\ \forall j = 1, .., m, \quad \begin{bmatrix} I & \alpha I \\ \alpha I & W \end{bmatrix} \geq 0 \tag{2.35}$$

$$\begin{bmatrix} \begin{bmatrix} He(A_iW + B_iY) & (Y + X)' - B_iS \\ * & -2S \end{bmatrix} & \begin{bmatrix} W & Y' \\ 0 & -S \end{bmatrix} \\ * & -\nu \begin{bmatrix} Q^{-1} & 0 \\ 0 & R^{-1} \end{bmatrix} \end{bmatrix} < 0,\ \forall i = 1, ..., N \tag{2.36}$$

where X_j denotes the j^{th} row of matrix X. Then, the selecting:

$$K = YW^{-1} \tag{2.37}$$

ensures:

1. *local exponential stability of the origin of system (2.33), (2.34) with region of attraction $\varepsilon(W^{-1}) = \{x \in \mathbb{R}^n : x'W^{-1}x \leq 1\}$ which contains the α-ball $\mathcal{B}(\alpha) := \{x \in \mathbb{R}^n : |x| \leq \alpha\}$;*
2. *for any initial condition $x(0) \in \varepsilon(W^{-1})$, the cost function J in (2.2) evaluated along the corresponding (unique) solution to (2.33), (2.34) satisfies $J \leq \nu x_0^T W^{-1} x_0$;*
3. *global exponential stability of the origin of system (2.33), (2.34) if the solution to (2.35), (2.36) is such that $X = 0$.*

Proof. The proof of this theorem follows the proof used in Theorem 2.3 using the convexity of the polytopic system as defined in 2.33. We verify that Theorem 2.3 holds for all the pairs (A_i, B_i), $\forall i = 1, .., N$.

In particular, following the steps of the proof of Theorem 2.3 without any change, but with reference to a generic pair (A_i, B_i), $\forall i = 1, .., N$, we get the equivalent equation to (2.28), corresponding to:

$$\begin{aligned} \mathcal{T}'\Pi_{0i}\mathcal{T} &= \begin{bmatrix} He(A_iW + B_iKW) & -B_iS + W(K+H)' \\ * & -2S \end{bmatrix} \\ &+ \begin{bmatrix} W & 0 \\ KW & -S \end{bmatrix}' \begin{bmatrix} \frac{Q}{\nu} & 0 \\ 0 & \frac{R}{\nu} \end{bmatrix} \begin{bmatrix} W & 0 \\ KW & -S \end{bmatrix} \end{aligned} \tag{2.38}$$

Then recalling that the uncertain matrices can be defined as

$$A = \sum_{i=1}^{N} \mu_i A_i x, \qquad B = \sum_{i=1}^{N} \mu_i B_i,$$

we may perform a convex combination of the above inequalities to obtain that $\dot{V}(x) + \frac{1}{\nu}\psi(x,s) < 0$. The rest of the proof follows the same steps as that of Theorem 2.3. □

Also for this specific case, the result of Theorem 2.4 implies the statement for the case without saturation, already introduced in Section 2.2.2.

2.3.4 Numerical Example

Continuing with the previous mass and spring example, we now introduce magnitude input saturation.

The problem can actually be approached in two different ways. Indeed, for a fixed value of ν, we can solve Eq. (2.17) or (2.36) while seeking for the maximum α in $\varepsilon(W^{-1})$. In this case, we are solving the LMI problem for a fixed value of performance while looking for the maximum region of attraction. It is also possible to consider a second formulation where, for a fixed domain of attraction defined by the radius α we optimize the performance of the solution by finding the minimum value of ν.

In the following, we will solve the first formulation for the LTI and the polytopic problem. We still consider that the parameters may vary between $f = \in [-0.011, -0.009]$ or $k = \in [0.9, 1.1]$ for the polytopic problem and $f = -0.01$ and $k = 1$ for the LTI problem. The magnitude saturation is $u_0 = 1$ and ν is varied. Using the same weights, the LTI problem in Theorem 2.3 for $f = -0.01$ and $k = 1$ and the polytopic problem in Theorem 2.4 are solved. The results are provided in Table 2.1.

ν	K	α	$K_{polytopic}$	$\alpha_{polytopic}$
0.1	$[-9.8923\ ,\ -1.9042]$	0.0766	$[-9.8870\ ,\ -1.9047]$	0.0763
1	$[-19.2088\ ,\ -5.0408]$	0.2218	$[-16.2966\ ,\ -4.2743]$	0.2200
2	$[-9.9360\ ,\ -2.8185]$	0.3008	$[-22.4522\ ,\ -6.6460]$	0.2976
5	$[-27.7767\ ,\ -9.5710]$	0.4467	$[-12.5273\ ,\ -4.3260]$	0.4399
10	$[-37.0232\ ,\ -14.6216]$	0.5998	$[-19.6186\ ,\ -7.8853]$	0.5876

TABLE 2.1: Solutions to the LMI problems for a LTI and polytopic system in presence of position saturation.

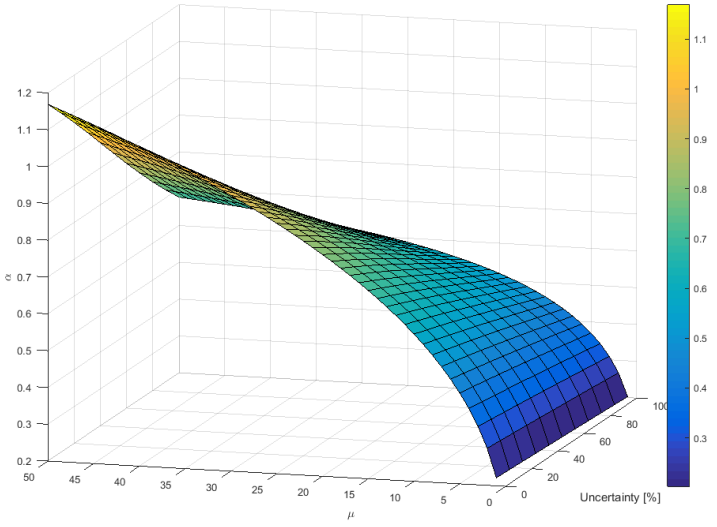

FIGURE 2.5: Evolution of α with variation of the uncertainties and ν

We can observe that in both cases, LTI or polytopic, the size of the attraction region, represented by the radius α of the ball $\mathcal{B}(\alpha)$, increased with ν, the performance index, which meets our expectations.

%	K	α
0	$[-19.2088\ ,\ -5.0408]$	0.2218
10	$[-16.2966\ ,\ -4.2743]$	0.2200
20	$[-11.4814\ ,\ -2.9670]$	0.2182

TABLE 2.2: Solutions to the LMI problems for polytopic system for various percentages of uncertainties in presence of position saturation.

Varying the percentage of uncertainties, we also observe on Table 2.1 or Table 2.2 , but also on Fig. 2.5 that α decreases with the increase of the uncertainties, which was also expected.

2.4 Linear Quadratic Regulator (LQR) in presence of Rate Saturation

2.4.1 Problem Formulation

A rate saturation is a dynamic saturation, where the rate of variation of the state considered is limited. In the sequel, we will study the rate saturation applied to an input command signal.

More specifically, given an input u, the rate saturation nonlinearity with saturation bounds $u_{r,0} = [u_{r,01}...u_{r,0m}]'$ provides an output s that can be written as $s = sat_r(u)$, which corresponds to reducing as much as possible the mismatch between u and s with the additional constraints that $\dot{s}_j \in [-u_{r,0j}, u_{r,0j}]$, where $\dot{s}_j$ denotes the j^{th} component of the time derivative of s, for all $j = 1, .., m$.

To model the rate saturation, a method is proposed in [6] consisting of using a position saturation and a set of integrators and gains inserted in a feedback loop. Additional models were presented in follow-up papers (see, e.g., the overview in [82]).

Rather than enforcing the rate saturation constraints *a posteriori*, we adopt here an alternative approach, which does not require using those models. This approach, which is a well-known strategy, consists in augmenting the closed-loop with an extra integrator at the input of the plant, so that saturating the input of this integrator results in saturating the rate of its output, that is, the rate of the plant input u.

Following this strategy, we obtain the augmented system where the augmented state vector is composed of the state x of the initial system augmented by the input command signals u_r (that is, the outputs of the artificial integrators). We could just as well call these states u, but we use the subscript r to remind the reader that these states will satisfy a rate saturation constraint:

$$\tilde{x} = \begin{bmatrix} x \\ u_r \end{bmatrix} \tag{2.39}$$

and

$$\tilde{y} = \begin{bmatrix} y \\ u_r \end{bmatrix} \tag{2.40}$$

The input signal that we now want to design is given by the time derivative of the initial input command, namely $\tilde{u} = \dot{u_r}$. The augmented system is given by

$$\begin{cases} \dot{\tilde{x}} = \tilde{A}\tilde{x} + \tilde{B}\tilde{u} \\ \dot{\tilde{y}} = \tilde{C}\tilde{x} + \tilde{D}\tilde{u} \end{cases}, \tag{2.41}$$

with:

$$\tilde{A} = \begin{bmatrix} A & B \\ 0 & 0 \end{bmatrix}, \ \tilde{B} = \begin{bmatrix} 0_{n,m} \\ I_m \end{bmatrix}.$$

$$\tilde{C} = \begin{bmatrix} C & D \\ 0 & I_m \end{bmatrix}, \ \tilde{D} = \begin{bmatrix} 0_{n,m} \\ 0_{m,m} \end{bmatrix}.$$

We can also express the augmented system as $\tilde{\mathcal{H}}(s)$:

$$\tilde{\mathcal{H}}(s) = \left[\begin{array}{cc|c} A & B & 0_{n,m} \\ 0 & 0 & I_m \\ \hline C & D & 0_{n,m} \\ 0 & I_m & 0 \end{array}\right] \tag{2.42}$$

2.4.2 LQR Synthesis for LTI System with Rate Saturation

The objective of this section is the use of the previous theorems in order to develop a constructive stabilization theorem for linear systems subject to rate input saturations. The considered control problem remains the linear system given by Eq.(2.12) and whose augmented system is given by:

$$\dot{\tilde{x}} = \tilde{A}\tilde{x} + \tilde{B}sat(\tilde{u}(t)) \tag{2.43}$$

where $\tilde{x} \in \mathbb{R}^{n+m}$ and $\tilde{u} \in \mathbb{R}^m$ represent the augmented state and the input of the system, respectively, where n and m are positive integers. Matrices $A \in \mathbb{R}^{n+m \times n+m}$ and $B \in \mathbb{R}^{n+m \times m}$ are constant and known. The saturation function has been defined in the previous sections. The control input $\tilde{u}$ results from a static state feedback control law given by

$$\tilde{u} = \tilde{K}\tilde{x}, \tag{2.44}$$

with $\tilde{K}$ the augmented static gain matrix.

Let us define the following quadratic cost function for the augmented system:

$$\tilde{J} = \int_0^\infty \left(x(t)'Qx(t) + u(t)'Ru(t) + \dot{u}(t)'\tilde{R}\dot{u}(t) \right) dt = \int_0^\infty \left(\tilde{x}(t)'\tilde{Q}\tilde{x}(t) + \tilde{u}(t)'\tilde{R}\tilde{u}(t) \right) dt, \tag{2.45}$$

where $\tilde{R} \in \mathbb{R}^{m\times m}$ is a positive definite matrix and $\tilde{Q} = \begin{bmatrix} Q & 0 \\ 0 & R \end{bmatrix}$ with $Q \in \mathbb{R}^{n\times n}$ and $R \in \mathbb{R}^{m\times m}$ are symmetric positive definite matrices that may be freely selected. The following theorem holds.

Theorem 2.5. *Given $\tilde{Q} = \tilde{Q}' > 0$ and $\tilde{R} > 0$, assume that there exists $W = W' > 0 \in \mathbb{R}^{n+m\times n+m}$, Y, X in $\mathbb{R}^{m\times n+m}$, a diagonal positive matrix $S > 0 \in \mathbb{R}^{m\times m}$ and positive scalars α, ν satisfying the following inequalities:*

$$\begin{bmatrix} W & X_j' \\ X_j & u_{r,0j}^2 \end{bmatrix} \geq 0, \ \forall j = 1, .., m, \quad \begin{bmatrix} I & \alpha I \\ \alpha I & W \end{bmatrix} \geq 0 \tag{2.46}$$

$$\begin{bmatrix} \begin{bmatrix} He(\tilde{A}W + \tilde{B}Y) & (Y+X)' - \tilde{B}S \\ * & -2S \end{bmatrix} & \begin{bmatrix} W & Y' \\ 0 & -S \end{bmatrix} \\ * & -\nu \begin{bmatrix} \tilde{Q}^{-1} & 0 \\ 0 & \tilde{R}^{-1} \end{bmatrix} \end{bmatrix} < 0, \tag{2.47}$$

where X_j denotes the j^{th} row of matrix X. Then, the selecting:

$$\tilde{K} = YW^{-1} \tag{2.48}$$

ensures:

1. *local exponential stability of the origin of system (2.43), (2.44) with region of attraction $\varepsilon(W^{-1}) = \{\tilde{x} \in \mathbb{R}^{n+m} : \tilde{x}'W^{-1}\tilde{x} \leq 1\}$ which contains the α-ball $\mathcal{B}(\alpha) := \{\tilde{x} \in \mathbb{R}^n \ : \ |\tilde{x}| \leq \alpha\}$;*
2. *for any initial condition $\tilde{x}(0) \in \varepsilon(W^{-1})$, the cost function $\tilde{J}$ in (2.45) evaluated along the corresponding (unique) solution to (2.43), (2.44) satisfies $\tilde{J} \leq \nu\tilde{x}_0^T W^{-1}\tilde{x}_0$;*
3. *global exponential stability of the origin of system (2.43), (2.44) if the solution to (2.46), (2.47) is such that $X = 0$.*

Proof. The proof of this theorem is straightforward using Theorem 2.3 and the augmented system 2.41 with the decentralized rate saturation. □

2.4.3 LQR Synthesis for Polytopic System with Rate Saturation

One more time, the objective of this section is to extend the optimization problem of Theorem 2.5 to the case of polytopic systems. To do this extension, let us introduce the model of polytopic systems using the augmented notation of the system introduced in the previous section as follows

$$\dot{\tilde{x}} = \sum_{i=1}^{N} \mu_i(t) \left(\tilde{A}_i \tilde{x} + \tilde{B}_i sat(\tilde{u}) \right), \tag{2.49}$$

where matrices $\tilde{A}_i \in \mathbb{R}^{n+m \times n+m}$ and $\tilde{B}_i \in \mathbb{R}^{n+m \times m}$ are constant and known, for all $i = 1, .., N$, where N is a positive integer. The coefficient $\mu_i \in [0, 1]$ are such that their sum is equal to 1. Consider the polytopic open-loop system defined in (2.49) and the rate saturation introduced in the previous section with

$$\tilde{u} = \tilde{K}\tilde{x}. \tag{2.50}$$

Theorem 2.6. *Given $\tilde{Q} = \tilde{Q}' > 0$ and $\tilde{R} > 0$, assume that there exists $W = W' > 0 \in \mathbb{R}^{n+m \times n+m}$, Y, X in $\mathbb{R}^{m \times n+m}$, a diagonal positive matrix $S > 0 \in \mathbb{R}^{m \times m}$ and positive scalars α, ν satisfying the following inequalities:*

$$\begin{bmatrix} W & X_j' \\ X_j & u_{r,0j}^2 \end{bmatrix} \geq 0, \ \forall j = 1, .., m, \quad \begin{bmatrix} I & \alpha I \\ \alpha I & W \end{bmatrix} \geq 0 \tag{2.51}$$

$$\begin{bmatrix} \begin{bmatrix} He(\tilde{A}_i W + \tilde{B}_i Y) & (Y + X)' - \tilde{B}_i S \\ * & -2S \end{bmatrix} & \begin{bmatrix} W & Y' \\ 0 & -S \end{bmatrix} \\ * & -\nu \begin{bmatrix} \tilde{Q}^{-1} & 0 \\ 0 & \tilde{R}^{-1} \end{bmatrix} \end{bmatrix} < 0, \forall i = 1, \ldots, n \tag{2.52}$$

where X_j denotes the j^{th} row of matrix X. Then, the selecting:

$$\tilde{K} = YW^{-1} \tag{2.53}$$

ensures:

1. *local exponential stability of the origin of system (2.49), (2.50) with region of attraction $\varepsilon(W^{-1}) = \{\tilde{x} \in \mathbb{R}^{n+m} : \tilde{x}' W^{-1} \tilde{x} \leq 1\}$ containing the α-ball $\mathcal{B}(\alpha) := \{\tilde{x} \in \mathbb{R}^n : |\tilde{x}| \leq \alpha\}$;*

2. *for any initial condition* $\tilde{x}(0) \in \varepsilon(W^{-1})$*, the cost function* $\tilde{J}$ *in (2.45) evaluated along the corresponding (unique) solution to (2.49), (2.50) satisfies* $\tilde{J} \leq \nu \tilde{x}_0^T W^{-1} \tilde{x}_0$*;*

3. *global exponential stability of the origin of system (2.49), (2.50) if the solution to (2.51), (2.52) is such that* $X = 0$*.*

Proof. The proof of this theorem is straightforward using Theorem 2.4 and the augmented system (2.41) with the decentralized rate saturation. □

2.4.4 Numerical Example

Let us consider again the example of the previous sections. We still consider that the parameters may vary between $f \in [-0.011, -0.009]$ or $k \in [9, 1.1]$. The rate saturation is $u_{r,0} = 1$. We consider the augmented plant:

$$\tilde{A} = \begin{bmatrix} 0 & 1 & 0 \\ -k/m & -f/m & 1/m \\ 0 & 0 & 0 \end{bmatrix}, \ \tilde{B} = \begin{bmatrix} 0 \\ 0 \\ 1 \end{bmatrix}, \tag{2.54}$$

where $m = 0.1$ represents the mass of the body, k is the spring's elastic constant (with nominal value 1), and f the damping coefficient (with nominal value 0.01). The nominal eigenvalues of the state matrix $\tilde{A}$ remain $\lambda_{1,2} = 0.05 \pm 3.1619i$ and $\lambda_{1,2} = 0$ due to the integrator. As the real part of the eigenvalues is positive, the open-loop system is unstable. We verify that the pair $(\tilde{A}, \tilde{B})$ is controllable as $rank([B_{aug}\ A_{aug}.B_{aug}\ A_{aug}^2.B_{aug}]) = 3$ using the Kalman criteria for controllability.

Using again the same weights, the LTI problem in Theorem 2.5 for $f = -0.01$ and $k = 1$ and the polytopic problem in Theorem 2.6 are solved considering the augmented system (2.54). The results are provided in Table 2.3 for various values of ν.

ν	$\tilde{K}$	α	$\tilde{K}_{polytopic}$	$\alpha_{polytopic}$
0.1	[1.8114 , 3.3436 , 8.2385]	0.0559	[2.5136 , 3.4671 , 8.3925]	0.0551
1	[1.9560 , 6.6378 , 19.7777]	0.1723	[2.6438 , 6.5077 , 19.4065]	0.1695
2	[0.5602 , 9.1569 , 30.0273]	0.2399	[1.2970 , 8.7293 , 28.6874]	0.2357
5	[−4.2206 , 13.2037 , 58.1396]	0.3513	[−3.0981 , 13.6986 , 58.1134]	0.3535
10	[−13.4073 , 12.9539 , 66.1501]	0.4151	[−9.2555 , 11.1194 , 54.4328]	0.4138

TABLE 2.3: Solutions to the LMI problems for a LTI and polytopic system in presence of rate saturation.

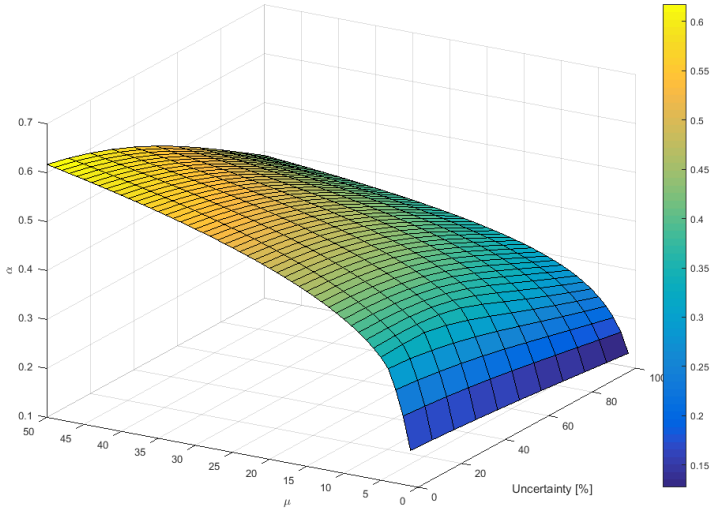

FIGURE 2.6: Evolution of α with variation of the uncertainties and ν

We can observe that in both cases, LTI or polytopic, the size of the attraction region, represented by the radius α of the ball $\mathcal{B}(\alpha)$, increased with ν, the performance index. This confirms our expectations.

%	$\tilde{K}$	α
0	[1.9560 , 6.6378 , 19.7777]	0.1723
10	[2.6438 , 6.5077 , 19.4065]	0.1695
20	[3.5745 , 6.6843 , 19.9715]	0.1662

TABLE 2.4: Solutions to the LMI problems for polytopic system for various percentage of uncertainties in presence of rate saturation.

%	$\tilde{K}$	α
0	[−1.5340 , 3.9374 , 16.6234]	0.3469
5	[−1.6900 , 6.4874 , 27.3318]	0.3483
10	[−1.9883 , 10.8906 , 45.5573]	0.3493
15	[−1.1465 , 6.0266 , 24.0099]	0.3495
20	[−2.8001 , 16.0014 , 61.4849]	0.3463

TABLE 2.5: Solutions to the LMI problems for polytopic system for various percentage of uncertainties in presence of rate saturation for $\nu = 4.75$.

Varying the percentage of the uncertainties, we also observe on Table 2.3, between the LTI and polytopic solutions, but also on Table 2.4 that α decreases with the increase of the uncertainties, which is also expected.

However, as we can see in Fig. 2.6 or in Table 2.5, $\alpha_{optimal}$ increases slightly as the uncertainties increase between 5% and 15% for $\nu \simeq 4.75$. This unexpected variation

remains local and with limited amplitude. This result is attributed to computational issues.

2.5 Chapter Summary

This chapter aimed at presenting controller synthesis methods for multi-affine polytopic systems. The varying parameters are supposed to be unknown and thus the gain scheduling or similar methods are not applicable. Optimal control has been selected to guarantee stability as well as performances in terms of errors and input command. These methods include several levels of saturation. The region of stability is assessed for each case.

In Chapter 3, these different methods will be applied to the model developed in Chapter 1 to tackle the flutter of a pitching wing.

Chapter 3

Application of Robust Control Methods to Stall Flutter Suppression

3.1 Introduction

As described earlier, flutter is an aeroelastic instability resulting from a coupling between the structure and the aerodynamic loads, which can be destructive for the aircraft. Two different types of flutter have been identified which are known as *classical flutter* and *stall flutter*.

- *Classical flutter* is an unstable mode of the wing involving coupled oscillations of pitch and plunge resulting from the coupling between the structural mode and aerodynamic loads. Classical flutter is well represented by a linear fluid-structural model, and has therefore been readily integrated into a variety of control approaches.
- *Stall flutter* results from a coupling between the nonlinear and unsteady process of *Dynamic stall*, where the flow alternatively separates from the wing and reattaches, and the torsional mode of the wing. This phenomenon leads to the emergence of oscillations, limited in amplitude, known as Limit Cycle Oscillations (LCO). *Stall flutter* can be experienced with only one structural degree of freedom, and primarily relies upon the coupling between the unsteady vorticity generation and the convection in the flow. Details can be found in [71].

In this work, the problem of *Stall flutter* suppression is addressed for a one degree of freedom pitching wing. Indeed, the model developed in Chapter 1 proves particularly interesting to predict the stall of the wing including the trailing edge and leading edge vortex shedding. Moreover, studying only one degree of freedom, i.e. the pitch oscillation, will allow us to only focus on the aerodynamics and the stall effect. However, this study can be later generalized to a full pitch and plunge system.

The problem of flutter suppression has been addressed in many works. In [83], a *dynamic stall* model for rotating blade is derived from Beddoes-Leishman. An adaptive controller is designed and simulated for various flutter conditions. In [43], a Linear Parameter Varying LQR controller is synthesized to suppress the LCO from *stall flutter*. The resulting auto-scheduled controller displays marginal robustness to airspeed variations. In [39], a mixed norm $\mathcal{H}_2 \setminus \mathcal{H}_\infty$ robust controller is designed. The model used is derived from the ONERA *dynamic stall* model in [59]. A similar model is used in [42] and solved using LQR theory. In [84], a polytopic linear dynamic inclusion is used to account for density and velocity. The problem is solved using an LMI formulation to guarantee stability. A feedback linearization method is used [9], which provides experimental validation

The present study differs from the previous works since the controllers designed in the previous works are mainly adaptive but also because the model used here includes the second vortex shedding based on both GK and ONERA BH theories. It is interesting to note that the model is based on previous Truong's model whose set of equations initially proposed may have suffered from a difficulty to apply due to these nonlinearities and switched characteristics as highlighted by the author himself in [67].

This work offers an original approach to tackle the initial difficulties to use this model in a closed-loop system. Indeed, following some similar approaches with Olalla & Al. [74] and Boyd & Al. [85], the nonlinear system will be conveniently formulated as an uncertain polytopic system. This interesting formulation allows us to use the control theory developed in Chapter 2. Especially, the different methods developed previously to tackle the specific problem of stall flutter on a wing will be applied and simulated. In particular, input saturation would be considered as magnitude and rate saturation.

3.2 Model Description

This section details the plant that will be used to address the stall flutter suppression problem based on the set of equations Eq. (1.22-1.25) presented in Chapter 1. However, the set of equations forms a nonlinear parameter varying system, including switched

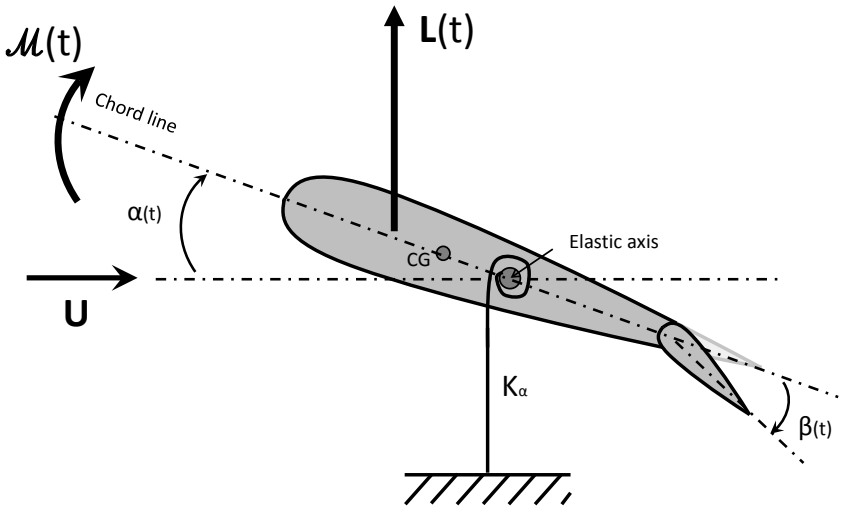

FIGURE 3.1: Model of the pitching equipped with a flap

dynamics, bilinear terms due to state multiplication. Introducing the flap actuator, the system is also limited in its position and rate command signal. Such a system proves to be complex and difficult to control in a control theory point of view. For this reason, a new formulation of the model is needed and will be provided in the sequel.

3.2.1 Adapted Aeroelastic Model

Chapter 1 provides a complete set of equations for a pitching and plunging wing. However, as mentioned previously, these equations need to be adapted to the dedicated problem of *Stall flutter* suppression on a one degree of freedom pitching wing as depicted on Fig. 3.1. The model is developed considering the moment at mid-chord which is experimentally measured contrarily to the lift. In such conditions, the set of equations in Eq. (1.22-1.25) are decoupled and simplified in so far as the plunge terms h and its derivatives are null. The linearized and decoupled equation of motion of the wing is consequently given by:

$$I_\alpha \ddot{\alpha} + C_\alpha \dot{\alpha} + K_\alpha \alpha = \mathcal{M}, \tag{3.1}$$

where we remind that K_α is the torsional stiffness, C_α is the torsional damping and I_α is the inertia around the center of rotation. $\mathcal{M}$ represents the total moment at the center of mid-chord and is split in three components such as

$$\mathcal{M} = \mathcal{M}_w + \mathcal{M}_\beta + \mathcal{M}_{ext}, \tag{3.2}$$

where $\mathcal{M}_w$ represents the aerodynamic moment produced by the wing, $\mathcal{M}_\beta$ is the aerodynamic moment produced by the flap. $\mathcal{M}_{ext}$ is the external moment which can possibly be applied. This moment can correspond for example to the torque produced by an electrical motor connected to the axis of rotation.

3.2.1.1 Aerodynamic Model Considerations

For the sake of readability, the moment set of equation Eq. (1.22-1.25) is detailed hereafter and notations are slightly adapted to transit from aerodynamic notations to a control perspective. In particular, we remind to the reader that x_s denotes location of the separation point and is such that

$$x_s \in [0, 1]. \tag{3.3}$$

This point corresponds to the distance from the leading edge, normalized by the chord length, where the flow is separated from the wing. Thus, picking $x_s = 0$ corresponds to a fully separated flow while $x_s = 1$ represents a fully attached flow. The dynamic of this point follows a first order equation:

$$\tau_1 \dot{x}_s = -x_s + x_{s,0}(\alpha - \tau_2 \dot{\alpha}), \tag{3.4}$$

where τ_1 and τ_2 are two constants and $x_{s,0}$ corresponds to the static separation point location, which can be modeled as a function of the angle α and its derivative $\dot{\alpha}$. The function $x_{s,0}$ has been evaluated experimentally using quasi-static data.

The moment produced by the wing has been slightly modified and is now given by (3.5).

$$\mathcal{M}_w = \frac{1}{2}\rho U^2 Sc \left[2\pi\alpha\eta(x_s) + C_{M_u} + C_{M\text{offset}}\right], \tag{3.5}$$

where

$$\eta(x_s) = \eta_2 x_s + \eta_1(1 - x_s), \tag{3.6}$$

and where η_2 and η_1 represent respectively the slope of the moment coefficient for a fully attached and fully detached flow. This two coefficients allow us to consider a variation between η_1 and η_2, respectively for $x_s = 0$ and $x_s = 1$. This formulation proves to be more convenient and consistent from a control point of view. Indeed, in control theory, A and B denote the state and command matrices, while A_M and $A_M + B_M$ in the aeroelastic model in Chapter 1 denote the coefficient of moment slope for fully detached flow and the coefficient of moment slope for fully attached flow. Thus, $\eta_1 = A_M$ and $\eta_2 = A_M + B_M$ using the former notation. $C_{M\text{offset}}$ is the offset value of the moment coefficient. C_{M_u} is the unsteady contribution to the moment coefficient. It has

been observed that the oscillations, for pure sinusoidal motion, were mainly following a second order behavior. For this reason, it is assumed that a second order with constant terms could be sufficient enough to reproduce the observed behavior. Thus, the second equation of Eq. (1.24) can be linearized around $(\dot{C}_{M_u}, C_{M_u}) = (0, 0)$ and we notice that the unsteady component now follows the following simplified second order dynamic:

$$\ddot{C}_{M_u} - w_S \beta_M(x) \dot{C}_{M_u} + w_S^2 C_{M_u} = -E_M(x) w_S \dot{\alpha}(t) - D_M(x) w_S \ddot{\alpha}(t) . \tag{3.7}$$

where w_s is a constant, and β_M, E_M and D_M are constants depending on α and $\dot{\alpha}$.

Remark 2. Note that the Van der Pol-like equation is now a harmonic oscillator equation. This point will be discussed later on. However, it has to be noticed that Eq.(3.7) is still switched.

Let us introduce again α_s and $\alpha_{d\, x_s = x_{s,c}}$, the critical angles of attack, as defined Chapter 1, and Ω_{ne}, the following set:

$$\Omega_{ne} := \Omega_{ne}^1 \cup \Omega_{ne}^2,$$

where

$$\begin{aligned} \Omega_{ne}^1 &= \left\{ (\alpha, \dot{\alpha}) \in [-180, 180] \times \mathbb{R}, \alpha \in \left[-\alpha_s, \alpha_{d\, x_s = x_{s,c}} \right] \, , \, \dot{\alpha} < 0 \right\}, \\ \Omega_{ne}^2 &= \left\{ (\alpha, \dot{\alpha}) \in [-180, 180] \times \mathbb{R}, \alpha \in \left[-\alpha_{d\, x_s = x_{s,c}}, \alpha_s \right] \, , \, \dot{\alpha} > 0 \right\}. \end{aligned}$$

We can now define β_M, E_M and D_M as a two-valued set of functions such as,

$$\{D_M, \beta_M, E_M\} = \begin{cases} \{D_{M,1}, \beta_{M,1}, E_{M,1}\} & , \text{if } (\alpha, \dot{\alpha}) \notin \Omega_{ne}, \\ \{D_{M,2} = 0, \beta_{M,2} < 0, E_{M,2} = 0\} & , \text{if } (\alpha, \dot{\alpha}) \in \Omega_{ne}, \end{cases}$$

where parameters $D_{M,i}$, $\beta_{M,i}$ and $E_{M,i}$, for $i = 1, 2$, are constant and known.

$\mathcal{M}_\beta$ is the moment produced by the trailing edge flap and is defined by

$$\mathcal{M}_\beta = \tfrac{1}{2} \rho U^2 S c C_{M,\beta} \beta, \tag{3.8}$$

where

- $C_{M,\beta}$ is a the slope of the actuator moment coefficient,
- β is the flap deflection angle which can possibly be limited as follows:

$$|\beta| \leq \bar{\beta} \tag{3.9}$$

$$|\dot{\beta}| \leq \bar{\dot{\beta}} \tag{3.10}$$

with $\bar{\beta}$ and $\bar{\dot{\beta}}$ constant.

The final set of equations for the aeroelastic model is consequently given by:

$$\begin{cases} I_\alpha \ddot{\alpha} & = & -C_\alpha \dot{\alpha} - K_\alpha \alpha + qSb\,[2\pi\alpha(A_M + B_M x_s) + C_{M\text{offset}} \\ & & +C_{M_u} + C_{M,\beta}\beta] \\ \tau_1 \dot{x}_s & = & -x_s + x_{s,0}(\alpha - \tau_2 \dot{\alpha}), \\ \ddot{C}_{M_u} + D_M(x) w_S \ddot{\alpha} & = & w_S \beta_M(x) \dot{C}_{M_u} - w_S^2 C_{M_u} - E_M(x) w_S \dot{\alpha} \end{cases} \tag{3.11}$$

3.2.1.2 Complete Aeroelastic Model

The resulting equations of the complete aeroelastic model of the wing are then given by Eq. (3.1), (3.11) and (3.8). The previous final set of equations can thus be formulated as the nonlinear system:

$$\begin{aligned} \dot{x} &= A(x, x_s)x + B(x)u \\ \tau_1 \dot{x}_s &= -x_s + x_{s,0}(x) \\ y &= C(x)x \\ z &= Fx \end{aligned} \tag{3.12}$$

where the vector $x \in \mathbb{R}^4$ is given by

$$x = [\ \dot{\alpha},\ \alpha,\ \dot{C}_{M_u},\ C_{M_u}\ ]', \tag{3.13}$$

and vector u $(= \beta)$, y and z are respectively the control input, the output and the measurement vectors of the system. Matrices A, B, C and F are given in (3.14).

Parameter	Value	Parameter	Value
I_α	$0.0037\ Nm/rad/s^2$	C_α	$0.072\ Nm/rad/s$
K_α	$2.78\ Nm/rad$	ρ	$0.9\ kg/m^3$
$C_{M,\beta}$	1	T	$292\ K$

TABLE 3.1: Model parameters used in the simulation study.

$$
A(x,x_s) = \begin{bmatrix} -\frac{C_\alpha}{I_\alpha} & \frac{\pi\rho U^2 Sc\eta(x_s)-K_\alpha}{I_\alpha} & 0 & \frac{\rho U^2 Sc}{2I_\alpha} \\ 1 & 0 & 0 & 0 \\ w_S\left(D_M(x)\frac{C_\alpha}{I_\alpha} - E_M(x)\right) & -w_S D_M(x)\left(\frac{\pi\rho U^2 Sc\eta(x_s)-K_\alpha}{I_\alpha}\right) & w_S\beta_M(x) & -w_S\left(w_S + \frac{D_M(x)\rho U^2 Sc}{2I_\alpha}\right) \\ 0 & 0 & 1 & 0 \end{bmatrix},
$$

$$
B = \tfrac{1}{2}\rho U^2 Sc C_{M,\beta}\begin{bmatrix} 1 & 0 & -w_S D_M(x) & 0 \end{bmatrix}'
$$

$$
C(x_s) = \begin{bmatrix} 0 & 2\pi\eta(x_s) & 0 & 1 \\ 0 & 1 & 0 & 0 \end{bmatrix}, \qquad F = \begin{bmatrix} 0 & 1 & 0 & 0 \end{bmatrix}. \tag{3.14}
$$

System (3.12) can be seen as a nonlinear switched system, for which a dedicated stability analysis needs to be provided. In order to solve this problem, we will provide in the next section a polytopic model for system (3.12), for which such an analysis is simplified.

3.2.2 Validation of the Aeroelastic Model in Stall Flutter Conditions

To validate the synthesis model, experimental data have been collected in [71] and compared to the prediction. The parameters of the aerodynamic model are identical to the ones used in Chapter 1. Indeed, as the amplitude of the oscillations experimented in flutter conditions are in the range of the cases used to validate the model, it seems relevant to use the same values. The values of the flow conditions as well as the structural parameters are listed in Table 3.1.

As we can see Fig. 3.2 and Fig. 3.4, the amplitude as well as the frequency of flutter oscillations are successfully reproduced for the 3 freestream velocities presented in Table 3.2 at an initial angle of attack of 10°. This initial angle of attack has been used to obtain flutter conditions at lower speed and with lower amplitudes.

Fig. 3.2 shows also the evolution of the steady (blue) and unsteady (purple) coefficients of moment. As observed in the first Chapter 1, the main contribution is provided by the steady moment coefficient responsible for the hysteresis.

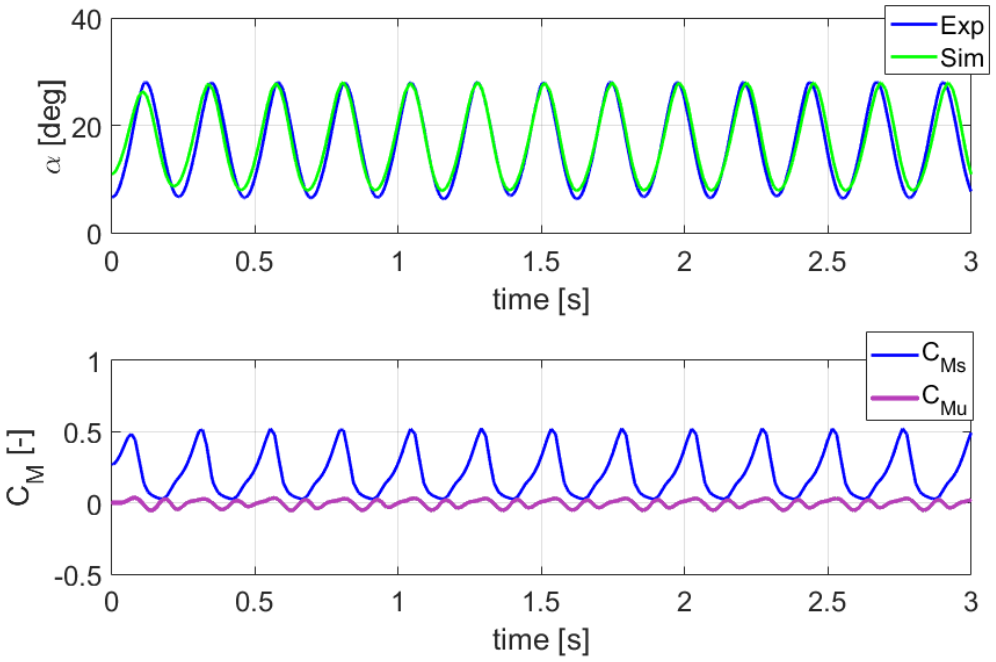

FIGURE 3.2: Experiment and simulation in flutter conditions (case 2) and steady and unsteady simulated moment coefficient.

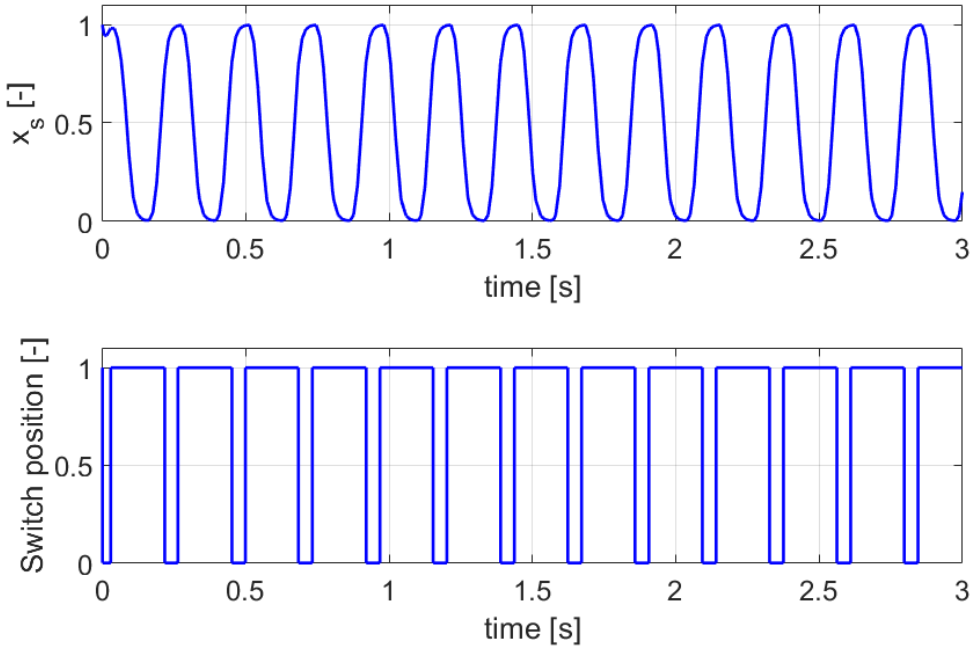

FIGURE 3.3: Variation of the separation and switch signal.

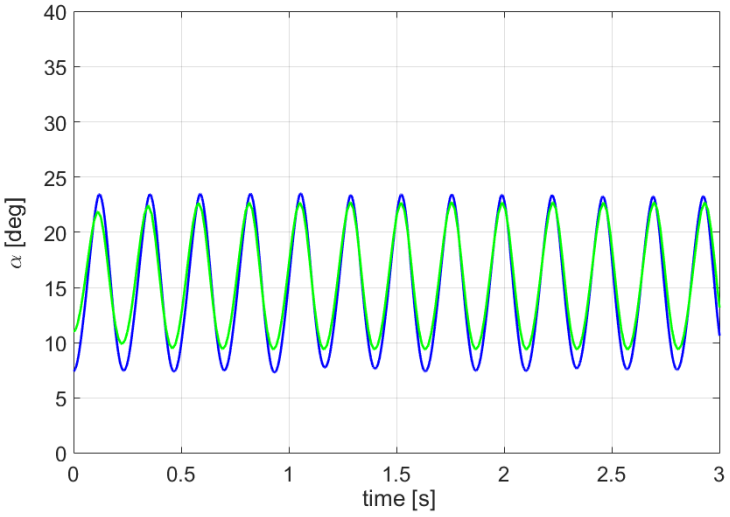

(a)

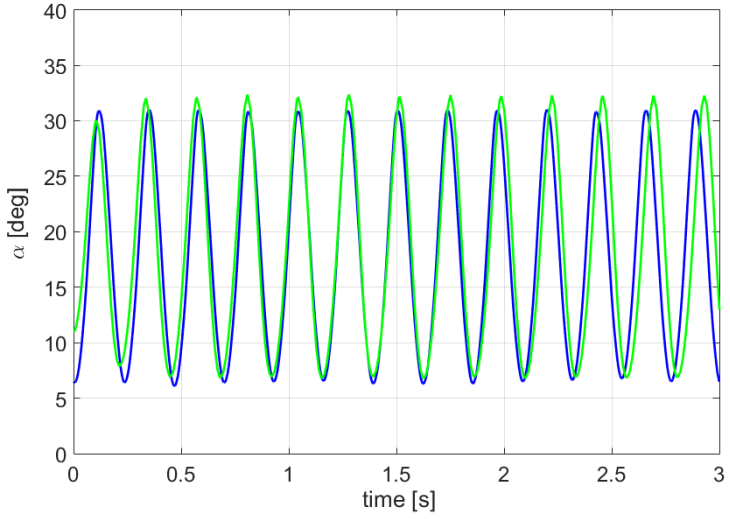

(b)

FIGURE 3.4: Experiment and simulation in stall flutter conditions: **a** Case 1, **b** Case 3

The time history of the separation point location and the switch signal of the values for unsteady moment coefficient equation are provided in Fig. 3.3. We can observe the periodic variation of these signals justifying that a LTI or Linear Time Invariant formulation would not be relevant for such system.

These observations validate the model in the range of variations described earlier. Especially, we can see that for the range of variations of the freestream velocity considered, the model provides a good agreement with experimental values.

Case	α_0	U_∞
1	$10°$	$17.5\ m/s$
2	$10°$	$20.3\ m/s$
3	$10°$	$22.3\ m/s$

TABLE 3.2: Parameters of the flutter cases.

3.3 Aeroelastic Model as an Uncertain Polytopic Plant

In this section, an uncertain polytopic system is developed. This formulation will conveniently allow us to deal with the uncertainties and nonlinearities in the previous equations.

3.3.1 Description of the Uncertain Polytopic Plant

As mentioned above, system (3.12) presents some nonlinearities due to the products in the dynamics of the variable x_s and also to bilinear terms which appear in the matrix $A(x, x_s)$ through the function $\eta(x_s)$. In order to simplify the model, we rewrite system (3.12) as an uncertain polytopic system where the uncertain parameters are listed in the following description.

$\eta(x_s)$: First, in order to suppress the product $\alpha \times \eta$ from the equation, let us consider η introduced previously in Eq. (3.6). We note that η is a linear combination of the state variable x_s. Since x_s cannot be directly measured, it is reasonable to consider as an uncertainty to the system and to use the fact that it lies in the interval $[0,\ 1]$. Therefore, parameter η verifies

$$\eta \in [\eta_1,\ \eta_2], \tag{3.15}$$

or equivalently, there exists a scalar function $\lambda_1 \in [0, 1]$ such that

$$\eta(x_s) = \lambda_1 \eta_1 + (1 - \lambda_1)\eta_2. \tag{3.16}$$

E_M, β_M, D_M: Secondly, instead of considering a switch of the constants $\{D_M, \beta_M, E_M\}$ in Eq. (3.11), a linear variation is conveniently introduced depending on an additional parameter. This technique has been successfully used in [74]. Therefore, there exists a function $\lambda_2 \in [0, 1]$ such that

$$\begin{aligned} \{D_M, \beta_M, E_M\} \ := \ & \lambda_2 \{D_{M,1}, \beta_{M,1}, E_{M,1}\} \\ & +(1 - \lambda_2) \{D_{M,2}, \beta_{M,2}, E_{M,2}\}. \end{aligned} \tag{3.17}$$

A particular attention should be brought to $\beta_{M,1}$. Indeed, as discussed earlier through the linearization of Eq. (1.24), the Van der pol equation at the origin of the Hopf bifurcation has become a harmonic oscillator equation. Especially, the coefficient is reduced to a scalar value. However, as the Hopf bifurcation admits in this case a LCO, then C_{M_u} is varying and bounded. Thus, we can consider that the damping coefficient β_M encapsulates the variation of the Van der pol equation's damping coefficient. Consequently, $\beta_{M,1}$ varies between these bounds, i.e. $\beta_{M,1} \in [\beta^+_{M,1}, \beta^-_{M,1}]$. For this reason, $\beta_{M,1} \to \beta^+_{M,1}$ and $\beta_{M,2} \to min(\beta_{M,2}, \beta^-_{M,1})$.

U^2: Finally, matrices A and B also depend on the uncertainties. Especially, the freestream velocity U can be considered uncertain due to the possible gusts of wind that can be encountered during flight, or just because of uncertainties on its measurement. Therefore, there exists a function $\lambda_3 \in [0, 1]$ such that

$$U^2 = \lambda_3 U_1^2 + (1 - \lambda_3) U_2^2. \tag{3.18}$$

Remark 3.1. The control algorithm derived in this paper is designed by considering the situation where the freestream velocity U may vary in a certain allowable set, but can be approximated by an (unknown) constant parameter during the dynamic evolution. Then, the moment in (3.5) introduces a constant bias affecting dynamics (3.1), whose magnitude depends on the constant $C_{M\text{offset}}$ and on the parameter U. When designing our controller, we will focus on the unperturbed dynamics resulting from $C_{M\text{offset}} = 0$, but it is clear that the developed results easily extend to the case of constant values of $C_{M\text{offset}}$ and U, because the corresponding effect is merely to shift the equilibrium point.

Even though we assumed that U be constant (and unknown) during motion, as well as the quantity λ_3 in (3.18), we consider a time-varying version of the uncertain vector $\lambda(t) = [\lambda_1(t)\ \lambda_2(t)\ \lambda_3(t)]'$ in $[0\ 1]^3$, comprising the coefficients λ_l, for any $l = 1, 2, 3$, which can vary with time and are not necessarily constant.

Based on this uncertain vector and on relations (3.16)–(3.18), we can derive a polytopic model of the uncertain system (3.12), corresponding to:

$$\begin{array}{rcl} \dot{x} & = & \sum_{i,j,k=1}^{2} \lambda_1^i \lambda_2^j \lambda_3^k \left(A_{i,j,k} x + B_{i,j,k} u\right) \\ & = & \sum_{i,j,k=1}^{2} \mu_{ijk} \left(A_{i,j,k} x + B_{i,j,k} u\right) \\ y & = & \sum_{i,j,k=1}^{2} \lambda_1^i \lambda_2^j \lambda_3^k C_{i,j,k} x = \sum_{i,j,k=1}^{2} \mu_{ijk} C_{i,j,k} x \\ z & = & Fx \end{array} \tag{3.19}$$

where $\lambda_l^1 = \lambda_l(t)$ and $\lambda_l^2 = 1 - \lambda_l(t)$, for $l = 1, 2, 3$, matrices $A_{i,j,k}$, $B_{i,j,k}$ and $C_{i,j,k}$ are given in (3.20), at the top of the next page, and where we introduced the scalars $\mu_{ijk} = \lambda_1^i \lambda_2^j \lambda_3^k$. These scalars, in particular, satisfy $\sum_{i,j,k=1}^{2} \mu_{ijk} = 1$, which reveals that

Vertex	μ	Eigenvalues
1	μ_{000}	$[5.52 \pm 66.12i, -24.91,\ 7.28]$
2	μ_{001}	$[5.81 \pm 66.39i, -9.1 \pm 6.87i]$
3	μ_{010}	$[5.46 \pm 65.83i, -8.74 \pm 25.34i]$
4	μ_{011}	$[5.79 \pm 66.26i, -9.08 \pm 25.44i]$
5	μ_{100}	$[-28.4 \pm 61.18i, -26.15, 6.7]$
6	μ_{101}	$[-28.4 \pm 61.18i, -9.72 \pm 5.7i]$
7	μ_{110}	$[-28.4 \pm 61.18i, -9.72 \pm 24.39i]$
8	μ_{111}	$[-28.4 \pm 61.18i, -9.72 \pm 24.79i]$

TABLE 3.3: Eigenvalues of the polytope vertices.

the multi-affine dynamics (3.12) can be written as a convex combination of $2^3 = 8$ linear time-invariant models corresponding to all possible selections of $i, j, k \in \{0, 1\}$ in (3.20) (see, e.g., [86, Prop. 2] for details).

$$
\begin{aligned}
&A_{i,j,k} = \\
&\begin{bmatrix}
-\frac{C_\alpha}{I_\alpha} & \frac{\pi\rho U_k^2 Sc\eta_i - K_\alpha}{I_\alpha} & 0 & \frac{\rho U_k^2 Sc}{2I_\alpha} \\
1 & 0 & 0 & 0 \\
w_S\left(D_{M,j}\frac{C_\alpha}{I_\alpha} - E_{M,j}\right) & -w_S D_{M,j}\left(\frac{\pi\rho U_k^2 Sc\eta_i - K_\alpha}{I_\alpha}\right) & w_S\beta_{M,j} & -w_S\left(w_S + \frac{D_{M,j}\rho U_k^2 Sc}{2I_\alpha}\right) \\
0 & 0 & 1 & 0
\end{bmatrix}, \\
&B_{i,j,k} = \tfrac{1}{2}\rho U_k^2 Sc C_{M,\beta}\begin{bmatrix}1 & 0 & -w_S D_{M,j} & 0\end{bmatrix}', \\
&C_{i,j,k} = \begin{bmatrix}0 & 2\pi\eta_i & 0 & 1 \\ 0 & 1 & 0 & 0\end{bmatrix}, \qquad F = \begin{bmatrix}0 & 1 & 0 & 0\end{bmatrix}.
\end{aligned}
\tag{3.20}
$$

3.3.2 Stability and Controllability Analysis

To study the stability and controllability of the system inside the defined polytope, it is necessary to consider the 8 vertices.

The eigenvalues are calculated for each matrix $A_i \ \forall\ i \in \{1, ..., 8\}$ and are presented in Table 3.3.

We can see in particular that the 4 last cases, which correspond to $\{D_M, E_M\} = \{0, 0\}$, are all stable.

Using the Kalman criteria we calculate the controllability of each pairs (A_i, B_i) in Table 3.4. We can observe that half of the pairs are not controllable. Looking at Eq. (3.20), we can actually observe that the equation of C_{M_u} is uncontrollable for $(\alpha, \dot{\alpha}) \in \Omega_{ne}$ as

Vertex	μ	$Rank(\left[B, AB, A^2B, A^3B\right]$
1	μ_{000}	4
2	μ_{001}	4
3	μ_{010}	4
4	μ_{011}	4
5	μ_{100}	2
6	μ_{101}	2
7	μ_{110}	2
8	μ_{111}	2

TABLE 3.4: Controllability of the polytope vertices pairs (A_i, B_i).

$\{D_M, E_M\} = \{0, 0\}$. However, as observed in Table 3.3, the uncontrollable eigenvalues are stable, which means that the pairs are all stabilizable. Using the convexity of the polytopic formulation, as each pair (A_i, B_i) is stabilizable, we can conclude that any pair (A, B) is also stabilizable inside the polytope.

Remark 3. The uncontrollability of two of the modes corresponds to the non-excited regime when the flow is attached or re-attaching and when we do not have any control on the leading edge vortex with the trailing edge flap.

3.4 Application to Flutter Suppression Control

In this section, the previous formulation will be used to solve the problem of flutter suppression. The synthesis techniques developed in Chapter 2 will be applied. First, a static state feedback will be computed by application of Theorem 2.2.

Fig. 3.5 provides an illustration of the architecture of the complete system to control, including the aeroelastic model and the controller to synthesize. In the *Stall flutter* suppression problem, the objective is to bring down the angle of attack when facing stall flutter conditions.

Then, since input saturations phenomenon are quite critical for this problem, we will also apply the design methods provided in Theorems 2.4 and 2.6 addressing the case of magnitude and rate saturation respectively as represented in Fig. 3.5 between the controller and the system.

A polytope is also defined to allow the variation of the unknown parameters of the polytopic formulation in Eq. (3.19–3.20). Indeed, if η and $\{D_M, \beta_M, E_M\}$ are bounded and known from the previous section, we need to define the margin of uncertainty of the freestream velocity to ensure some robustness to this parameter. The nominal value

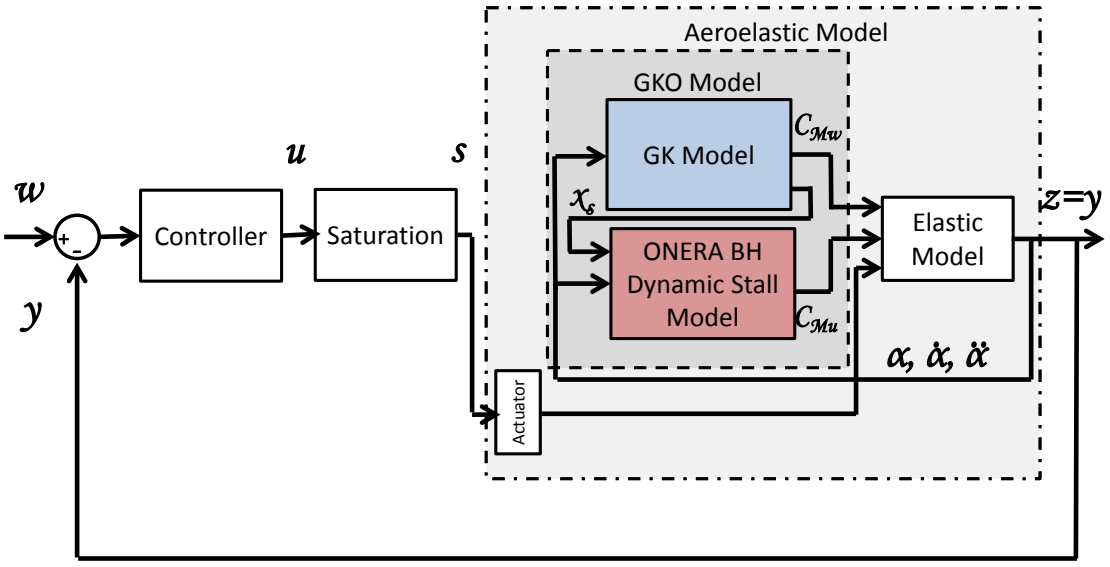

FIGURE 3.5: Closed-loop architecture of the aeroelastic system.

selected is 20 m/s. We allow some variation of $\pm 2.5 m/s$ which provides a variation range $[U_{min}, U_{max}] = [17.5\ m/s, 22.5\ m/s]$.

3.4.1 LMI-based Selection of an LQR Controller using a Polytopic Formulation

We will first apply the control theory to the case without saturation. This essential step is necessary to demonstrate the validity of the formulation proposed in this chapter. In particular, it is important to show that the formulation proposed in Eq. (3.19–3.20) to synthesize the static state feedback controller is adapted to the full size system. Theorem 2.2 will be used to synthesize the controller.

3.4.1.1 Numerical results

In order to use Theorem 2.2, it is necessary to select the appropriate weighting matrices of the cost function. Their selection has to ensure that the flutter is suppressed after a reasonable time and also that the input vector remains limited in amplitude.

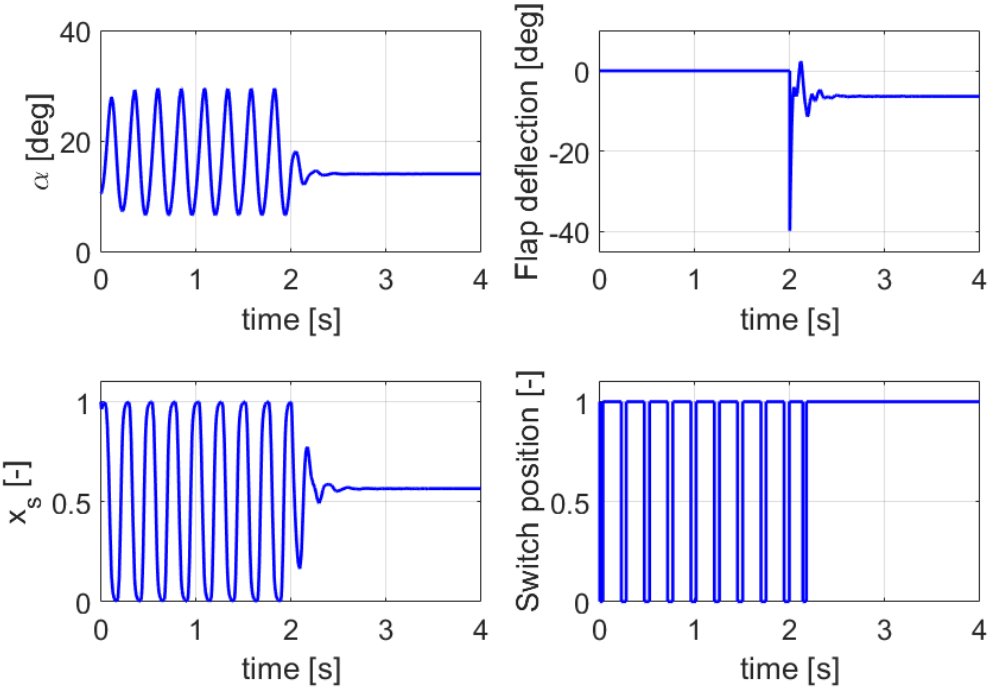

FIGURE 3.6: Angle of attack (deg), flap deflection (deg), x_s and switch signal as function of the time (s) for $U = 20\ m/s$. The controller is activated after 2 s.

After trials and errors, the matrices have been chosen $Q = \text{diag}\{1, 0.1, 0.01, 0.01\}$ and $R = 100$. This choice is initially driven by the willingness of reducing quickly the flutter, which explains the higher weight put on the first state corresponding to the time derivative of the angular position relatively to the other states. To have reasonable a control input, the matrix R had to be selected with a relative high weight.

The convex optimization in Theorem 2.2 is then solved using the Robust Control Toolbox [87, 88] available in MATLAB R2017a. The resulting static state feedback controller K, is given by:

$$K = [0.1246,\ 1.7496,\ 0.3036,\ -1.3672].$$

This controller is then evaluated using the non-linear set of equation derived in Chapter 1.

The results for three different airspeeds are presented in Fig. 3.6–3.7. As already observed in Remark 3.1, while the controller design was performed without the presence of the external disturbance $C_{M\text{offset}}$, in the simulation we consider a more realistic case of a nonzero value of $C_{M\text{offset}}$ (see Table 3.1). As expected, the different values of U considered in our three simulations, correspond to different equilibrium points reached by the closed-loop system.

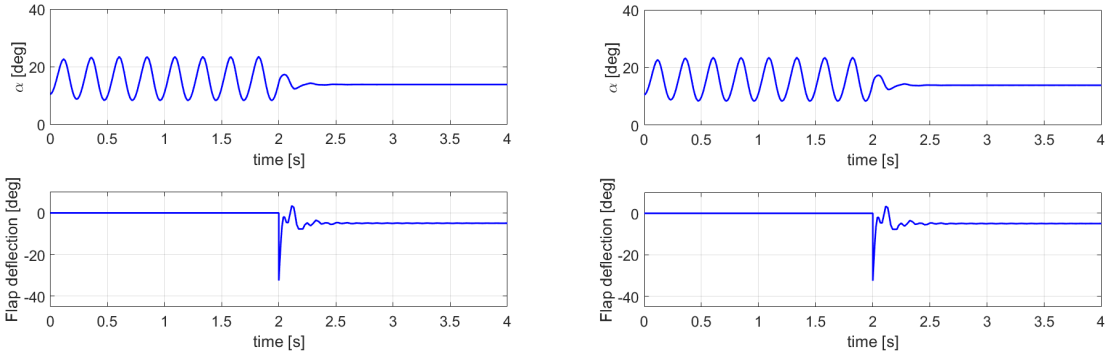

(a) (b)

FIGURE 3.7: Angle of attack (deg) and flap deflection (deg) as function of the time (s) for: (a) $U = 17.5\ m/s$ and (b) $U = 22.5\ m/s$. The controller is activated after 2 s.

The simulation results illustrate how the same feedback gain is able to stabilize the system to this equilibrium point for the three different values of freestream velocities while the other parameters are varying, as it can be seen on x_s and the switch position graphs given in Fig. 3.6. The controller successfully suppresses the flutter phenomenon, which is visible in all three simulations, before the controller activation, which always occurs at time $t = 2s$.

We can observe on Fig. 3.6, which corresponds to a freestream velocity of $U = 20\ m/s$, that the flutter is suppressed at time $t = 0.15\ s$ after the activation of the controller. To obtain this quick response, a command of almost 40° of deflection is necessary. Such deflection may be considered as relatively high. Especially, this could eventually lead to the partial separation of the flow over the flap and would be partially inefficient.

Using the LQR formulation, it is possible to vary the command input by adjusting the relative weight R. Fig. 3.8 and 3.9 illustrate the time responses using respectively $R = 10$ and $R = 500$ in the synthesis of the controller. We can notice as expected that a smaller value of the weighting matrix R results in an increase of the input signal but a faster suppression of the flutter. On the contrary, increasing R will reduce the input signal, but will slow the convergence of the output.

3.4.1.2 Conclusion

The numerical results illustrate the efficiency of the synthesis method developed in Theorem 2.2. Especially, we can observe that the polytopic formulation used to synthesize the controller captures the nonlinearities and parameter variations of the set of equation. This formulation allows us to apply the design technique to compute an adapted

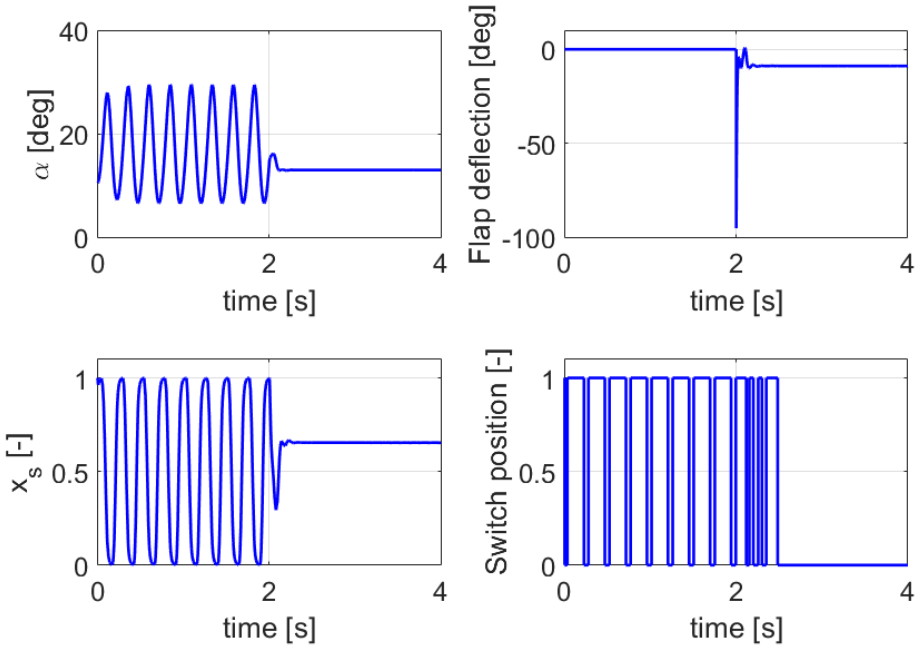

FIGURE 3.8: Angle of attack (deg), flap deflection (deg), x_s and switch signal as function of the time (s) for $U = 20\ m/s$ synthesized with $R = 10$. The controller is activated after 2 s.

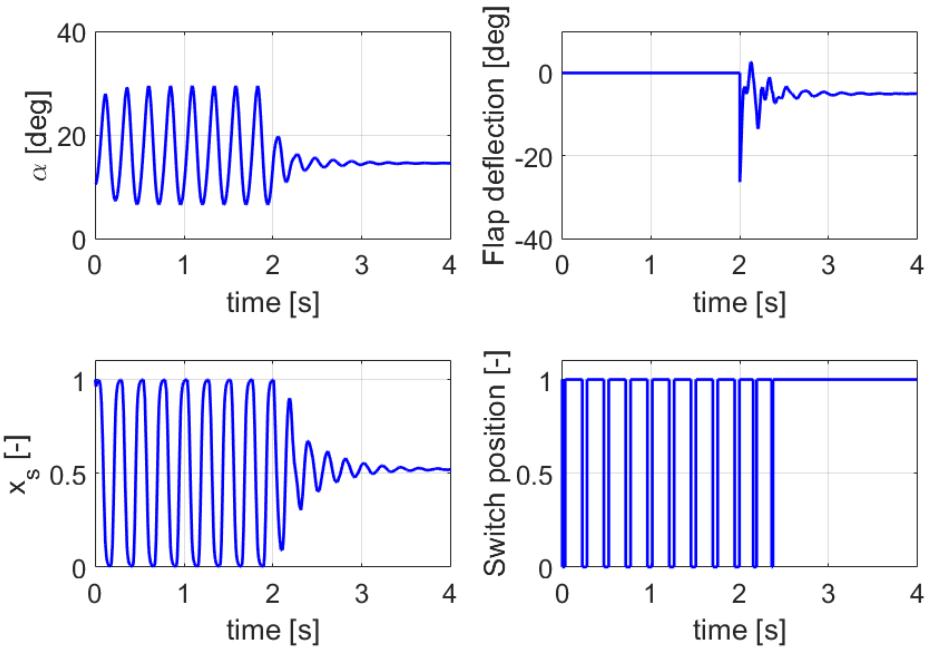

FIGURE 3.9: Angle of attack (deg), flap deflection (deg), x_s and switch signal as function of the time (s) for $U = 20\ m/s$ synthesized with $R = 500$. The controller is activated after 2 s.

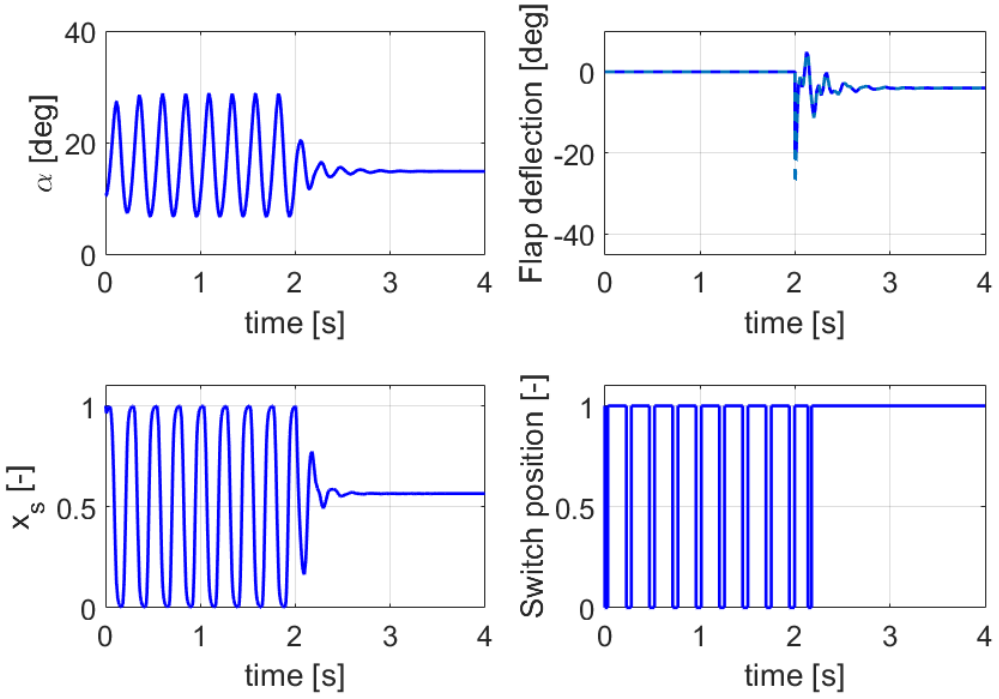

FIGURE 3.10: Angle of attack (deg) and flap deflection (deg) as function of the time (s) for $U = 20\ m/s$ with saturation. The controller is activated after 2 s.

controller. Not only the controller successfully stabilizes the unknown parameter varying system and suppresses flutter, but it also includes uncertainties on the freestream velocity.

3.4.2 LQR Controller using a Polytopic Formulation with Magnitude Input Saturation

The previous section has shown the ability of the polytopic formulation to synthesize an adapted controller. In this section, a magnitude input saturation is considered using the same approach. In particular, Theorem 2.4 will be applied to synthesize the controller of the closed-loop system.

3.4.2.1 Numerical Results

The magnitude input saturation has been selected $|\beta| \leq \bar{\beta} = 20°$. Once again, the weighting matrices need to be selected to obtain the desire closed-loop behavior. The matrices used are similar to the previous case and remain consequently $Q = \text{diag}\{1, 0.1, 0.01, 0.01\}$ and $R = 100$. The convex optimization proposed in Theorem 2.4 is solved and the resulting state feedback gain is obtained:

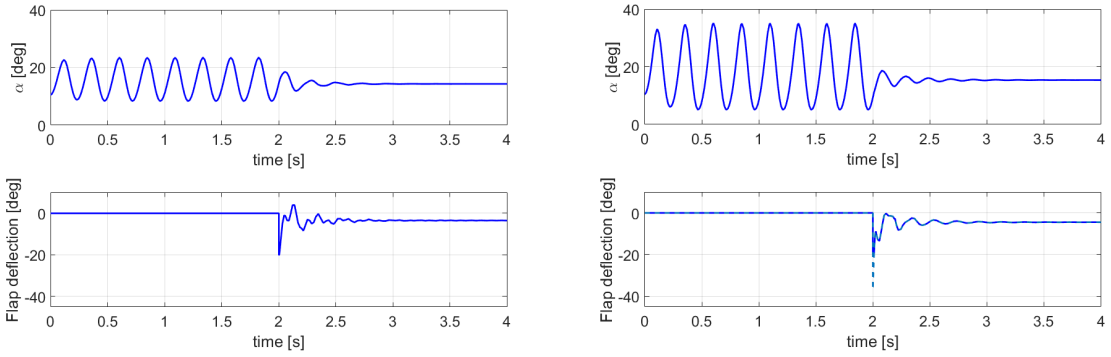

(a) (b)

FIGURE 3.11: Angle of attack (deg) and flap deflection (deg) with saturation as function of the time (s) for: (a) $U = 17.5\ m/s$ and (b) $U = 22.5\ m/s$. The controller is activated after 2 s.

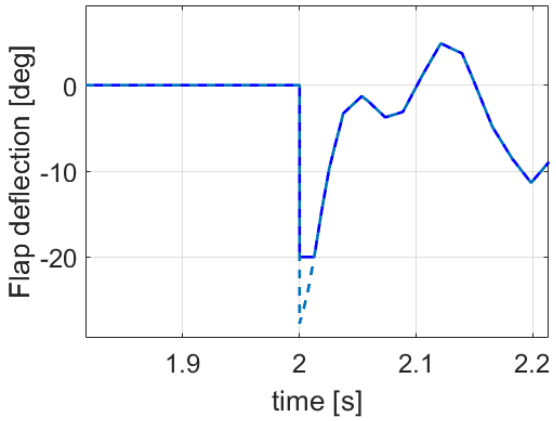

FIGURE 3.12: Enlargement of flap deflection (deg) as function of the time (s) for $U = 20\ m/s$.

$$K = [0.098,\ 0.9160,\ 0.2174,\ -4.764].$$

The performance index has been maintained to $\nu = 1$ which provides a radius of the region of attraction $\alpha = 0.0265$. This value proves to be really small which is an expression of the conservatism involved in the method. Indeed, the uncertainties introduced in the polytopic formulation is a loss of information which induces some conservatism. The solution is then evaluated using temporal simulations for the three different velocities given in Fig. 3.10–3.12. We can observe the ability of the controller to suppress the flutter in presence of magnitude saturation on the control input in a reasonable time for the three considered cases.

In order to increase the radius of the region of attraction, it is possible to relax the constraint on the cost function by increasing the performance index to $\nu = 10$. In this

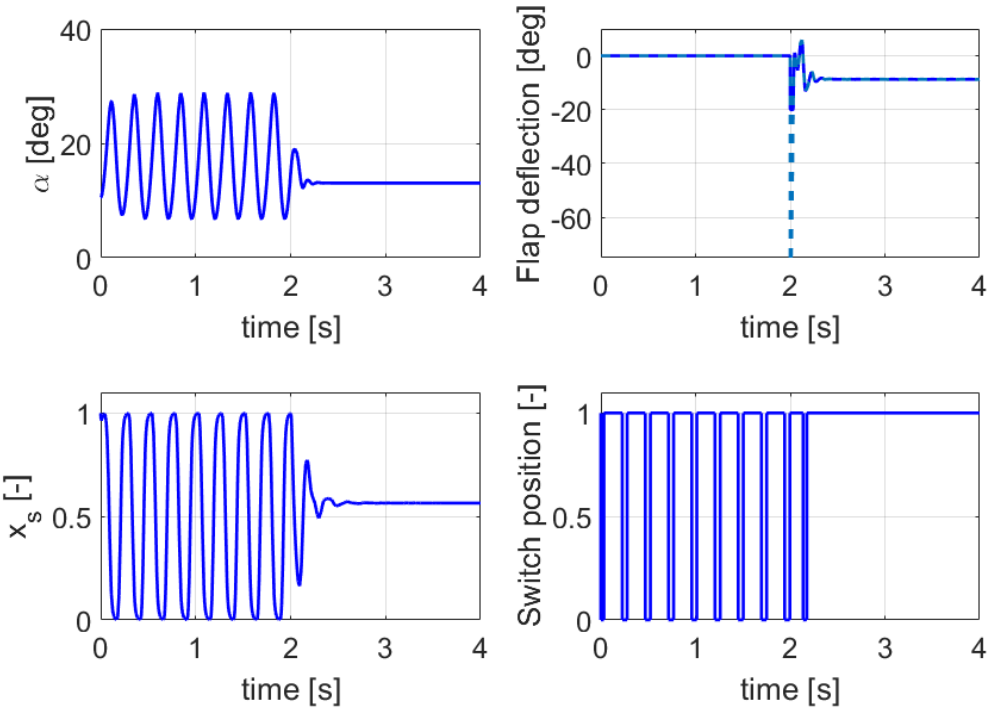

FIGURE 3.13: Angle of attack (deg) and flap deflection (deg) as function of the time (s) for $U = 20\ m/s$ with $\nu = 10$. The controller is activated after 2 s.

condition, the radius is increased as expected with $\alpha = 0.0421$. The controller has also been synthesized using a value of this performance index. It is interesting to see in Fig. 3.13 that the command is then larger and the convergence faster. Indeed, the performance is relative to the weighting matrices Q and R. Thus, decreasing the cost performance or increasing J, can result in being less demanding on the states or the input.

3.4.2.2 Conclusion

The numerical results show the ability of Theorem 2.4 to compute a controller gain in presence of saturation. Especially, one can observe that the constraint on the saturation is considered during the synthesis and results in an adapted controller. However, because of the conservatism induced by the polytopic formulation, the region of attraction proved to be extremely reduced and does not necessarily include the flutter conditions, depending on the values used for the wing, flow conditions and input saturation.

3.4.3 LQR Controller using a Polytopic Formulation with Rate Input Saturation

Finally, a rate input saturation is considered. Following the approach detailed in Section 2.4.1, an augmented system is now considered as introduced in (2.41) and is given by:

$$\begin{aligned} \dot{\tilde{x}} &= \sum_{i,j,k=1}^{2} \lambda_1^i \lambda_2^j \lambda_3^k \left(\tilde{A}_{i,j,k} \tilde{x} + \tilde{B}_{i,j,k} \tilde{u} \right) \\ &= \sum_{i,j,k=1}^{2} \mu_{ijk} \left(\tilde{A}_{i,j,k} \tilde{x} + \tilde{B}_{i,j,k} \tilde{u} \right) \end{aligned} \tag{3.21}$$

where $\tilde{x} = [x,\ u]'$ and the matrices $\tilde{A}_{i,j,k}$ and $\tilde{B}_{i,j,k}$ are given in (3.22). The scalars $\mu_{ijk} = \lambda_1^i \lambda_2^j \lambda_3^k$ remain identical to the initial formulation and still satisfy $\sum_{i,j,k=1}^{2} \mu_{ijk} = 1$, which reveals that the multi-affine dynamics remains a convex combination of $2^3 = 8$ linear time-invariant models.

$$\tilde{A}_{i,j,k} = \begin{bmatrix} -\frac{C_\alpha}{I_\alpha} & \frac{\pi \rho U_k^2 S c \eta_i - K_\alpha}{I_\alpha} & 0 & \frac{\rho U_k^2 S c}{2 I_\alpha} & \frac{1}{2} \rho U_k^2 S c C_{M,\beta} \\ 1 & 0 & 0 & 0 & 0 \\ w_S \left(D_{M,j} \frac{C_\alpha}{I_\alpha} - E_{M,j} \right) & -w_S D_{M,j} \left(\frac{\pi \rho U_k^2 S c \eta_i - K_\alpha}{I_\alpha} \right) & w_S \beta_{M,j} & -w_S \left(w_S + \frac{D_{M,j} \rho U_k^2 S c}{2 I_\alpha} \right) & -\frac{1}{2} \rho U_k^2 S c C_{M,\beta} w_S D_{M,j} \\ 0 & 0 & 1 & 0 & 0 \\ 0 & 0 & 0 & 0 & 0 \end{bmatrix},$$

$$\tilde{B}_{i,j,k} = \begin{bmatrix} 0 & 0 & 0 & 0 & 1 \end{bmatrix}'. \tag{3.22}$$

3.4.3.1 Numerical Results

The magnitude input saturation has been selected $|\dot{\beta}| \leq \bar{\dot{\beta}} = 60°/0.2s$. This value has been selected based on performance of small UAV actuators. Concerning the weighting matrices, the dimension had been adapted to the augmented system. After trials and errors, the values had been adjusted as follows: $Q = \text{diag}\{1, 0.1, 0.01, 0.01\}$ and $R = 100$ and $\tilde{R} = 10$. Theorem 2.6 is then used to compute the controller which gives a controller:

$$K = [0.0976,\ 2.31,\ 0.157,\ -7.089].$$

Once again, the radius of region of attraction is small with $\alpha = 0.000043$. This results from the conservatism of the polytopic formulation but also from the method itself.

The results of the time simulations of the closed-loop system are given Fig. 3.14–3.15. The figures demonstrate the capability of the controller to suppress flutter for all three freestream velocities while limiting the rate of the flap deflection.

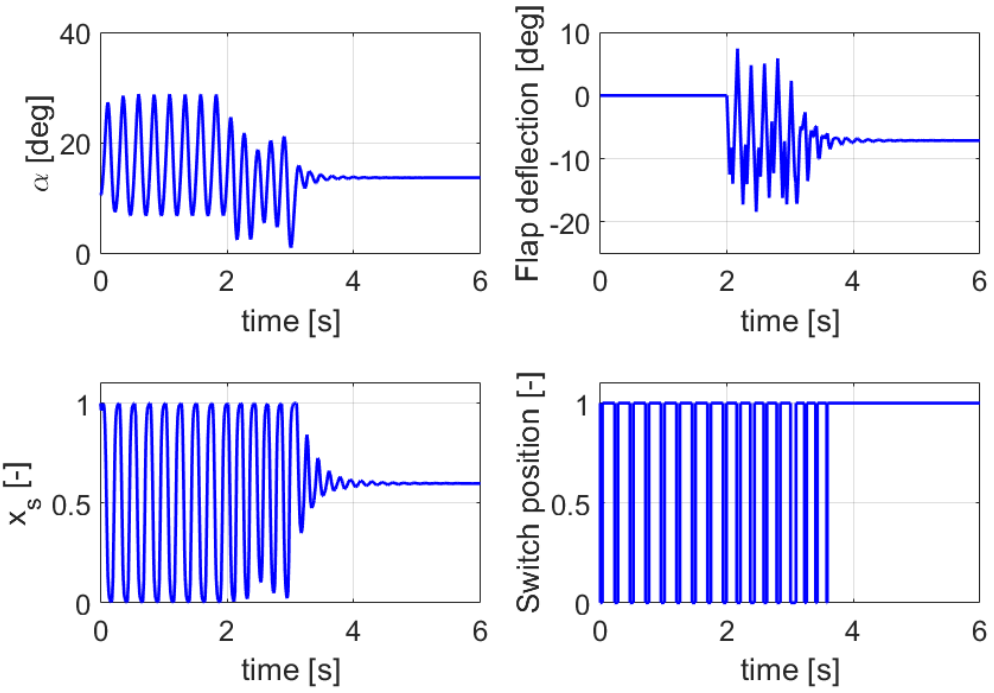

FIGURE 3.14: Angle of attack (deg) , flap deflection (deg), x_s and switch signal as function of the time (s) for $U = 20\ m/s$ with rate saturation. The controller is activated after 2 s.

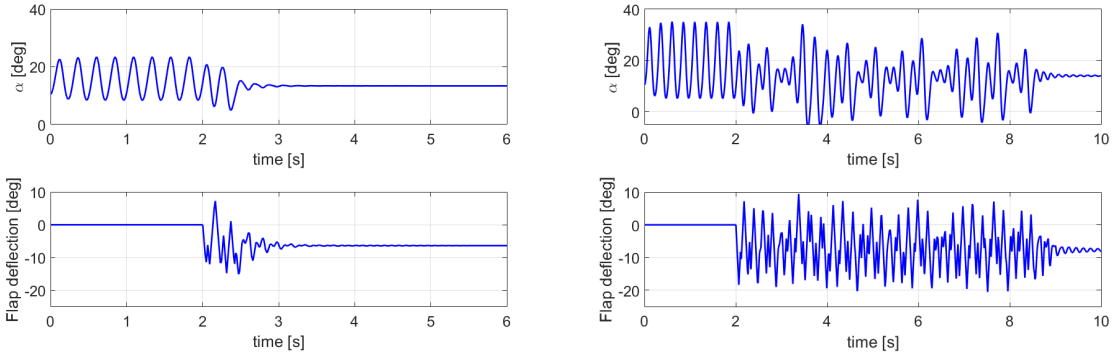

(a) (b)

FIGURE 3.15: Angle of attack (deg) and flap deflection (deg) with rate saturation as function of the time (s) for: (a) $U = 17.5\ m/s$ and (b) $U = 22.5\ m/s$. The controller is activated after 2 s.

3.4.3.2 Conclusion

These numerical examples show how Theorem 2.6 is able to synthesize a controller for a polytopic formulation in presence of rate saturation. However, the region of attraction is one more time limited due to the conservatism introduced by the polytopic formulation but also due to the method itself. Indeed, the formulation of the rate saturation used in Theorem 2.6 requires to augment the system with the input command signal. This signal is now encapsulated in the state vector which is constrained by the definition of the region of attraction. Thus, the problem has now a direct constraint on the input rate and an indirect constraint on the magnitude.

3.5 Chapter Summary

In this chapter, the set of equations developed in Chapter 1 is adapted to the specific problem of stall flutter. Especially, the problem is reduced to a one dimension pitching airfoil. To deal with the nonlinearities present in the aerodynamic equations, a polytopic formulation with uncertain parameters is conveniently introduced. In particular, this formulation allows us to use the control theory to solve the problem. Numerical results are provided to illustrate the ability of each theorem presented in Chapter 2 to stabilize and suppress flutter. The first case considered allows us to validate that the polytopic formulation is adapted to the synthesis of a static feedback controller. The two other cases deal with magnitude and rate input saturation. However, if the controller successfully suppresses flutter, its region of attraction, where the convergence is guaranteed, does not include the flutter conditions. This illustrates the conservatism induced by the problem formulation as well the theorems themselves.

This work provides an interesting basis in view of being applied to an active flow control using blowing actuation which proves to be extremely challenging. Indeed, this complex method has a highly nonlinear dynamic including saturations and is widely state vector dependent. Thus, this work intends to provide the necessary tools for control under constraints to be applied to a wide class of actuators including AFC.

Conclusion

Due to the diversity of nonlinearities which are often present in aeroelastic model, the problem of controlling such class of complex systems is often reduced to a linearization of the equations in order to apply more classical techniques. This work aims at applying nonlinear control theory to aeroelastic systems. Especially, nonlinearities such as switched parameters depending on the state, bilinear terms or uncertainties are considered as well as saturation in order to offer a general approach to aeroelastic control. This work tends to be general enough to be extended to the case of active flow control, such as blowing actuation.

Contributions

In Chapter 1, an aeroelastic model is developed. The validity of the aerodynamic model is demonstrated for a NACA 0018 pitching wing oscillating in a flow at low Reynolds number which exhibits separation and vortex shedding. The model is particularly efficient at predicting the leading edge vortex shedding. If more identification could be performed using a wide range of variations of the different angles and the reduced frequencies, the parameters obtained allow us to validate the model and especially its ability to capture the hysteresis as well as the vortex shedding on an oscillating wing. However, like many advanced aeroelastic models, nonlinearities are present which can make the associated control problem challenging.

In the second chapter, linear quadratic results are presented for LTI systems and extended to polytopic systems with unknown varying parameters. Especially, magnitude and rate saturations are considered. Using LMI formulations, the theorems allow us not only to provide a design technique to synthesize a controller but also define a region of attraction guaranteeing the local stability. The rate saturation formulation proves to be an extension of the magnitude saturation where an augmented system is considered.

In the third chapter, the structure of the initial model developed in Chapter 1 is studied. Indeed, the model proposed presents various nonlinearities such as switching parameters,

shifted states or bilinear terms. Moreover, the actuators have non-negligible saturations, which need to be taken into account. To study this complex system, the set of equations are conveniently manipulated to encapsulate all these nonlinearities. Especially, the following approach was used to address each nonlinearity type:

Bilinear terms: one of the states of the system was bounded but not directly measurable. Therefore, it was considered as an uncertain varying parameter.

Switched system: following the technique used in [74], the set of parameters, which takes only two values depending on the state of the system, is conveniently assumed to vary linearly between these two values. As the switching signal is not accurately accessible, this bounded varying set of parameters is then considered as uncertain.

Uncertainties: Uncertainties on the freestream velocity are also considered. The variation is supposed to be bounded and then considered also as an uncertain parameter.

The bounded uncertain parameters define a polytope, which leads to a multiaffine formulation, allowing us to apply the control theory presented in the previous chapter.

The technique proves to be successful in all the different cases covered in this study. Especially, the design methods presented in Chapter 2 allow us to successfully obtain a controller in the presence of magnitude saturation and also rate saturation over the polytope defined by the uncertainties considered in the formulation. However, due to the formulation of the model, some conservatism is involved. The guarantee of stability provided by the theorem is no longer determined in flutter conditions as the initial conditions are not included in the regions of attraction. Relaxation on the cost function but also adjustment of the weighting functions involved in the LQ techniques should be considered. However, due to numerical issues, probably due to the matrix conditioning, the consideration of these options has been limited.

Future Work

As mentioned previously, the aerodynamic model proposed in Chapter 1 predicts particularly well the hysteresis and oscillations due to the vortex shedding on the range of the angles of attack and reduced frequencies considered by the experiments. However, it could be interesting to collect more data on a wider range of variation in order to better train the model. Especially, in the case of flutter suppression, the amplitude of the angle of attack can rapidly grow, even if it is bounded. Also, although the approach only focuses on the pitch oscillations to obtain a better understanding of the phenomenon involved, a combined pitch and plunge motion can be considered.

A natural extension of this work would eventually consist of experimental validations of the controllers developed and simulated. For this purpose, it will be necessary to consider output feedback control. Developing observers could also be beneficial to reduce the conservatism involved in the model as the dynamics of the state would now be considered. A similar approach in [89], based on Takagi-Sugeno theorem [47], has been used following these considerations. More generally, Linear Parameter Varying tools could be investigated.

The approach used in this work concerning the switched system proves to be particularly conservative. Considering the theory developed for such a class of system could be beneficial.

Finally, one of the main extensions considered, and which has motivated the approach of this PhD thesis, concerns the application to Active Flow Control. The model developed in the first chapter proves to be interesting in the sense that it provides a low computational model, involving few parameters, and predicting LEV shedding. Active Flow Control, especially blowing air at the leading edge, tends to control the boundary layer including separation and vorticity. From that perspective, the model developed earlier can be extremely beneficial. If the early work realized until now has not permitted us to obtain the necessary controllability because of the weak quantity of air blown, some trends have been identified and are encouraging to apply the previous model and control to the wing equipped with AFC [29].

Bibliography

[1] WJ McCroskey, LW Carr, and KW McAlister. Dynamic stall experiments on oscillating airfoils. *AIAA Journal*, 14(1):57–63, 1976.

[2] Mikhail Goman and Alexander Khrabrov. State-space representation of aerodynamic characteristics of an aircraft at high angles of attack. *Journal of Aircraft*, 31 (5):1109–1115, 1994.

[3] Konstantinos Zikidis, Alexios Skondras, and Charisios Tokas. Low observable principles, stealth aircraft and anti-stealth technologies. *Journal of Computations & Modelling*, 4(1):129–165, 2014.

[4] Narendra Kumar and Sampat R. Vadera. Stealth materials and technology for airborne systems. In *Aerospace Materials and Material Technologies*, pages 519–537. Springer, 2017.

[5] David R Williams and Jürgen Seidel. Crossed-actuation AFC for lateral-directional control of an ICE-101/saccon ucav. In *8th AIAA Flow Control Conference*, page 3167, 2016.

[6] Lars Rundqwist and Karin Stahl-Gunnarsson. Phase compensation of rate limiters in unstable aircraft. In *Control Applications, 1996., Proceedings of the 1996 IEEE International Conference on*, pages 19–24. IEEE, 1996.

[7] Bei Lu et al. Linear parameter-varying control of an F-16 aircraft at high angle of attack. 2005.

[8] David R Williams, Xuanhong An, Simeon Iliev, Rudibert King, and Florian Reißner. Dynamic hysteresis control of lift on a pitching wing. *Experiments in Fluids*, 56(5):1–12, 2015.

[9] Shakir Jiffri, Sebastiano Fichera, John E Mottershead, and Andrea Da Ronch. Experimental nonlinear control for flutter suppression in a nonlinear aeroelastic system. *Journal of Guidance, Control, and Dynamics*, 2017.

[10] Arnaud Malher. *Amortisseurs passifs non linéaires pour le contrôle de l'instabilité de flottement*. PhD thesis, Paris Saclay, 2016.

[11] Michael Amitay and Ari Glezer. Controlled transients of flow reattachment over stalled airfoils. *International Journal of Heat and Fluid Flow*, 23(5):690–699, 2002.

[12] Yuehan Tan, Thomas M Crittenden, and Ari Glezer. Aerodynamic control of a dynamically pitching vr-12 airfoil using discrete pulsed actuation. In *54th AIAA Aerospace Sciences Meeting*, page 321, 2016.

[13] Stefan Vey, Christian N Nayeri, Christian O Paschereit, and David Greenblatt. Plasma flow control on low aspect ratio wings at low Reynolds numbers. *AIAA paper*, 1222:4–7, 2010.

[14] Casey Fagley, John Farnsworth, Chris Porter, Jürgen Seidel, Thomas McLaughlin, Jinik Lee, and Eunseok Lee. Open-loop dynamics of the asymmetric vortex wake behind a von Kármán ogive at high incidence. *International Journal of Flow Control*, 5(1):59–78, 2013.

[15] Chris Porter, Casey Fagley, John Farnsworth, Jürgen Seidel, and Thomas McLaughlin. Closed-loop flow control of a forebody at a high incidence angle. *AIAA Journal*, 52(7):1430–1440, 2014.

[16] Roeland De Breuker, Mostafa Abdalla, Attilio Milanese, and Pier Marzocca. Optimal control of aeroelastic systems using synthetic jet actuators. In *49th AIAA Structures, Structural Dynamics, and Materials Conference*, page 1726, 2008.

[17] Wesley Kerstens, Jens Pfeiffer, David Williams, Rudibert King, and Tim Colonius. Closed-loop control of lift for longitudinal gust suppression at low Reynolds numbers. *AIAA journal*, 49(8):1721–1728, 2011.

[18] David Greenblatt, Hanns Mueller-Vahl, David Williams, and Florian Reissner. Goman-Khrabrov model on pitching airfoils with flow control. In *8th AIAA Flow Control Conference*, page 4240, 2016.

[19] Hanns F Müller-Vahl, Christoph Strangfeld, Christian N Nayeri, Christian O Paschereit, and David Greenblatt. Control of thick airfoil, deep dynamic stall using steady blowing. *AIAA Journal*, 53(2):277–295, 2014.

[20] Hanns Friedrich Müller-Vahl, Christian Navid Nayeri, Christian Oliver Paschereit, and David Greenblatt. Dynamic stall control via adaptive blowing. *Renewable Energy*, 97:47–64, 2016.

[21] Avraham Seifert, A Darabi, and Israel Wyganski. Delay of airfoil stall by periodic excitation. *Journal of Aircraft*, 33(4):691–698, 1996.

[22] David Greenblatt and Israel J Wygnanski. The control of flow separation by periodic excitation. *Progress in Aerospace Sciences*, 36(7):487–545, 2000.

[23] S Scott Collis, Ronald D Joslin, Avi Seifert, and Vassilis Theofilis. Issues in active flow control: theory, control, simulation, and experiment. *Progress in Aerospace Sciences*, 40(4):237–289, 2004.

[24] Xuanhong An, David R Williams, Jeff Eldredge, and Tim Colonius. Modeling dynamic lift response to actuation. In *54th AIAA Aerospace Sciences Meeting*, 2016.

[25] Xuanhong An, Lou Grimaud, and David R Williams. Feedforward control of lift hysteresis during periodic and random pitching maneuvers. In *Active Flow and Combustion Control 2014*, pages 55–69. Springer, 2015.

[26] Maxime Feingesicht, Cédric Raibaudo, Andrey Polyakov, Franck Kerherve, and Jean-Pierre Richard. A bilinear input-output model with state-dependent delay for separated flow control. In *Control Conference (ECC), 2016 European*, pages 1679–1684. IEEE, 2016.

[27] Maxime Feingesicht, Andrey Polyakov, Franck Kerhervé, and Jean-Pierre Richard. Model-based feedforward optimal control applied to a turbulent separated flow. In *IFAC 2017-20th World Congress of the International Federation of Automatic Control*, page 6, 2017.

[28] Maxime Feingesicht, Andrey Polyakov, Franck Kerhervé, and Jean-Pierre Richard. Sliding mode control for turbulent flows. In *IFAC 2017-20th World Congress of the International Federation of Automatic Control*, page 8, 2017.

[29] Fabien Niel, Casey Fagley, Jürgen Seidel, and Thomas McLaughlin. Modeling of transient blowing actuation using pulse width modulation on a dynamically pitching NACA 0018 airfoil. In *35th AIAA Applied Aerodynamics Conference*, page 3564, 2017.

[30] Wanan Sheng, Rodderic Galbraith, and Frank Coton. A modified dynamic stall model for low Mach numbers. *Journal of Solar Energy Engineering*, 130(3):031013, 2008.

[31] Shao Song, Zhu Qinghua, Chenglin Zhang, and Ni Xianping. Airfoil aeroelastic flutter analysis based on modified leishman-beddoes model at low Mach number. *Chinese Journal of Aeronautics*, 24(5):550–557, 2011.

[32] Jeesoon Choi, Tim Colonius, and David R Williams. Surging and plunging oscillations of an airfoil at low Reynolds number. *Journal of Fluid Mechanics*, 763: 237–253, 2015.

[33] Chen Gang, Sun Jian, and Li Yueming. Active flutter suppression control law design method based on balanced proper orthogonal decomposition reduced order model. *Nonlinear Dynamics*, 70(1):1–12, 2012.

[34] Steven L Brunton and Clarence W Rowley. Empirical state-space representations for Theodorsen's lift model. *Journal of Fluids and Structures*, 38:174–186, 2013.

[35] Andrea Mannarino. *Nonlinear aeroservoelasticity: reduced order modeling and active control*. PhD thesis, 2016.

[36] Gang Chen, Jian Sun, and Yue-Ming Li. Adaptive reduced-order-model-based control-law design for active flutter suppression. *Journal of Aircraft*, 49(4):973–980, 2012.

[37] Thomas W Strganac, Jeonghwan Ko, David E Thompson, and Andrew J Kurdila. Identification and control of limit cycle oscillations in aeroelastic systems. *Journal of Guidance Control and Dynamics*, 23(6):1127–1133, 2000.

[38] Jean-Jacques E Slotine, Weiping Li, et al. *Applied nonlinear control*, volume 199. Prentice hall Englewood Cliffs, NJ, 1991.

[39] Sohrab Haghighat, Zhiwei Sun, Hugh HT Liu, and Junqiang Bai. Robust stall flutter suppression using $\mathcal{H}_2/\mathcal{H}_\infty$ control. In *ASME 2014 Dynamic Systems and Control Conference*. American Society of Mechanical Engineers, 2014.

[40] Hugo Lhachemi, David Saussie, and Guchuan Zhu. Flutter suppression for a two degree of freedom aeroelastic wing section: a structured h-infinity-based gain-scheduling approach with explicit hidden coupling terms handling. In *AIAA Guidance, Navigation, and Control Conference*, page 1735, 2017.

[41] Zhiwei Sun, Sohrab Haghighat, Hugh HT Liu, and Junqiang Bai. Time-domain modeling and control of a wing-section stall flutter. *Journal of Sound and Vibration*, 340:221–238, 2015.

[42] Wen Fan, Hugh HT Liu, and Raymond HS Kwong. Linear parameter-varying control of a wing-section stall flutter. In *ASME 2014 Dynamic Systems and Control Conference*, pages V001T01A003–V001T01A003. American Society of Mechanical Engineers, 2014.

[43] Zebb Prime, Ben Cazzolato, Con Doolan, and Thomas Strganac. Linear-parameter-varying control of an improved three-degree-of-freedom aeroelastic model. *Journal of Guidance, Control, and Dynamics*, 33(2):615–619, 2010.

[44] George Platanitis and Thomas W Strganac. Control of a nonlinear wing section using leading-and trailing-edge surfaces. *Journal of Guidance, Control, and Dynamics*, 27(1):52–58, 2004.

[45] Steven L Brunton and Bernd R Noack. Closed-loop turbulence control: Progress and challenges. *Applied Mechanics Reviews*, 67(5):050801, 2015.

[46] Jinwu Xiang, Yongju Yan, and Daochun Li. Recent advance in nonlinear aeroelastic analysis and control of the aircraft. *Chinese Journal of Aeronautics*, 27(1):12–22, 2014.

[47] Tomohiro Takagi and Michio Sugeno. Fuzzy identification of systems and its applications to modeling and control. *IEEE transactions on systems, man, and cybernetics*, (1):116–132, 1985.

[48] Van Khiem Truong. A 2-d dynamic stall model based on a Hopf bifurcation. In *European Rotorcraft Forum*. Associazione Italiana di Aeronautica ed Astronautica, 1993.

[49] Fabien Niel, Alexandre Seuret, Luca Zaccarian, and Casey Fagley. Robust LQR control for stall flutter suppression: A polytopic approach. In *IFAC-PapersOnLine*, volume 50, pages 11367–11372. Elsevier, 2017.

[50] Fabien Niel, Casey P Fagley, Jurgen Seidel, and Thomas E McLaughlin. Reduced order modeling of a dynamically pitching NACA 0018 airfoil. In *55th AIAA Aerospace Sciences Meeting*, 2017.

[51] Fabien Niel, Yann Ameho, Jean-Marc Biannic, François Defaÿ, and Caroline Bérard. A novel parameter varying controller synthesis method for quadrotor control. In *Proceedings of the AIAA Guidance, Navigation, and Control Conference*, 2013.

[52] Yann Ameho, Fabien Niel, François Defaÿ, Jean-Marc Biannic, and Caroline Bérard. Adaptive control for quadrotors. In *Robotics and Automation (ICRA), 2013 IEEE International Conference*, pages 5396–5401. IEEE, 2013.

[53] Thomas E Noll, John M Brown, Marla E Perez-Davis, Stephen D Ishmael, Geary C Tiffany, and Matthew Gaier. Investigation of the Helios prototype aircraft mishap. *Mishap Report, NASA Report*, 1, 2004.

[54] Theodore Theodorsen. General theory of aerodynamic instability and the mechanism of flutter. Technical Report 496, NASA, 1935.

[55] Ramin Modarres. *Semi-Empirical Modeling of Two-Dimensional and Three-Dimensional Dynamic Stall*. PhD thesis, 2016.

[56] Laurent Beaudet. *Etude expérimentale et numérique du décrochage dynamique sur une éolienne à axe vertical de forte solidité*. PhD thesis, Université de Poitiers, 2014.

[57] Wayne Johnson. Rotorcraft dynamics models for a comprehensive analysis. In *Annual Forum Proceedings-American Helicopter Society*, volume 54, pages 452–471. American Helicopter Society, 1998.

[58] WAAM Bierbooms. A comparison between unsteady aerodynamic models. *Journal of Wind Engineering and Industrial Aerodynamics*, 39(1):23–33, 1992.

[59] R Dat, CT Tran, and Didier Petot. Modèle phénomènologique de décrochage dynamique sur profil d'hélicoptère. *TP ONERA 1979-149*, 1979.

[60] Loren A Ahaus. *An airloads theory for morphing airfoils in dynamic stall with experimental correlation*. Washington University in St. Louis, 2010.

[61] Murray Tobak and Gary T Chapman. Nonlinear problems in flight dynamics involving aerodynamic bifurcations. *NASA Technical Memorandum*, 1985.

[62] J Gordon Leishman. Challenges in modelling the unsteady aerodynamics of wind turbines. *Wind energy*, 5(2-3):85–132, 2002.

[63] J Gordon Leishman and TS Beddoes. A semi-empirical model for dynamic stall. *Journal of the American Helicopter society*, 34(3):3–17, 1989.

[64] J Gordon Leishman. *Principles of Helicopter Aerodynamics with CD Extra*. Cambridge university press, 2006.

[65] Xavier Amandolese, Sébastien Michelin, and Maxime Choquel. Low speed flutter and limit cycle oscillations of a two-degree-of-freedom flat plate in a wind tunnel. *Journal of Fluids and Structures*, 43:244–255, 2013.

[66] Van Khiem Truong. Prediction of helicopter rotor airloads based on physical modeling of 3-D unsteady aerodynamics. 1996.

[67] Khiem Van Truong. Modeling aerodynamics, including dynamic stall, for comprehensive analysis of helicopter rotors. *Aerospace*, 4(2):21, 2017.

[68] Albert Medina, V Michael, David Williams, Xuanhong An, and Maziar Hemati. Modeling of conventional flaps at high deflection-rate. In *55th AIAA Aerospace Sciences Meeting*, page 1230, 2017.

[69] David R Williams, Florian Reissner, David Greenblatt, Hanns Mueller-Vahl, and Christoph Strangfeld. Modeling lift hysteresis with a modified Goman-Khrabrov model on pitching airfoils. In *45th AIAA Fluid Dynamics Conference*, 2015.

[70] Natalie Ramos Pedroza, William MacKunis, and Vladimir Golubev. A new method of synthetic jet actuator-based lco suppression using an output feedback control strategy. In *Control, Automation and Systems (ICCAS), 2015 15th International Conference on*, pages 1463–1468. IEEE, 2015.

[71] Casey Fagley, Jürgen Seidel, and Thomas McLaughlin. Cyber-physical flexible wing for aeroelastic investigations of stall and classical flutter. *Journal of Fluids and Structures*, 67:34–47, 2016.

[72] Norizham Abdul Razak, Thomas Andrianne, and Grigorios Dimitriadis. Flutter and stall flutter of a rectangular wing in a wind tunnel. *AIAA journal*, 49(10): 2258–2271, 2011.

[73] Lennart Ljung. *MATLAB: System Identification Toolbox: User's Guide Version 4*. The Mathworks, 1995.

[74] Carlos Olalla, Ramon Leyva, Abdelali El Aroudi, and Isabelle Queinnec. Robust LQR control for pwm converters: an LMI approach. *IEEE Transactions on industrial electronics*, 56(7):2548–2558, 2009.

[75] Luca Zaccarian and Andrew R Teel. *Modern anti-windup synthesis: control augmentation for actuator saturation*. Princeton University Press, 2011.

[76] Tingshu Hu and Zongli Lin. *Control systems with actuator saturation: analysis and design*. Springer, 2001.

[77] Sophie Tarbouriech, Germain Garcia, João Manoel Gomes da Silva Jr., and Isabelle Queinnec. *Stability and stabilization of linear systems with saturating actuators*. Springer-Verlag London Ltd., 2011.

[78] Sergio Galeani, Sophie Tarbouriech, Matthew Turner, and Luca Zaccarian. A tutorial on modern anti-windup design. *European Journal of Control*, 15(3-4):418–440, 2009.

[79] Sophie Tarbouriech, Christophe Prieur, and João Manoel Gomes Da Silva. Stability analysis and stabilization of systems presenting nested saturations. *IEEE Transactions on Automatic Control*, 51(8):1364–1371, 2006.

[80] Luca Zaccarian and Andrew R Teel. Analysis and synthesis of feedback systems: quadratic functions and LMIs. 2009.

[81] Alexandre Seuret, Christophe Prieur, Sophie Tarbouriech, and Luca Zaccarian. Lq-based event-triggered controller co-design for saturated linear systems. *Automatica*, 74:47–54, 2016.

[82] Sergio Galeani, Simona Onori, Andrew Richard Teel, and Luca Zaccarian. A magnitude and rate saturation model and its use in the solution of a static anti-windup problem. *Systems and Control Letters*, 57(1):1–9, 2008.

[83] Nailu Li, Mark J Balas, Hua Yang, and Wei Jiang. Flow control and stability analysis of rotating wind turbine blade system. *Journal of Guidance, Control, and Dynamics*, 2016.

[84] Douglas D Bueno, Clayton R Marqui, Luiz Góes, and Paulo JP Gonçalvez. Aeroelastic stability analysis using linear matrix inequalities. *Journal of the Brazilian Society of Mechanical Sciences and Engineering*, 34(SPE2):545–551, 2012.

[85] Stephen Boyd, Laurent El Ghaoui, Eric Feron, and Venkataramanan Balakrishnan. *Linear matrix inequalities in system and control theory*. SIAM, 1994.

[86] Calin Belta, Luc C.G.J.M. Habets, and Vijay Kumar. Control of multi-affine systems on rectangles with applications to hybrid biomolecular networks. In *Decision and Control, 2002, Proceedings of the 41st IEEE Conference on*, volume 1, pages 534–539, 2002.

[87] Pascal Gahinet, Arkadii Nemirovskii, Alan J Laub, and Mahmoud Chilali. The LMI control toolbox. In *Decision and Control, 1994., Proceedings of the 33rd IEEE Conference on*, volume 3, pages 2038–2041. IEEE, 1994.

[88] Gary Balas, Richard Chiang, Andy Packard, and Michael Safonov. Robust control toolbox. *For Use with Matlab. User's Guide, Version*, 3, 2005.

[89] Víctor Costa da Silva Campos, Anh-Tu Nguyen, and Reinaldo Martinez Palhares. LMI-based adaptive control for uncertain polytopic systems. In *Decision and Control (CDC), 2016 IEEE 55th Conference on*, pages 3222–3227. IEEE, 2016.

THÈSE

En vue de l'obtention du

DOCTORAT DE L'UNIVERSITÉ DE TOULOUSE

Délivré par :

Institut Supérieur de l'Aéronautique et de l'Espace

Présentée et soutenue par :
Fabien NIEL

le vendredi 26 janvier 2018

Titre :

Modélisation et contrôle d'une aile en présence d'oscillations Aéroélastiques de grande amplitude et à faible nombre de Reynolds

Modeling and control of a wing at low Reynolds number with high amplitude aeroelastic oscillations

---

École doctorale et discipline ou spécialité :
EDSYS : Automatique 4200046

Unité de recherche :
Laboratoire d'Analyse et d'Architecture des Système - CNRS

Directeur/trice(s) de Thèse :

M. Luca ZACCARIAN et M. Alexandre SEURET

Jury :
Mme Isabelle QUEINNEC - Président du Jury
M. Marc JUNGERS - Rapporteur
M. Marco LOVERA - Rapporteur
M. Charles POUSSOT-VASSAL - Membre du Jury
M. Giorgio VALMORBIDA - Membre du Jury
M. Luca ZACCARIAN - Directeur de thèse

Résumé

A fort angles d'attaque ou à faible nombre de Reynolds, l'écoulement sur les ailes d'avion ou les pales d'hélicoptères ou d'éoliennes peut se séparer, ce qui peut éventuellement mener à des couplages aéroélastiques tels que le phénomène de flottement (flutter). Ces instabilités peuvent être particulièrement limitantes pour de nombreuses applications, voire destructrices. L'objectif de cette thèse est de s'intéresser à la modélisation et au contrôle d'une aile oscillant dans des conditions de flutter ainsi que de fournir une approche générale pour aborder ce problème. Tout d'abord, un modèle aéroélastique est développé en s'appuyant sur de précédents travaux. Le modèle est une extension de celui proposé par Goman-Khrabrov, et modifié par Williams, par l'utilisation du modèle ONERA BH. Si la première composante de ce modèle permet de rendre compte du phénomène d'hystérésis des charges aérodynamiques d'une aile en oscillation, la seconde permet d'inclure le détachement des tourbillons ainsi que le phénomène de décrochage dynamique qui peut être observé. Cette seconde composante est particulièrement délicate à prédire alors qu'elle joue un rôle important dans la dynamique de l'aile. Le modèle aérodynamique est alors entraîné et comparé avec succès aux résultats expérimentaux obtenus pour une aile rigide de type NACA 0018 oscillant autour de son axe de tangage. Ce modèle, comme de nombreux modèles aéroélastiques ou aérodynamiques, souffre d'une complexité inhérente et de non-linéarités qui rendent son analyse et son contrôle particulièrement compliqués du point de vue de l'automatique. Pour cette raison, l'ensemble d'équations a été modifié afin d'inclure les non-linéarités dans une formulation polytopique dont les paramètres sont incertains. Des stratégies dédiées aux systèmes à temps invariant sont alors étendues aux systèmes polytopiques. De plus, les saturations en vitesse ou en position qui sont un problème majeur et récurent de la dynamique du vol, sont considérées comme une contrainte supplémentaire dans la boucle d'asservissement. S'appuyant sur la théorie de la commande linéaire quadratique, plusieurs théorèmes sont alors développés en utilisant une formulation à partir des inégalités des matrices linéaires, afin de permettre non seulement de synthétiser un correcteur stabilisant mais aussi de définir une région d'attraction. Les théorèmes sont alors appliqués avec succès au cas du flottement de décrochage (stall flutter), stabilisant le système en boucle fermée en présence de saturations en position et en vitesse, ce qui montre le potentiel des contributions développées dans ce travail de thèse.

Résumé court

L'objectif de cette thèse est de fournir une approche générale permettant d'aborder les problèmes de contrôle aéroélastique. Tout d'abord, un modèle d'aile oscillante est développé afin de rendre compte des phénomènes d'hystérésis des charges aérodynamiques et de décrochage dynamique qui peut être observé, particulièrement à fort angles d'attaque ou à faible nombre de Reynolds. Le modèle est alors entraîné et comparé avec succès aux résultats expérimentaux obtenus pour une aile NACA 0018. Ce modèle, comme de nombreux modèles aérodynamiques, souffre d'une complexité inhérente et de non-linéarités qui rendent son analyse et son contrôle complexes. Par conséquent, le modèle a été modifié afin d'inclure les non-linéarités dans une formulation polytopique aux paramètres incertains. S'appuyant sur la théorie de la commande linéaire quadratique et utilisant les inégalités des matrices linéaires, plusieurs théorèmes sont développés, considérant les saturations qui sont un problème majeur et récurent de la dynamique du vol. Les théorèmes sont alors appliqués avec succès au cas du stall flutter en présence de saturations en position et en vitesse.

Contents

À ma femme et à mes enfants à qui j'ai manqué si souvent...

Introduction

Contexte et motivation

Si les avions de combat ou bombardiers modernes tendent à augmenter leurs performances en termes de charges utiles, de rayon d'action, de plafond, d'efficacité ou encore de manœuvrabilité, l'une des caractéristiques principales des avions actuels comme des avions futurs, reste la *furtivité*. La *furtivité* est définie par la capacité d'un véhicule à réduire sa signature Radar, acoustique, infra-rouge ou visible afin de le rendre faiblement observable. Bénéficiant de géométries et de matériaux adaptés, les avions Lockheed Martin F-117A Nighthawk, Lockheed Martin F-22 Raptor ou F-35 Lightning II, Northrop Grumman X-47B ou le Dassault nEUROn, avion expérimental de combat sans pilote inspiré du Northrop B-2 Spirit, sont d'excellents exemples des efforts réalisés par les constructeurs pour obtenir cette capacité essentielle [1, 2].

En effet, malgré l'exceptionnelle manœuvrabilité dont font preuve les nouveaux avions de chasse, un combat air-air de type dogfight semble de moins en moins probable au regard des avancées importantes en termes de détection ou de ciblage longue distance. Les systèmes d'avioniques récents de même que les missiles, ont amélioré leur portée et leur efficacité de façon si importante que les armements sont délivrés bien avant le contact visuel de la cible. Par conséquent, l'une des clés de réussite réside dans la capacité à pouvoir intervenir aussi discrètement que possible, c'est-à-dire aussi furtivement que possible. La section Radar (RCS) est l'une des mesures de la furtivité d'un avion. Réduire la section Radar d'un avion implique un choix adapté de matériaux et de géométries des différentes parties de l'avion, dont la stratégie de contrôle de vol fait sans aucun doute partie. En effet, les mouvements des différents actionneurs de l'avion viennent modifier plus ou moins temporairement la forme de l'avion, transformant ainsi la signature Radar. Il convient donc de développer des techniques de contrôle adaptées garantissant non seulement la stabilité et le haut niveau de performance de l'avion, mais aussi sa faible visibilité. Si les valeurs restent difficilement accessibles dans la littérature,

il est reconnu que les saturations des actionneurs tant en amplitude qu'en vitesse permettent de maintenir le niveau de furtivité désiré en réduisant l'exposition des surfaces de réflexion.

Les surfaces de contrôle classiques comme les volets, les ailerons ou les gouvernes de profondeur sont utilisées pour assurer le contrôle de l'avion. Cependant, le contrôle actif de l'écoulement, *active flow control* en anglais, présente également de nombreux avantages, notamment dans cette perspective de furtivité. En effet, ce type d'actionneur permet de souffler ou d'aspirer de l'air dans l'écoulement afin de modifier celui-ci et d'obtenir les effets désirés en termes de force résultante ou de moment. Ces techniques permettent clairement de s'affranchir de surfaces amovibles pouvant altérer la signature Radar. L'*active flow control* n'est pas nouveau puisque celui-ci à été utilisé très tôt dans l'aviation, notamment en soufflant de grosses quantités d'air sur les ailes dans les phases critiques comme le décollage. Ceci se révélait particulièrement intéressant sur les avions présents sur les porte-avions, nécessitant rapidement de grandes performances du fait des longueurs limites des pistes de décollage. Cependant, ces techniques ont souffert des poids importants des actionneurs, tout comme des débits massiques d'air nécessaire extrait directement des moteurs. De plus, l'amélioration des performances aérodynamiques des avions actuels ont rendu obsolètes ces méthodes.

Si ces technologies ne semblent donc plus adaptées à des augmentations de portance, l'*active flow control* peut aussi être envisagé pour améliorer la contrôlabilité en vol des avions. Des projets ambitieux comme l'*Innovative Control Effectors* (ICE) [3], visent pour des questions de furtivité à remplacer complètement les contrôles de surface par de puissants actionneurs soufflant de l'air. Cependant, il est possible d'envisager des solutions hybrides pour améliorer la dynamique du vol dans de telles conditions. Le problème de la dynamique du vol demeure particulièrement complexe du fait des nombreux sous-problèmes qu'il peut contenir en termes de performances globales, d'efficacité, de phénomènes de pompage, ou *Pilot induced oscillations* (PIO) [4], de manœuvrabilité à haute incidence [5] ou encore d'instabilités aéroélastiques comme le flottement ou le galop parmi tant d'autres. Tous ces problèmes restent divers et délicats, particulièrement sur un avion complet.

Pour obtenir une meilleure compréhension de ces phénomènes complexes, notamment pour les questions aéroélastiques, le problème général est bien souvent restreint à l'étude d'une aile oscillante. D'apparence beaucoup plus simple, il n'en demeure pas moins tout à fait approprié et complexe du fait des nombreuses non-linéarités dans la description de la dynamique de l'écoulement. Ces questions d'instabilité aéroélastique étant un problème majeur en dynamique du vol, de nombreux travaux de recherche ont été publiés à ce

sujet. Si ces travaux concernent principalement les surfaces de contrôle classique, de nombreux autres travaux, notamment récents, s'intéressent à l'*active flow control* [6, 7].

L'*active flow control* (AFC) est l'action de modifier activement l'écoulement autour d'un objet afin d'obtenir un effet désiré. Cette définition inclut les surfaces de contrôle mobiles comme les volets ou les gouvernes, mais également les actionneurs soufflant ou aspirant de l'air. Contrairement à l'AFC, on peut définir du contrôle passif pour lequel les actionneurs ne nécessitent pas d'ajout d'énergie. C'est le cas des matériaux ou oscillateurs passifs tels que définis dans [8], ou encore des systèmes à géométrie fixe comme les générateurs de tourbillons positionnés sur les ailes, notamment sur les gouvernes de profondeurs. Cependant, dans ce manuscrit, seul l'*active flow control* sera considéré et limité aux actionneurs de soufflage ou d'aspiration.

De nombreux actionneurs ont été développés et étudiés en AFC. Ces études ont permis de comprendre leur fonctionnement, d'évaluer leur performance, de les optimiser pour réduire les masses d'air employées, de faire varier leurs éventuelles fréquences, mais également de modéliser leur dynamique [9]. On peut citer parmi les principaux actionneurs : les actionneurs à air pulsé [10], à plasma [11–13], à jet synthétique [14], ou encore les actionneurs à aspiration ou à soufflage [15].

Les actionneurs soufflant de l'air connaissent un intérêt grandissant, comme le montrent les récents travaux conduits par Williams [6], Greenblatt [16] et Muller-Vahl [17, 18]. Ces études présentent l'effet sur le coefficient de portance des actionneurs soufflant en continu et proposent une modélisation basée sur les travaux de Goman et Khrabrov. En utilisant ces techniques, la quantité d'air peut être ajustée en variant la vitesse du jet de l'actionneur. Une faible quantité d'air s'avère être peu efficace voire diminue les performances de l'aile.

Cependant, l'efficacité de la pulsation période pour exciter la couche limite et obtenir un contrôle de l'écoulement a aussi été démontrée à travers l'emploi de différents actionneurs [19]. Une synthèse de ces différentes recherches peut être trouvée dans les travaux de Greenblatt & Wygnanski [20] ou Collis [21].

Malgré les diverses études publiées sur ce sujet, la modélisation et la compréhension de l'AFC restent extrêmement délicates. De récents travaux ont été réalisés en ce sens, notamment en utilisant des actionneurs soufflant de l'air [22–26]. La quantité d'air soufflée peut éventuellement être modifiée et être utilisée comme signal de commande. Dans [27], une technique de modulation d'amplitude (PWM) est employée à partir d'une pression d'air constante. L'objectif est d'obtenir un signal de commande variable basée sur le rapport cyclique. Bien que des effets encourageants ont été observés, la faible

quantité d'air pulsé n'a pas permis de développer un modèle précis de l'effet de ce type d'actionneur.

Cependant, dans tous les cas, le contrôle considéré souffre du manque d'un modèle précis ou d'un degré de modélisation trop important, qui limite le développement de correcteur avancé. Particulièrement, les actionneurs soufflant en bord d'attaque interagissent avec les nappes tourbillonnaires qui peuvent se produire à cet endroit. La modélisation et le contrôle de cette vorticité en bord d'attaque, ou bord de fuite, restent très délicats. Du fait de leur faible énergie et de leurs propriétés de séparation, les faibles nombres de Reynolds sont des cas particulièrement intéressants pour illustrer ces phénomènes complexes et ont focalisé l'attention dans de nombreuses recherches [28–30].

La compréhension et la modélisation de l'écoulement demeurent un champ de recherche fertile. De nombreuses techniques et stratégies ont été utilisées pour traiter le problème de la modélisation, en essayant par exemple de capturer un maximum d'énergie présente dans l'écoulement [31] ou les principaux modes de sa dynamique. Cependant, ces méthodes peuvent souffrir d'un manque de sens physique des différents et souvent nombreux états du modèle. D'un autre côté, des modèles semi-empiriques plus proches de la physique des systèmes peuvent être développés, mais restent souvent limités par leur apparente simplicité. Si les modèles plus précis semblent donc logiquement plus attractifs, leur complexité et leur grand nombre d'états les rendent peu adaptés aux techniques de contrôle. En effet, en théorie du contrôle, un correcteur est réalisé pour calculer une commande permettant d'obtenir la sortie désirée. Ce type de commande correspond à du contrôle en boucle ouverte. Au contraire, il est possible de calculer à chaque instant une commande en utilisant les informations de l'état du système ou de ses sorties. On parle dans ce cas de boucle fermée, qui permet d'être beaucoup plus robuste aux perturbations extérieures, c'est-à-dire qu'elle permet de conserver les performances désirées malgré des variations imprévisibles de l'état (rafale de vent, conditions initiales...). Néanmoins, les performances du système en boucle fermée dépendent largement de la nature des perturbations, des incertitudes ou même du correcteur lui-même. La théorie du contrôle permet de synthétiser des correcteurs pour une large gamme de systèmes, de perturbations, d'incertitudes et de performances recherchées. La complexité des correcteurs dépend de tous ces paramètres. En particulier, la théorie du contrôle s'appuie, sauf pour certaines synthèses particulières, sur un modèle de synthèse qui peut être différent du modèle de simulations au plus près du système réel. En effet, afin d'appliquer un contrôle classique et obtenir un correcteur simple (évitant des calculs et des temps de calcul inutiles), le modèle de synthèse doit être aussi simple que possible tout en préservant les performances en boucle fermée. Ceci nous permet de comprendre le nécessaire compromis entre :

- *Un modèle trop complexe* qui permet de reproduire précisément les états d'un système. Cependant, il souffre d'un ordre du système important qui complexifie son contrôle.

- *Et un modèle trop simple* qui permet d'appliquer simplement les outils de la théorie du contrôle mais peut ne pas reproduire assez fidèlement le comportement du système.

Ce compromis s'applique tout particulièrement au contrôle des écoulements dont les équations du système peuvent être particulièrement complexes. Pour cette raison, les Modèles d'ordre réduit (ROM) pour le contrôle des écoulements sont devenus un axe de recherche important afin d'appliquer des méthodes de contrôle plus avancées, obtenant ainsi un meilleur compromis entre complexité et fidélité du système [32–34].

Les non-linéarités qui sont souvent présentes dans les équations du système sont l'une de ces complexités. Plusieurs travaux abordent cette problématique [7, 35]. La linéarisation par bouclage à été très utilisée dans ce contexte. Dans cette méthode, les non-linéarités sont encapsulées dans la commande par inversion de la dynamique du système. Le système résultant est un système linéaire dont le contrôle est particulièrement bien décrit par la théorie. Cependant, la linéarisation par bouclage peut ne pas être adaptée pour les systèmes singuliers et n'est pas robuste aux incertitudes et paramètres inconnus [36]. Dans [37], un correcteur robuste est développé en utilisant une norme mixte $\mathcal{H}_2/\mathcal{H}_\infty$ prenant en compte les variations de vitesse. Dans [38], une méthode de variation de gain $\mathcal{H}_\infty$ est développée. Le contrôle quadratique linéaire a également été largement utilisé, notamment dans [31, 35, 39, 40] ou [41], qui considère une raideur non linéaire en torsion et une variation de vitesse. Dans [42], un correcteur de bord d'attaque et bord de fuite est développé. Une synthèse des nombreux travaux réalisés dans ces domaines est effectuée dans [43, 44]. La plupart de ces travaux utilisent des méthodes de contrôle par correcteurs adaptatifs, c'est-à-dire que le correcteur varie avec les paramètres variants du système. Lorsque ceux-ci sont linéaires, on parle alors de Système linéaire à paramètres variants (LPV). Le fait que le correcteur puisse varier avec les paramètres assure une plus grande robustesse en boucle fermée. Cette approche est motivée par le théorème de Takagi-Sugeno [45], établissant que chaque système peut être représenté par un système LPV ou un système polytopique. Cependant, les paramètres du système ne sont pas nécessairement connus et les méthodes présentées précédemment ne sont alors plus applicables.

Contributions

L'objectif de ce travail est de contrôler une aile rigide soumise à des oscillations en tangage de forte amplitude et à faible nombre de Reynolds. Bien que ces problèmes aient été abordés en utilisant des méthodes de contrôle conventionnelles avec un volet de bord de fuite, ce travail a pour objectif de pouvoir être étendu aux méthodes par *active flow control*. En effet, du fait de sa complexité, le problème d'*active flow control* doit être adressé par étapes, consistant tout d'abord en la proposition d'un modèle permettant une modélisation et une compréhension du phénomène de séparation et de lâcher tourbillonnaire. Ce modèle doit ensuite être étendu à une modélisation des effets d'*active flow control* puis en l'application d'une méthode de contrôle adaptée. Si le modèle de l'actionneur d'AFC n'a pu être complété lors de ces travaux, trois contributions principales permettent d'apporter des réponses à cette problématique. Tout d'abord, un modèle aérodynamique incluant une représentation du décrochage dynamique est développé à faible nombre de Reynolds, afin de prédire la séparation et le lâcher tourbillonnaire. Dans un second temps, des résultats de la théorie quadratique linéaire sont développés en présence de saturation et étendus aux systèmes polytopiques. Enfin, la dernière contribution consiste en une proposition de formulation intéressante du modèle non linéaire aéroélastique en un système polytopique incertain, permettant d'offrir une solution au problème de flottement de décrochage pour une aile rigide.

Organisation du manuscrit

A partir de ces objectifs, le manuscrit est organisé en trois chapitres, comme suit :

Le Chapitre 1 présente un nouveau modèle d'ordre réduit d'une aile oscillante basé sur les travaux de l'équipe du Dr. William et du Dr. Truong. Le système d'équations à paramètres variants permet notamment de modéliser le lâcher de nappes tourbillonnaires sur une aile oscillante. Les paramètres de ce modèle sont identifiés pour une aile oscillante de type NACA 0018 à partir de données expérimentales. Les résultats du modèle du coefficient de moment sont comparés aux résultats expérimentaux. Une fois la structure du modèle validée, celui-ci peut être utilisé pour une analyse et un contrôle du système.

Le Chapitre 2 présente plusieurs résultats théoriques concernant l'analyse et le contrôle optimal du système linéaire et étendu aux systèmes multi-affines en présence de saturations. Les théorèmes détaillés sont formulés à partir d'Inégalités matricielles quadratiques (LMI). Un exemple académique d'un système masse-ressort est utilisé afin d'illustrer numériquement les différents théorèmes.

Le Chapitre 3 présente la contribution principale de cette thèse, consistant en l'application des théorèmes présents dans le Chapitre 2 au problème spécifique du flottement de décrochage. L'application est limitée à l'oscillation en tangage d'une aile rigide, sur un degré de liberté, en présence éventuelle de saturation. Ce chapitre vise à fournir une approche pratique permettant d'appliquer des techniques de contrôle avancées à des systèmes aéroélastiques non linéaires. En particulier, les incertitudes et les non-linéarités tels que les dynamiques commutées, les paramètres variants inconnus et les saturations sont encapsulées dans une formulation polytopique multi-affine. Les résultats de simulations numériques sont fournis et des remarques sont formulées concernant les régions d'attraction, le conservatisme et les limitations éventuelles de cette méthode.

Enfin, après avoir présenté les remarques, quelques perspectives sont proposées afin de prolonger ce travail.

Chapter 1

Modélisation aéroélastique

1.1 Introduction

De nombreuses applications telles que les éoliennes, les drones, les hélicoptères ou les avions de combat cherchent à améliorer leurs performances et/ou étendre leur enveloppe de vol grâce aux avancées technologiques, notamment dans le domaine de la structure. De telles modifications restent limitées par les interactions entre les modes aérodynamiques et les modes structuraux, qui peuvent conduire à des instabilités aéroélastiques. Celles-ci peuvent se développer rapidement et être particulièrement destructrices, comme a pu le montrer le prototype d'aile volante solaire Helios, qui a rencontré de violentes oscillations aussi imprévisibles que catastrophiques [46].

La modélisation précise de ces phénomènes se développant au sein des systèmes {Aile-Ecoulement} et le développement de stratégies de contrôle robuste sont les clés pour de futures avancées et améliorations.

Cependant, utiliser un modèle trop complexe peut être extrêmement limitant pour le développement des correcteurs adaptés. Un compromis est généralement nécessaire entre un modèle complexe, reproduisant fidèlement la réalité du système mais souvent non utilisable du point de vue du contrôle, et un modèle plus simpliste qui permet d'appliquer des outils de théorie du contrôle mais qui risque de ne pas reproduire la dynamique du système considéré. Les modèles aéroélastiques utilisés pour décrire l'écoulement autour d'une aile correspondent parfaitement à cette situation où une description complète de l'écoulement, en utilisant directement les équations non linéaires de Navier-Stokes à chaque point de fluide, serait complètement inutile du point de vue de l'automatique. Au contraire, un modèle trop simpliste ne serait pas représentatif de la physique de l'écoulement.

Ce chapitre vise à développer un modèle précis, mais d'ordre réduit, capable de prédire la portance et le moment sur un profil oscillant, incluant la séparation des tourbillons de bord d'attaque et de bord de fuite. Tout d'abord, un modèle aéroélastique général est présenté. La charge aérodynamique est ensuite détaillée et un nouveau modèle du coefficient de portance et de moment, basé sur de précédents travaux du Dr Williams et du Dr Truong, est proposé. Ce modèle fournit la précision nécessaire tout en gardant un faible nombre de paramètres en vue de faciliter plus tard son contrôle. En utilisant des données expérimentales statiques et dynamiques, le modèle aérodynamique est formé et comparé avec succès aux résultats expérimentaux.

1.2 Modèle aéroélastique

Dans cette partie, une aile rigide oscillante en rotation et en translation est considérée telle que présentée Fig. 1.1.

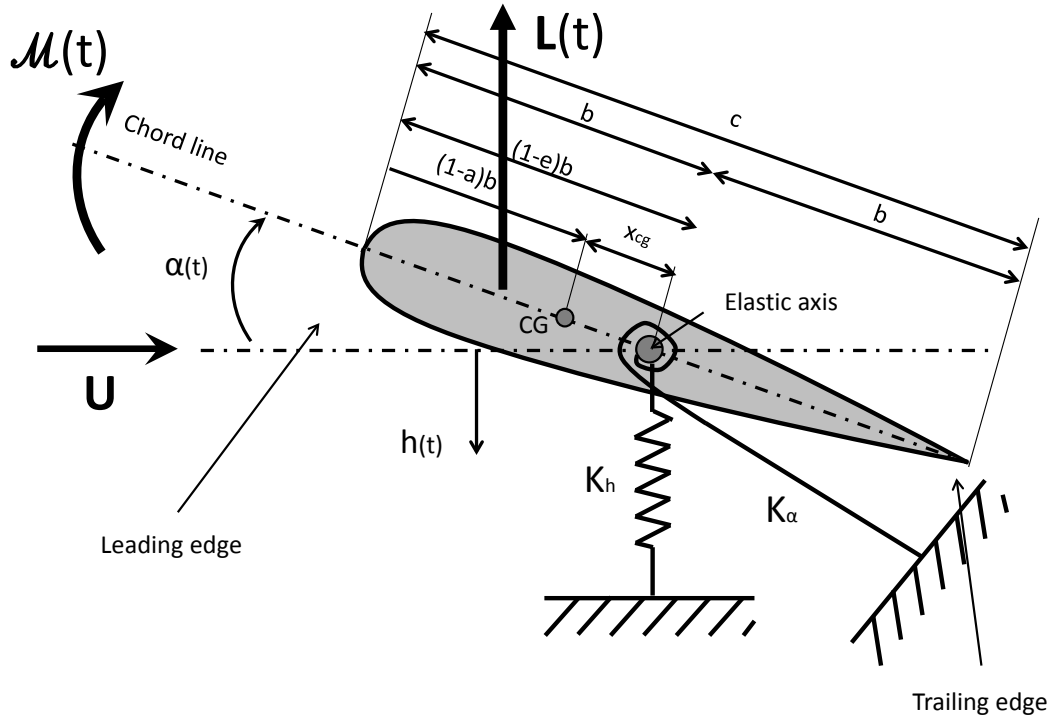

FIGURE 1.1: Modèle aéroélastique d'une aile rigide oscillante.

L'équation simplifiée du mouvement s'écrit alors :

$$\begin{bmatrix} m & mx_{CG} \\ mx_{CG} & I_\alpha \end{bmatrix} \begin{bmatrix} \ddot{h} \\ \ddot{\alpha} \end{bmatrix} + \begin{bmatrix} C_h & 0 \\ 0 & C_\alpha \end{bmatrix} \begin{bmatrix} \dot{h} \\ \dot{\alpha} \end{bmatrix} + \begin{bmatrix} K_h & 0 \\ 0 & K_\alpha \end{bmatrix} \begin{bmatrix} h \\ \alpha \end{bmatrix} = \begin{bmatrix} -L_{tot} \\ \mathcal{M}_{tot} \end{bmatrix} \tag{1.1}$$

où

- c est la corde,
- b est la demi-corde, $(b = c/2)$,
- e est la distance entre le milieu de la corde et l'axe élastique, normalisée par b. L'axe élastique est défini comme la ligne de l'aile composée des points pour lesquels aucune torsion n'est générée lorsque l'on applique une force, ou lorsqu'il n'y a pas de translation lorsque l'on applique un couple. Dans le cas considéré ici, l'axe de rotation correspond à l'axe élastique et $e = 0$,
- a est la distance entre le milieu de la corde et le centre de masse normalisé par b,
- $x_{CG} = (a - e)b$ correspond à la distance entre le centre élastique et le centre de masse,
- K_h, K_α sont respectivement la raideur en torsion et en translation,
- I_α est l'inertie par rapport à l'axe y,
- m est la masse de la section d'aile,
- C_h, C_α sont les coefficients d'amortissements respectifs,
- L_{tot} et $\mathcal{M}_{tot}$ sont respectivement la portance et le moment aérodynamique,
- h est le déplacement vertical,
- α est la déflection en torsion, ou angle d'attaque, entre la vitesse de l'écoulement libre et la corde de l'aile.

En définissant la pression dynamique, $q = \frac{1}{2}\rho U^2$, la surface de l'aile $2bl = S$, avec l l'envergure, la portance et le moment sont définis par :

$$\begin{bmatrix} L_{tot} \\ \mathcal{M}_{tot} \end{bmatrix} = \begin{bmatrix} qS\left[C_L(t, x(t)) + C_{L,act}(t, x(t), u(t))\right] \\ qSc\left[C_{\mathcal{M}}(t, x(t)) + C_{\mathcal{M},act}(t, x(t), u(t))\right] \end{bmatrix} \tag{1.2}$$

où $x(t)$ représente le vecteur d'état, $C_L(t, x(t))$ et $C_{\mathcal{M}}(t, x(t))$ sont respectivement les coefficients de portance et de moment de l'aile sans actionneur et $C_{L,act}(t, x(t), u(t))$ et $C_{\mathcal{M},act}(t, x(t), u(t))$ les coefficients des contributions de l'actionneur à la portance et au moment.

En utilisant le modèle développé par Theodorsen, la portance et le moment ont une contribution liée à la rotation et une contribution liée à la translation. Si la contribution

en translation est conservée, la contribution en rotation est modifiée afin d'une part de rendre compte des phénomènes de lâchers tourbillonnaires et d'autre part de conserver un ordre limité du système.

Pour cela, le modèle développé dans [6] est considéré. Ces travaux s'appuient sur les travaux de Goman et Khrabrov dans [47] permettant de relier l'évolution du point de séparation à l'évolution du coefficient de portance tel que présenté en Fig. 1.2 et 1.3.

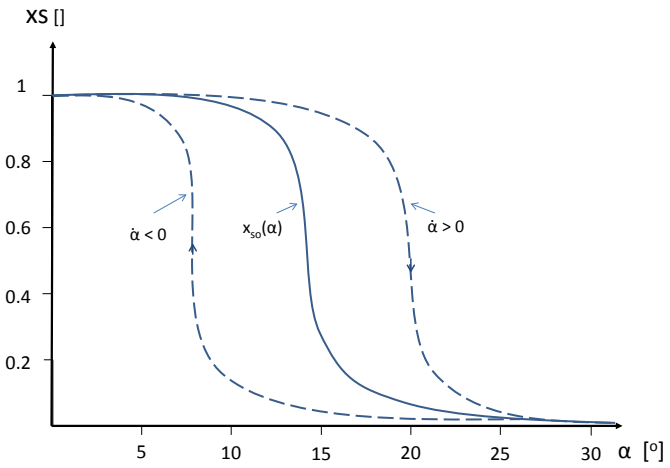

FIGURE 1.2: Evolution du point de séparation en fonction de α, adapté de [47].

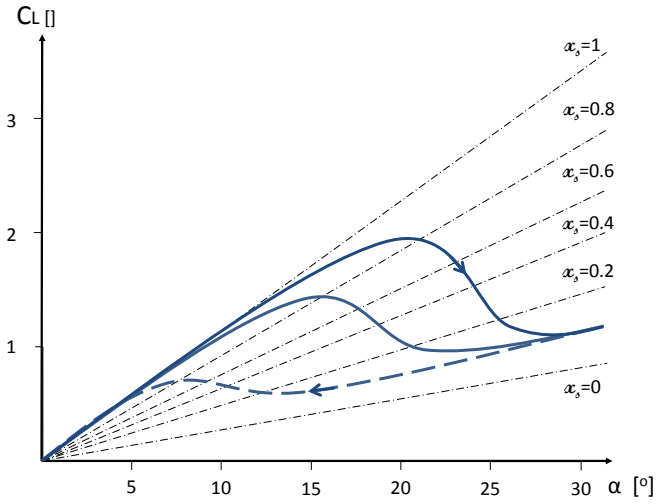

FIGURE 1.3: Evolution de C_L en fonction de α, adapté de [47].

Cependant, si ce modèle s'avère particulièrement adapté pour reproduire l'hystérésis présente lors du mouvement d'oscillation de l'aile, celui-ci ne rend pas compte des lâchers tourbillonnaires de bord d'attaque.

Le modèle est donc enrichi en intégrant et en adaptant sensiblement la partie instationnaire du modèle ONERA BH s'appuyant sur la théorie de la bifurcation [48].

Un nouveau modèle aérodynamique appelé *GKO* pour Goman-Khrabrov et ONERA BH est obtenu.

Un modèle simplifié de la contribution en portance et en moment de l'actionneur est ensuite présenté.

Le modèle aéroélastique est alors défini par les équations suivantes :

$$\begin{bmatrix} m & mx_{CG} \\ mx_{CG} & I_\alpha \end{bmatrix} \begin{bmatrix} \ddot{h} \\ \ddot{\alpha} \end{bmatrix} + \begin{bmatrix} C_h & 0 \\ 0 & C_\alpha \end{bmatrix} \begin{bmatrix} \dot{h} \\ \dot{\alpha} \end{bmatrix} + \begin{bmatrix} K_h & 0 \\ 0 & K_\alpha \end{bmatrix} \begin{bmatrix} h \\ \alpha \end{bmatrix} = \begin{bmatrix} -qS\left[C_L(t,x(t)) + C_{L,act}(t,x(t),u(t))\right] \\ qSc\left[C_{\mathcal{M}}(t,x(t)) + C_{\mathcal{M},act}(t,x(t),u(t))\right] \end{bmatrix} \tag{1.3}$$

$$\begin{cases} C_L(t) = C_{L,\alpha} C(k) \frac{\dot{h}(t)}{U} + \pi \frac{b}{U^2} \ddot{h}(t) + 2\pi\alpha(t)(A_L + B_L x_s(t)) + C_{L\text{offset}} + C_{L_u}(t) \\ C_M(t) = C_{M,\alpha} C(k) \frac{\dot{h}(t)}{U} + \frac{\pi}{2} \frac{ab}{U^2} \ddot{h}(t) + 2\pi\alpha(t)(A_M + B_M x_s(t)) + C_{M\text{offset}} + C_{M_u}(t) \end{cases} \tag{1.4}$$

avec

$$\begin{cases} \tau_1 \dot{x_s} + x_s &= x_{s,0}(\alpha - \tau_2 \frac{d\alpha}{dt}), \\ \ddot{C}_{M_u} + D_M(x) w_S \ddot{\alpha}\,(t) &= w_S(\beta_M(x) - \gamma_M(x) C_{M_u}^2)\dot{C}_{M_u} - w_S^2 C_{M_u}(1 - \eta_M(x) C_{M_u}^2 \\ & \quad - a_{2,M}(x) C_{M_u}) - E_M(x) w_S \dot{\alpha}\,(t)\,, \\ \ddot{C}_{L_u} + D_L(x) w_S \ddot{\alpha}\,(t) &= w_S(\beta_L(x) - \gamma_L(x) C_{L_u}^2)\dot{C}_{L_u} - w_S^2 C_{L_u}(1 - \eta_L(x) C_{L_u}^2 \\ & \quad - a_{2,L}(x) C_{L_u}) - E_L(x) w_S \dot{\alpha}\,(t)\,. \end{cases} \tag{1.5}$$

$$\begin{cases} L_\beta &= \frac{1}{2}\rho U^2 S C_{L,\beta}\beta, \\ \mathcal{M}_\beta &= \frac{1}{2}\rho U^2 S c C_{M,\beta}\beta. \end{cases} \tag{1.6}$$

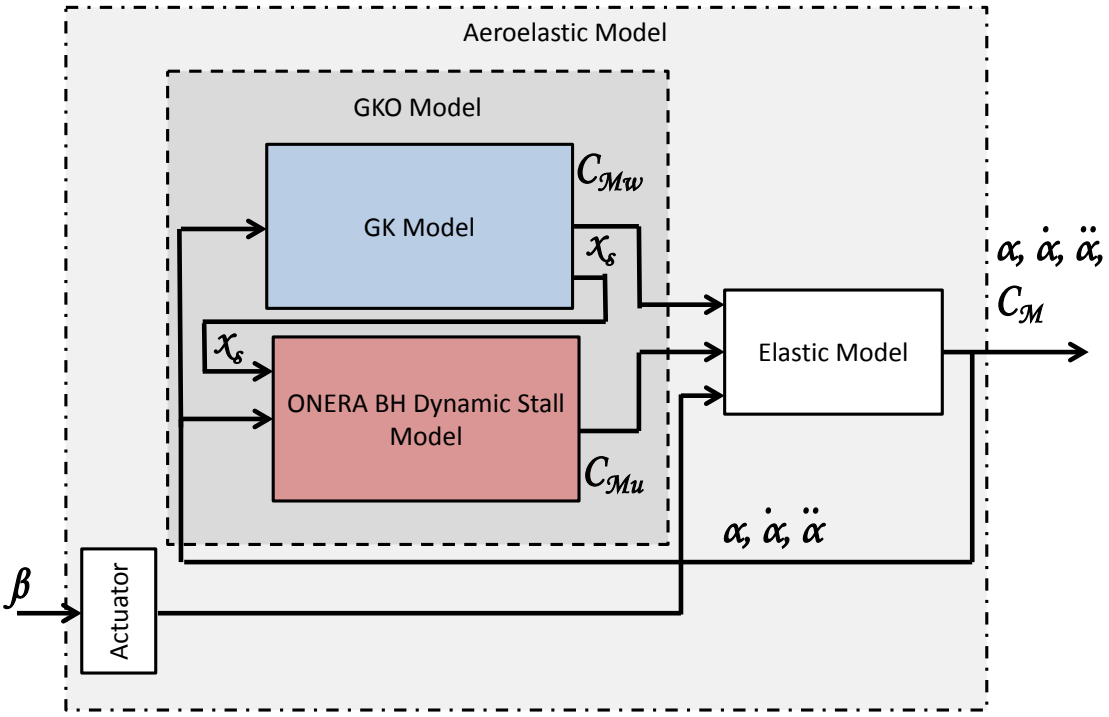

FIGURE 1.4: Architecture du système aéroélastique.

1.3 Résultats expérimentaux et validation du modèle aérodynamique

Cette partie vise à valider le modèle, particulièrement le modèle aérodynamique *GKO* développé précédemment. Pour cela, des données expérimentales ont été collectées au sein du Laboratoire d'aérodynamique de l'*United States Air Force Academy* aux Etats-Unis pour une aile de type NACA 0018. L'aile, sélectionnée pour ses caractéristiques liées au décrochage dynamique, présente une corde de $c = 0.15\ m$ et une envergure de $l = 0.45\ m$. L'aile est en oscillation forcée autour de son axe de tangage au milieu de la corde.

Les paramètres du modèle aérodynamique GKO sont alors identifiés en utilisant les données expérimentales statiques et dynamiques. Les prédictions du coefficient de moment sont alors comparées avec succès aux résultats expérimentaux comme présenté Fig. 1.5.

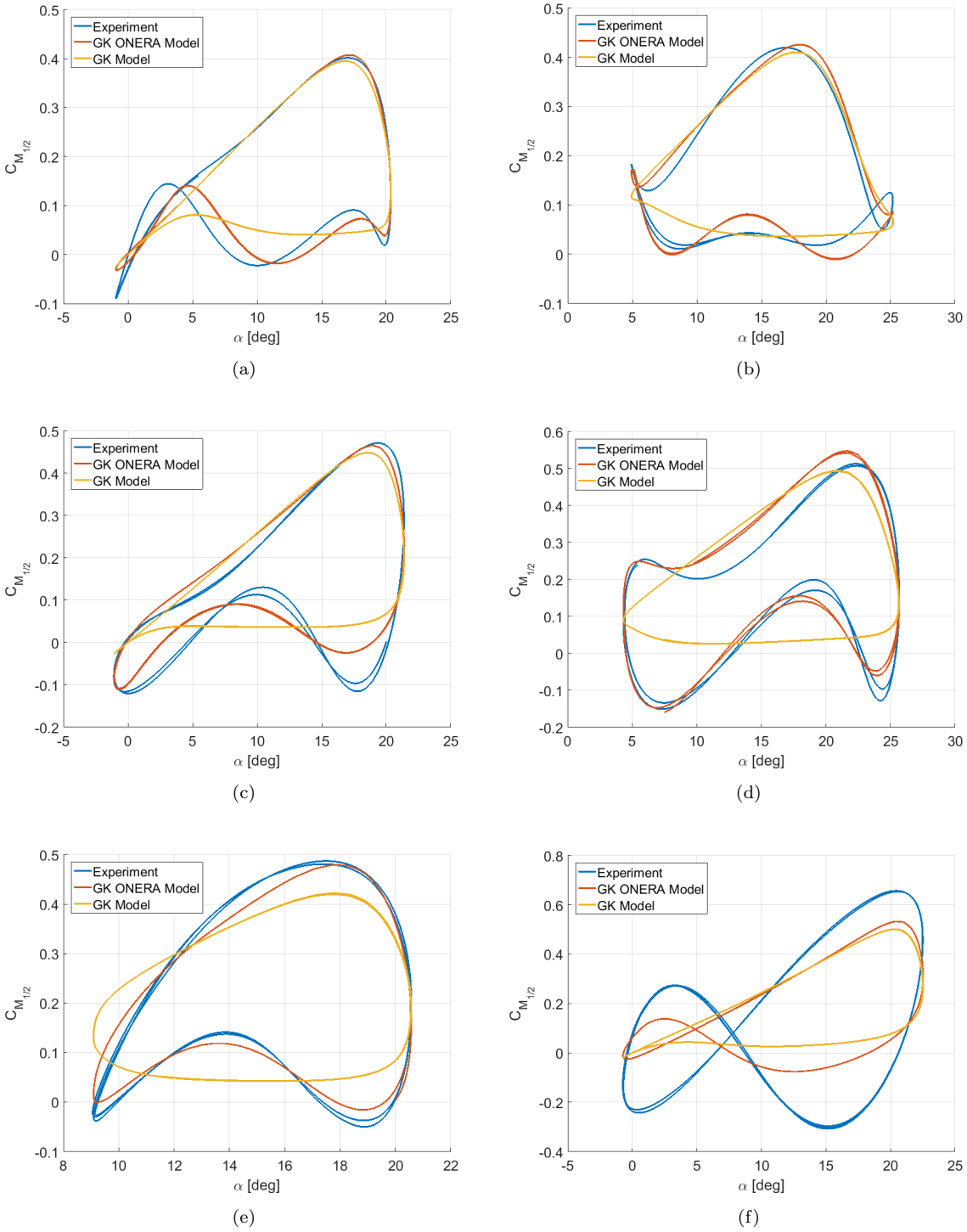

FIGURE 1.5: Prédictions du coefficient de moment et mesures pour différentes fréquences, amplitudes et valeurs moyennes : **a** Cas 1, **b** Cas 2, **c** Cas 3 , **d** Cas 4, **e** Cas 5 et **f** Cas 6.

1.4 Conclusion du chapitre

Le Chapitre 1 a permis d'établir un ensemble d'équations aéroélastiques pour une aile lors d'un mouvement d'oscillation et de translation verticale. Un nouveau modèle aérodynamique permettant de prédire l'évolution de la portance et du moment lors d'un mouvement d'oscillation de tangage est détaillé, en s'appuyant d'une part sur le modèle de Goman et Khrabrov et d'autre part sur le modèle de l'ONERA BH.

Les données expérimentales ont permis d'une part d'identifier les différents coefficients présents dans le modèle et d'autre part de valider celui-ci en comparant les résultats expérimentaux dynamiques aux prédictions du modèle et ce pour une gamme intéressante de fréquences d'oscillation, d'amplitudes ou de valeurs moyennes. Ce modèle capturant le phénomène d'hystérésis comme les lâchers tourbillonnaires peut donc être utilisé de façon intéressante dans le cas de l'AFC où un contrôle de la couche limite est recherché. Ce modèle reste cependant extrêmement non linéaire. Il convient donc de chercher à en obtenir une formulation plus adaptée pour une approche de la théorie du contrôle telle que développée dans le Chapitre 2.

Chapter 2

Contrôle robuste par approche polytopique en présence de saturation

2.1 Introduction

Les performances d'un système en boucle fermée peuvent être affectées par les saturations de l'actionneur. La saturation fait généralement référence au fait qu'une non-linéarité statique ou dynamique limitant l'amplitude ou le taux de variation de l'entrée affecte l'entrée de la commande demandée et entraîne une variation entre la sortie du contrôleur (entrée de l'installation commandée) et l'entrée réelle de l'installation.

Si la théorie liée à la stabilité et au contrôle propose de nombreuses solutions de contrôle efficaces, beaucoup d'entre elles sont difficilement applicables en pratique aux industries, précisément à cause de ces limitations rendant difficiles les hypothèses classiques de linéarité.

Des techniques comme l'anti-windup ont émergé afin de fournir une réponse intéressante aux problèmes ci-dessus. Adresser directement le problème de la saturation peut permettre de garantir certaines performances du système en boucle fermée, particulièrement pour des applications industrielles. L'inconvénient de ces méthodes avancées reste cependant leur relative complexité du fait de l'ordre du système en boucle ouverte et la précision du modèle développé.

Dans ce chapitre, une méthode de contrôle quadratique linéaire est considérée pour des systèmes linéaires à temps invariants (LTI), garantissant la stabilité ainsi que la minimisation d'une fonction de coût. Les résultats sont étendus à des systèmes incertains

représentés comme des systèmes multi-affines. Les paramètres incertains sont considérés comme bornés et variants à l'intérieur d'un polytope. Des saturations en position sont alors considérées. La stabilité locale et globale est étudiée. Dans le cas de la stabilité locale, une région d'attraction est définie et maximisée tout en garantissant un coût minimum. Le cas de la saturation en vitesse est également étudié en utilisant une formulation augmentée du système initial. Chaque théorème est appliqué à un exemple académique de système masse-ressort.

2.2 Correcteur *Linear Quadratic Regulator* (LQR)

Tout d'abord, le cas du système LTI sans saturation est considéré.

$$\dot{x}(t) = Ax(t) + Bu(t) \tag{2.1}$$

On définit la fonction de coût :

$$J = \int_0^\infty \left(x(t)'Qx(t) + u(t)'Ru(t) \right) dt, \tag{2.2}$$

où $R \in \mathbb{R}^{m\times m}$ est une matrice définie positive et $Q \in \mathbb{R}^{n\times n}$ est une matrice symétrique définie positive qui peut être librement choisie.

Theorem 2.1. *Etant donnés $Q = Q' > 0$ et $R > 0$, et en supposant qu'il existe $W = W' > 0 \in \mathbb{R}^{n\times n}$, Y, $X \in \mathbb{R}^{m\times n}$, une matrice diagonale positive $S > 0 \in \mathbb{R}^{m\times m}$ et un scalaire ν satisfaisant l'inégalité suivante :*

$$\begin{bmatrix} He(AW + BY) & W & Y' \\ * & -\nu Q^{-1} & 0 \\ * & * & -\nu R^{-1} \end{bmatrix} < 0. \tag{2.3}$$

Alors en choisissant $K = YW^{-1}$ on garantit :

1. *la stabilité globale exponentielle de l'origine du système (2.1) avec $u = Kx$;*
2. *pour une condition initiale $x(0) \in \varepsilon(W^{-1})$, la fonction de coût J définie Eq. (2.2) et évaluée le long de la solution (unique) correspondante de (2.1), K satisfait $J \leq \nu x_0^T W^{-1} x_0$.*

Le résultat est ensuite étendu aux systèmes polytopiques incertains définis comme suit :

$$\dot{x} = \sum_{i=1}^{N} \mu_i(t) \left(A_i x + B_i u \right), \tag{2.4}$$

où les matrices $A_i \in \mathbb{R}^{n\times n}$ et $B_i \in \mathbb{R}^{n\times m}$ sont constantes et connues, pour tout $i = 1,..,N$, où N est un nombre entier positif. Les coefficients $\mu_i \in [0,1]$ sont tels que leur somme est égale à 1. L'objectif est maintenant de trouver un signal de contrôle d'entrée optimal $u = Kx$ qui minimise de façon suboptimale la fonction de coût (2.2).

Le théorème suivant est alors obtenu.

Theorem 2.2. *Etant donnés $Q = Q' > 0$ et $R > 0$, et en supposant qu'il existe $W = W' > 0 \in \mathbb{R}^{n\times n}$, Y, $X \in \mathbb{R}^{m\times n}$, une matrice diagonale positive $S > 0 \in \mathbb{R}^{m\times m}$ et un scalaire ν satisfaisant l'inégalité suivante :*

$$\begin{bmatrix} He(A_iW + B_iY) & W & Y' \\ * & -\nu Q^{-1} & 0 \\ * & * & -\nu R^{-1} \end{bmatrix} < 0, \quad \forall i = 1,\dots,n \tag{2.5}$$

Alors en choisissant $K = YW^{-1}$ on garantit :

1. *la stabilité globale exponentielle de l'origine du système (2.4) avec $u = Kx$;*
2. *pour une condition initiale $x(0) \in \varepsilon(W^{-1})$, la fonction de coût J définie Eq. (2.2) et évaluée le long de la solution (unique) correspondante de (2.4), K satisfait $J \leq \nu x_0^T W^{-1} x_0$.*

Un exemple académique est fourni afin d'illustrer les deux théorèmes présentés ainsi que l'influence des paramètres.

2.3 Correcteur LQR en présence de saturation en position

Le problème des saturations est ensuite abordé.

Des saturations en position décentralisée sont considérées au niveau de la commande. Le système s'écrit donc :

$$\dot{x}(t) = Ax(t) + Bsat(u(t)) \tag{2.6}$$

où $sat(u)$ représente la saturation en position du signal de commande u s'écrivant lui-même au moyen de la matrice de gain statique tel que :

$$u = Kx \tag{2.7}$$

Des conditions de secteurs sont alors formulées afin d'obtenir la formulation LMI suivante.

Theorem 2.3. *[49] Etant donnés $Q = Q' > 0$ et $R > 0$, et en supposant qu'il existe $W = W' > 0 \in \mathbb{R}^{n\times n}$, Y, $X \in \mathbb{R}^{m\times n}$, une matrice diagonale positive $S > 0 \in \mathbb{R}^{m\times m}$ et deux scalaires α, ν satisfaisant les inégalités suivantes :*

$$\begin{bmatrix} W & X_j' \\ X_j & u_{0,j}^2 \end{bmatrix} \geq 0, \ \forall j = 1, .., m, \tag{2.8}$$

$$\begin{bmatrix} I & \alpha I \\ \alpha I & W \end{bmatrix} \geq 0 \tag{2.9}$$

$$\begin{bmatrix} He(AW + BY) & (Y + X)' - BS & W & Y' \\ * & -2S & 0 & -S \\ * & * & -\nu Q^{-1} & 0 \\ * & * & * & -\nu R^{-1} \end{bmatrix} < 0, \tag{2.10}$$

où X_j représente la j^{eme} ligne de la matrice X. Alors en choisissant :

$$K = YW^{-1} \tag{2.11}$$

1. *la stabilité locale exponentielle à l'origine du système (2.6), (2.7) avec une région d'attraction $\varepsilon(W^{-1}) = \{x \in \mathbb{R}^n : x'W^{-1}x \leq 1\}$ contenant la α-boule $\mathcal{B}(\alpha) := \{x \in \mathbb{R}^n \ : \ |x| \leq \alpha\}$;*

2. *pour une condition initiale $x(0) \in \varepsilon(W^{-1})$, la fonction de coût J définie (2.2) et évaluée le long de la solution (unique) correspondante de (2.6), (2.7) satisfait $J \leq \nu x_0^T W^{-1} x_0$;*

3. *la stabilité globale exponentielle de l'origine du système (2.6), (2.7) si la solution de (2.9), (2.10) est telle que $X = 0$.*

Le résultat est également étendu aux systèmes polytopiques incertains.

Afin d'étendre ce résultat, le système polytopique générique est introduit en présence de saturation :

$$\dot{x} \ = \ \sum_{i=1}^{N} \mu_i \left(A_i x + B_i sat(u)\right), \tag{2.12}$$

où les matrices $A_i \in \mathbb{R}^{n\times n}$ et $B_i \in \mathbb{R}^{n\times m}$ sont constantes et connues, pour tout $i = 1, .., N$, où N est un nombre entier positif. Les coefficients $\mu_i \in [0, 1]$ sont tels que leur somme est égale à 1. Le signal d'entrée u résulte de la loi de contrôle de retour d'état

calculée à partir de la matrice de gain statique telle que :

$$u = Kx. \tag{2.13}$$

On obtient alors le théorème suivant.

Theorem 2.4. *Etant donnés $Q = Q' > 0$ et $R > 0$, et en supposant qu'il existe $W = W' > 0 \in \mathbb{R}^{n\times n}$, Y, $X \in \mathbb{R}^{m\times n}$, une matrice diagonale positive $S > 0 \in \mathbb{R}^{m\times m}$ et deux scalaires α, ν satisfaisant les inégalités suivantes :*

$$\begin{bmatrix} W & X_j' \\ X_j & u_{0,j}^2 \end{bmatrix} \geq 0,\ \forall j = 1,..,m, \quad \begin{bmatrix} I & \alpha I \\ \alpha I & W \end{bmatrix} \geq 0 \tag{2.14}$$

$$\begin{bmatrix} \begin{bmatrix} He(A_iW + B_iY) & (Y+X)' - B_iS \\ * & -2S \end{bmatrix} & \begin{bmatrix} W & Y' \\ 0 & -S \end{bmatrix} \\ * & -\nu \begin{bmatrix} Q^{-1} & 0 \\ 0 & R^{-1} \end{bmatrix} \end{bmatrix} < 0,\ \forall i = 1,...,N \tag{2.15}$$

où X_j représente la j^{eme} ligne de la matrice X. Alors en choisissant :

$$K = YW^{-1} \tag{2.16}$$

on garantit :

1. *la stabilité locale exponentielle à l'origine du système (2.12), (2.13) avec une région d'attraction $\varepsilon(W^{-1}) = \{x \in \mathbb{R}^n : x'W^{-1}x \leq 1\}$ contenant la α-boule $\mathcal{B}(\alpha) := \{x \in \mathbb{R}^n \ : \ |x| \leq \alpha\}$;*
2. *pour une condition initiale $x(0) \in \varepsilon(W^{-1})$, la fonction de coût J définie Eq.(2.2) et évaluée le long de la solution (unique) correspondante de (2.12), (2.13) satisfait $J \leq \nu x_0^T W^{-1} x_0$;*
3. *la stabilité globale exponentielle de l'origine du système (2.12), (2.13) si la solution de (2.14), (2.15) est telle que $X = 0$.*

L'exemple académique introduit précédemment est utilisé afin d'illustrer les deux théorèmes présentés, ainsi que l'influence des différents paramètres.

2.4 Correcteur LQR en présence de saturation en vitesse

Dans cette section, le cas des saturations en vitesse est envisagé.

Suivant l'approche employée dans [4], un système augmenté permettant de modéliser la saturation en vitesse par une saturation en position est proposé. Cela permet alors d'utiliser les théorèmes précédents et d'obtenir les deux théorèmes suivants.

Le système augmenté est donné par le système générique suivant :

$$\dot{\tilde{x}} = \tilde{A}\tilde{x} + \tilde{B}sat(\tilde{u}(t)) \tag{2.17}$$

où $\tilde{x} \in \mathbb{R}^{n+m}$ et $\tilde{u} \in \mathbb{R}^m$ représentent respectivement les états et entrées du système augmenté, avec n et m des nombres entiers positifs. Les $\tilde{A} \in \mathbb{R}^{n+m\times n+m}$ et $\tilde{B} \in \mathbb{R}^{n+m\times m}$ sont constantes et connues. La fonction de saturation correspond dans ce cas à la saturation en position équivalente dans le système augmenté à la saturation en vitesse. Le signal de commande $\tilde{u}$ résulte de la loi de commande par retour d'état calculée à partir de la matrice de gain statique telle que :

$$\tilde{u} = \tilde{K}\tilde{x}. \tag{2.18}$$

Il convient également de définir une nouvelle fonction de coût quadratique pour le système augmenté :

$$\tilde{J} = \int_0^\infty \Big(x(t)'Qx(t) + u(t)'Ru(t) + \dot{u}(t)'\tilde{R}\dot{u}(t)\Big)\,dt = \int_0^\infty \Big(\tilde{x}'\tilde{Q}\tilde{x} + \tilde{u}(t)'\tilde{R}\tilde{u}(t)\Big)\,dt, \tag{2.19}$$

où $\tilde{R} \in \mathbb{R}^{m\times m}$ est une matrice définie positive et $\tilde{Q} = \begin{bmatrix} Q & 0 \\ 0 & R \end{bmatrix}$ avec $Q \in \mathbb{R}^{n\times n}$ et $R \in \mathbb{R}^{m\times m}$ des matrices symétriques définies positives pouvant être librement choisies. Dans ce cas, on obtient le théorème suivant.

Theorem 2.5. *Etant donnés $Q = Q' > 0$ et $R > 0$, et en supposant qu'il existe $W = W' > 0 \in \mathbb{R}^{n+m\times n+m}$, Y, $X \in \mathbb{R}^{m\times n+m}$, une matrice diagonale positive $S > 0 \in \mathbb{R}^{m\times m}$ et deux scalaires α, ν satisfaisant les inégalités suivantes :*

$$\begin{bmatrix} W & X_j' \\ X_j & u_{r,0j}^2 \end{bmatrix} \geq 0,\ \forall j = 1,..,m, \quad \begin{bmatrix} I & \alpha I \\ \alpha I & W \end{bmatrix} \geq 0 \tag{2.20}$$

$$\begin{bmatrix} \begin{bmatrix} He(\tilde{A}W + \tilde{B}Y) & (Y+X)' - \tilde{B}S \\ * & -2S \end{bmatrix} & \begin{bmatrix} W & Y' \\ 0 & -S \end{bmatrix} \\ * & -\nu \begin{bmatrix} \tilde{Q}^{-1} & 0 \\ 0 & \tilde{R}^{-1} \end{bmatrix} \end{bmatrix} < 0, \tag{2.21}$$

où X_j représente la j^{eme} ligne de la matrice X. Alors en choisissant :

$$\tilde{K} = YW^{-1} \tag{2.22}$$

on garantit que :

1. *la stabilité locale exponentielle à l'origine du système (2.17), (2.18) avec une région d'attraction $\varepsilon(W^{-1}) = \{\tilde{x} \in \mathbb{R}^{n+m} : \tilde{x}'W^{-1}\tilde{x} \leq 1\}$ contenant la α-boule $\mathcal{B}(\alpha) := \{\tilde{x} \in \mathbb{R}^n : |\tilde{x}| \leq \alpha\}$;*
2. *pour une condition initiale $\tilde{x}(0) \in \varepsilon(W^{-1})$, la fonction de coût $\tilde{J}$ définie (2.19) et évaluée le long de la solution (unique) correspondante de (2.17), (2.18) satisfait $\tilde{J} \leq \mu\tilde{x}_0^T W^{-1}\tilde{x}_0$;*
3. *la stabilité globale exponentielle de l'origine du système (2.17), (2.18) si la solution de (2.20), (2.21) est telle que $X = 0$.*

Le résultat est une fois de plus étendu aux systèmes polytopiques incertains.

On introduit donc de la même façon le système polytopique augmenté en présence de saturation en vitesse exprimée à partir d'une saturation en position :

$$\dot{\tilde{x}} = \sum_{i=1}^{N} \mu_i(t) \left(\tilde{A}_i\tilde{x} + \tilde{B}_i sat(\tilde{u}) \right), \tag{2.23}$$

avec

$$\tilde{u} = \tilde{K}\tilde{x}. \tag{2.24}$$

Theorem 2.6. *Etant donnés $Q = Q' > 0$ et $R > 0$, et en supposant qu'il existe $W = W' > 0 \in \mathbb{R}^{n+m\times n+m}$, Y, $X \in \mathbb{R}^{m\times n+m}$, une matrice diagonale positive $S > 0 \in \mathbb{R}^{m\times m}$ et deux scalaires α, ν satisfaisant les inégalités suivantes :*

$$\begin{bmatrix} W & X_j' \\ X_j & u_{r,0j}^2 \end{bmatrix} \geq 0, \ \forall j = 1, .., m, \quad \begin{bmatrix} I & \alpha I \\ \alpha I & W \end{bmatrix} \geq 0 \tag{2.25}$$

$$\begin{bmatrix} \begin{bmatrix} He(\tilde{A}_i W + \tilde{B}_i Y) & (Y+X)' - \tilde{B}_i S \\ * & -2S \end{bmatrix} & \begin{bmatrix} W & Y' \\ 0 & -S \end{bmatrix} \\ * & -\nu \begin{bmatrix} \tilde{Q}^{-1} & 0 \\ 0 & \tilde{R}^{-1} \end{bmatrix} \end{bmatrix} < 0, \forall i = 1, \ldots, n \tag{2.26}$$

où X_j représente la j^{eme} ligne de la matrice X. Alors en choisissant :

$$\tilde{K} = YW^{-1} \tag{2.27}$$

on garantit que :

1. *la stabilité locale exponentielle à l'origine du système (2.23), (2.24) avec une région d'attraction $\varepsilon(W^{-1}) = \{\tilde{x} \in \mathbb{R}^{n+m} : \tilde{x}' W^{-1} \tilde{x} \leq 1\}$ contenant la α-boule $\mathcal{B}(\alpha) := \{\tilde{x} \in \mathbb{R}^n \ : \ |\tilde{x}| \leq \alpha\}$;*
2. *pour une condition initiale $\tilde{x}(0) \in \varepsilon(W^{-1})$, la fonction de cout $\tilde{J}$ définie (2.19) et évaluée le long de la solution (unique) correspondante de (2.23), (2.24) satisfait $\tilde{J} \leq \mu \tilde{x}_0^T W^{-1} \tilde{x}_0$;*
3. *la stabilité globale exponentielle de l'origine du système (2.23), (2.24) si la solution de (2.25), (2.26) est telle que $X = 0$.*

L'exemple académique est utilisé une nouvelle fois afin d'illustrer les deux théorèmes présentés, ainsi que l'influence des différents paramètres.

2.5 Conclusion du chapitre

Ce chapitre a présenté des méthodes de synthèse de contrôleurs pour des systèmes polytopiques multi-affines en présence de saturation. Les paramètres variables étant supposés inconnus, le "*gain scheduling*" ou les méthodes similaires ne sont pas applicables. Un contrôle optimal à été choisi afin de garantir la stabilité ainsi que des performances en termes d'erreurs et de commande d'entrée. Ces méthodes comprennent plusieurs niveaux de saturation. La région de stabilité a été évaluée pour chaque cas.

Dans le Chapitre 3, ces différentes méthodes seront appliquées au modèle développé dans le Chapitre 1 pour s'attaquer au battement d'une aile de tangage.

Chapter 3

Application des méthodes de contrôle robuste au problème de flottement de décrochage

3.1 Introduction

Dans le Chapitre 3, le problème de flottement de décrochage est étudié pour une aile oscillante à un degré de liberté. Ce travail s'appuiera d'une part sur le modèle réalisé dans la première partie mais également sur les résultats de commande LQR développés dans la deuxième partie. En effet, le modèle développé dans le Chapitre 1 s'avère particulièrement intéressant pour prédire le décrochage de l'aile en considérant les tourbillons de bord de fuite mais également de bord d'attaque. De plus, la restriction de l'étude à un seul degré de liberté, c'est-à-dire l'oscillation en tangage, permet de se concentrer sur les effets aérodynamiques et le phénomène de décrochage. Cependant, cette étude peut être aisément généralisée à un système complet en tangage et pompage. Le problème de la suppression des oscillations de flottement à été abordé dans de nombreux travaux. Dans [50], un modèle de *décrochage dynamique* pour aile rotative est dérivé des travaux de Beddoes-Leishman. Un correcteur adaptatif est proposé et simulé pour diverses conditions de flottement. Dans [41], un correcteur linéaire LQR à paramètres variants est synthétisé afin de supprimer le LCO lié au phénomène de *flottement de décrochage*. Le correcteur obtenu montre une robustesse marginale aux variations de vitesse. Dans [37], un correcteur de norme mixte $\mathcal{H}_2 \setminus \mathcal{H}_\infty$ est proposé. Le modèle utilisé est dérivé du modèle de *décrochage dynamique* de l'ONERA détaillé dans [51]. Un modèle similaire est utilisé dans [40] afin de formuler une approche s'appuyant sur la théorie LQR. Dans [52], une inclusion dynamique linéaire polytopique est utilisée pour prendre en compte

les variations de masse volumique et de vitesse. Le problème est résolu en utilisant une formulation LMI pour garantir la stabilité. Une méthode de *feedback linearization* est utilisée dans [7] proposant notamment des résultats expérimentaux.

La présente étude diffère des travaux précédents dans la mesure où les correcteurs proposés dans ces travaux sont principalement adaptatifs mais également du fait que le modèle utilisé ici inclut une modélisation avancée de la séparation des tourbillons de bord d'attaque basée sur les théories GK et ONERA BH. Il est intéressant de noter que le modèle est basé sur le modèle du Dr. Truong, dont l'ensemble d'équations initialement proposé a souffert d'une difficulté d'application en raison de ces non-linéarités et de ces caractéristiques de commutation, comme souligné par l'auteur lui-même dans [53].

Ce travail offre donc une approche originale pour aborder les difficultés initiales d'utilisation de ce modèle et réaliser un contrôle du système en boucle fermée. En effet, suivant une approche similaire à celles présentées dans Olalla & Al. [54] et Boyd & Al. [55], le système non linéaire sera formulé comme un système polytopique incertain. Cette formulation intéressante permet d'utiliser la théorie de contrôle développée dans le Chapitre 2. En particulier, les différentes méthodes développées précédemment seront mises en œuvre et simulées pour adresser le problème spécifique du flottement de décrochage d'une aile. En particulier, les problèmes liés à la saturation de la commande telles que la saturation en position et en vitesse, seront considérés.

3.2 Description du modèle

Le problème considéré est maintenant réduit à une oscillation pure autour de l'axe de tangage.

Les équations sont manipulées afin de s'adapter au problème spécifique de contrôle. Notamment, certains paramètres sont légèrement modifiés et renommés.

Le modèle résultant est décrit par le système non linéaire suivant :

$$\begin{aligned} \dot{x} &= A(x, x_s)x + B(x)u \\ \tau_1 \dot{x}_s &= -x_s + x_{s,0}(x) \\ y &= C(x)x \\ z &= Fx \end{aligned} \tag{3.1}$$

où le vecteur $x \in \mathbb{R}^4$ est donné par :

$$x = [\ \dot{\alpha},\ \alpha,\ \dot{C}_{M_u},\ C_{M_u}\ ]', \tag{3.2}$$

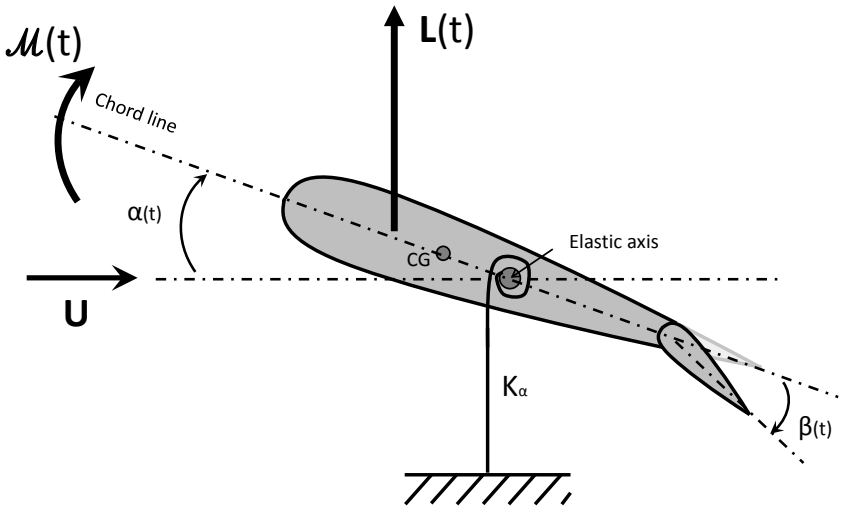

FIGURE 3.1: Modèle d'une aile rigide oscillante équipée d'un volet.

et les vecteurs u $(= \beta)$, y et z sont respectivement le signal de commande, le signal de sortie et les signaux à contrôler. Les matrices A, B, C et F sont données dans (3.3).

$$A(x, x_s) = \begin{bmatrix} -\frac{C_\alpha}{I_\alpha} & \frac{\pi\rho U^2 Sc\eta(x_s) - K_\alpha}{I_\alpha} & 0 & \frac{\rho U^2 Sc}{2I_\alpha} \\ 1 & 0 & 0 & 0 \\ w_S\left(D_M(x)\frac{C_\alpha}{I_\alpha} - E_M(x)\right) & -w_S D_M(x)\left(\frac{\pi\rho U^2 Sc\eta(x_s) - K_\alpha}{I_\alpha}\right) & w_S\beta_M(x) & -w_S\left(w_S + \frac{D_M(x)\rho U^2 Sc}{2I_\alpha}\right) \\ 0 & 0 & 1 & 0 \end{bmatrix},$$

$$B = \tfrac{1}{2}\rho U^2 Sc C_{M,\beta}\begin{bmatrix} 1 & 0 & -w_S D_M(x) & 0 \end{bmatrix}'$$

$$C(x_s) = \begin{bmatrix} 0 & 2\pi\eta(x_s) & 0 & 1 \\ 0 & 1 & 0 & 0 \end{bmatrix}, \qquad F = \begin{bmatrix} 0 & 1 & 0 & 0 \end{bmatrix}. \tag{3.3}$$

En utilisant les valeurs du modèle identifié dans le Chapitre 1, des simulations temporelles du système décrit précédemment sont réalisées et comparées aux résultats expérimentaux en conditions de flottement de décrochage. Il est notamment vérifié que le point de séparation et le signal de commutation varient au cours des ces simulations. Les résultats sont donnés pour trois vitesses d'écoulement différentes. La bonne adéquation entre les simulations et résultats expérimentaux permet de justifier l'emploi du modèle développé.

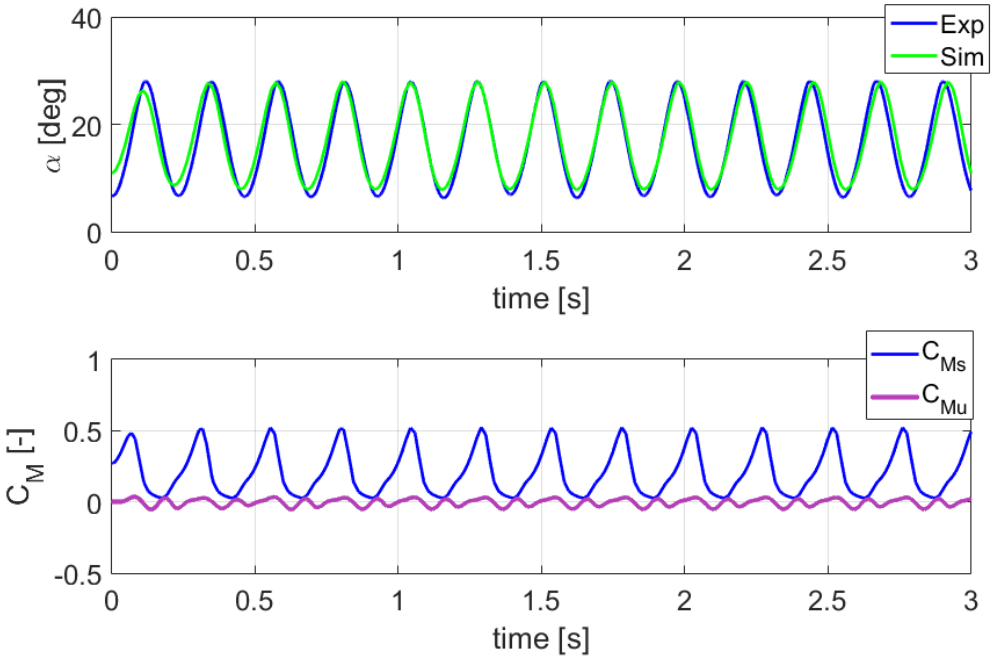

FIGURE 3.2: Résultats expérimentaux et simulation temporelle en condition de flottement (cas 2) et coefficients de moment simulés stationnaire et instationnaire.

3.3 Modélisation aéroélastique comme système polytopique incertain

Afin de prendre en compte les non-linéarités du modèle, le système est maintenant considéré comme un système polytopique à paramètres incertains.

On introduit le vecteur de paramètres incertains $\lambda(t) = [\lambda_1(t)\ \lambda_2(t)\ \lambda_3(t)]' \in [0\ 1]^3$.

On obtient alors une variation linéaire des trois paramètres considérés :

$\eta(x_s)$ **:** la pente qui était une combinaison linéaire de la position du point de séparation non difficilement mesurable.

$$\eta(x_s) = \lambda_1\eta_1 + (1-\lambda_1)\eta_2. \tag{3.4}$$

E_M, β_M, D_M **:** les paramètres de l'équation à commutation. Cette technique de variation linéaire est similaire à celle employée dans [54].

$$\begin{aligned}\{D_M, \beta_M, E_M\} \quad := \quad & \lambda_2 \{D_{M,1}, \beta_{M,1}, E_{M,1}\} \\ & +(1-\lambda_2)\{D_{M,2}, \beta_{M,2}, E_{M,2}\}.\end{aligned} \tag{3.5}$$

U^2 **:** la vitesse de l'écoulement est supposée variable. Cette valeur au carré est proportionnelle à la pression dynamique de l'écoulement.

$$U^2 = \lambda_3 U_1^2 + (1 - \lambda_3) U_2^2. \tag{3.6}$$

Le système paramétrique est maintenant un système linéaire aux paramètres variants à l'intérieur d'un polytope. La stabilisabilité du système est vérifiée aux $2^3 = 8$ sommets du polytope.

3.4 Application au contrôle du flottement de décrochage

Les différentes techniques de synthèse de correcteur sont ensuite appliquées à la formulation du système précédent. Des simulations temporelles sont réalisées en vérifiant la variation des paramètres incertains définis précédemment et pour différentes valeurs de vitesse de l'écoulement en présence de flottement de décrochage. Les principaux résultats sont présentés ci-dessous.

3.4.1 Synthèse LMI d'un correcteur LQR par formulation polytopique

Le système polytopique est tout d'abord considéré sans aucune saturation permettant d'appliquer le Théorème 2.2. Pour cela, les matrices Q et R ont été choisies telles que $Q = \text{diag}\{1, 0.1, 0.01, 0.01\}$ et $R = 100$. En utilisant la *Robust Control Toolbox* [56, 57] de MATLAB R2017a, on obtient la matrice de gain statique du correcteur par retour d'état K, suivant :

$$K = [0.1246,\ 1.7496,\ 0.3036,\ -1.3672].$$

On vérifie alors sur la simulation temporelle Fig. 3.3 que le correcteur, activé après 2 s, supprime bien les oscillations liées au flottement de décrochage qui s'était établi. On constate également sur les Fig. 3.3 et Fig. 3.4 que le correcteur statique fonctionne pour des vitesses d'écoulement différentes et pour une variation des paramètres au sein du polytope défini précédemment.

Le correcteur est également calculé et simulé pour différentes valeurs des matrices de pondérations afin d'illustrer leur influence sur la méthode de synthèse.

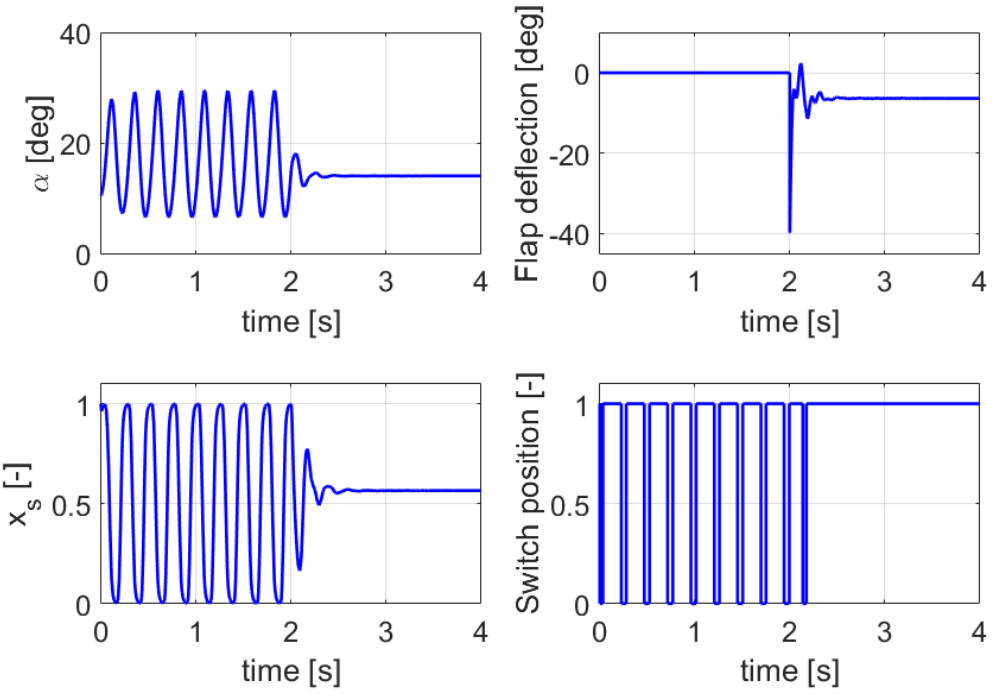

FIGURE 3.3: Angle d'attaque (deg), déflexion du volet (deg), x_s et signal de commutation en fonction du temps (s) pour $U = 20\ m/s$.

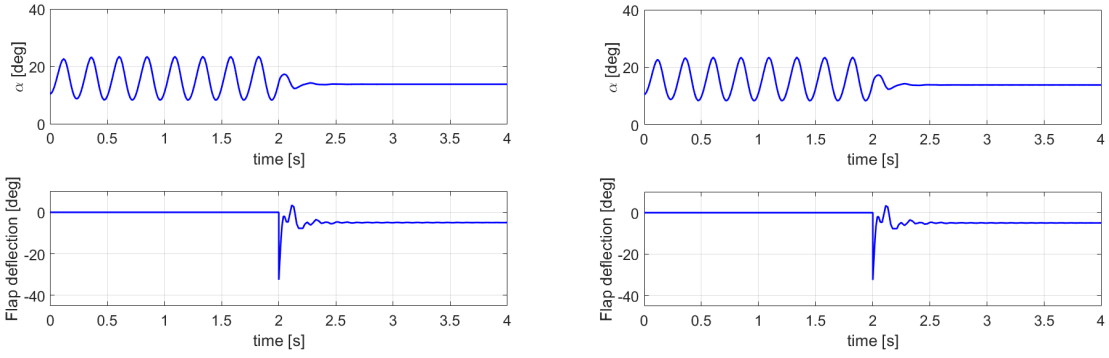

(a) (b)

FIGURE 3.4: Angle d'attaque (deg) et angle de déflexion du volet (deg) en fonction du temps (s) pour : (a) $U = 17.5\ m/s$ et (b) $U = 22.5\ m/s$.

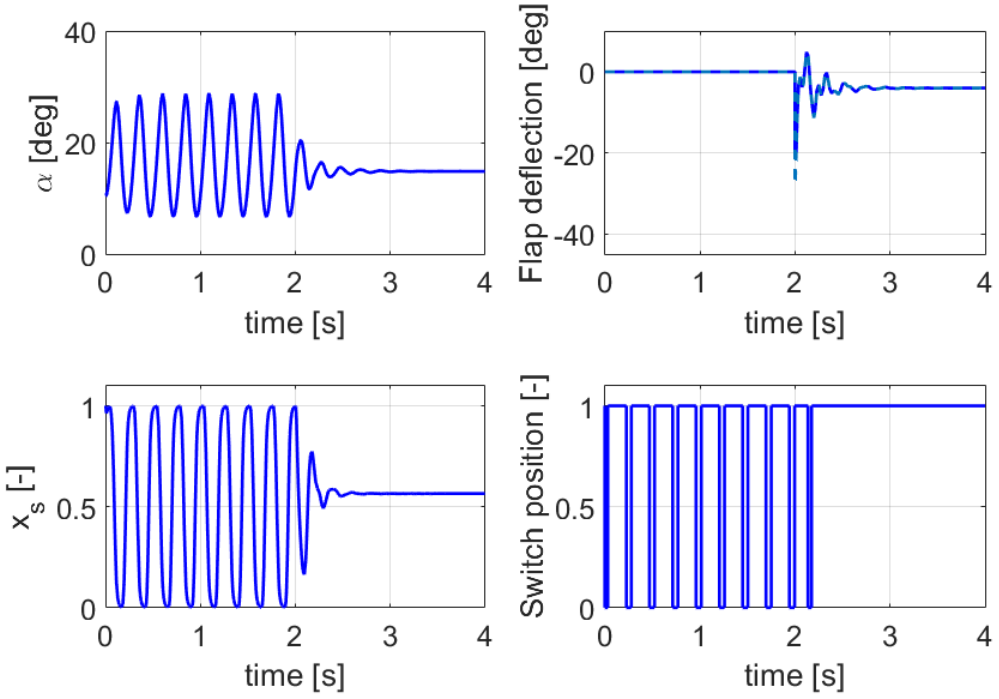

FIGURE 3.5: Angle d'attaque (deg), déflexion du volet (deg), x_s et signal de commutation en fonction du temps (s) pour $U = 20\ m/s$ avec saturation en position.

3.4.2 Synthèse LMI d'un correcteur LQR par formulation polytopique avec saturation en position

On s'intéresse ensuite au cas avec saturation en position.

L'amplitude de la saturation a été sélectionnée telle que $|\beta| \leq \bar{\beta} = 20°$. Une nouvelle fois, les matrices de pondération de la fonction de coût sont sélectionnées afin de garantir le fonctionnement désiré en boucle fermée. Les matrices sont similaires au cas précédent et sont donc $Q = \text{diag}\{1, 0.1,\ \ 0.01, 0.01\}$ et $R = 100$. Le problème d'optimisation convexe proposé dans le Théorème 2.4 est résolu en fournissant la matrice de gain statique :

$$K = [0.098,\ 0.9160,\ 0.2174,\ -4.764].$$

L'indice de performance est maintenu égal à $\nu = 1$, ce qui fournit un rayon de la boule de la région d'attraction $\alpha = 0.0265$. Cette valeur s'avère très réduite, ce qui est une conséquence directe du conservatisme de cette méthode.

La solution est alors évaluée en utilisant des simulations temporelles pour différentes vitesses telles que celles fournies Fig. 3.5. On constate une nouvelle fois la capacité à supprimer l'oscillation de flottement.

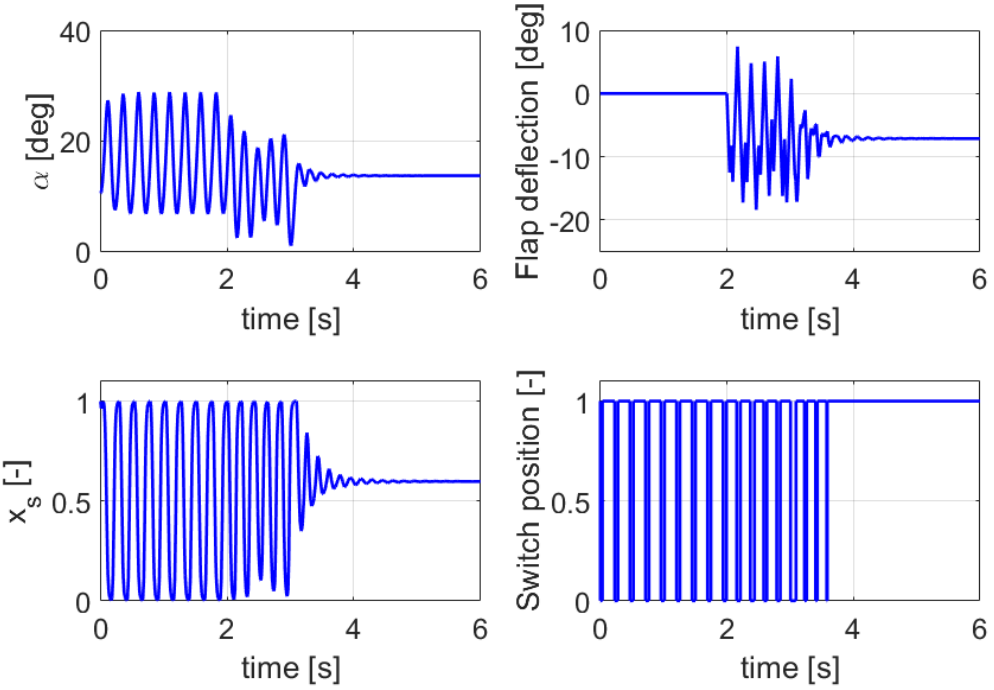

FIGURE 3.6: Angle d'attaque (deg), déflexion du volet (deg), x_s et signal de commutation en fonction du temps (s) pour $U = 20\ m/s$ avec saturation en vitesse.

Le correcteur est également calculé et simulé pour différentes valeurs d'indice de performance ν afin d'illustrer son influence notamment sur le domaine d'attraction.

3.4.3 Synthèse LMI d'un correcteur LQR par formulation polytopique avec saturation en vitesse

Enfin, le cas avec saturation en vitesse est considéré.

En suivant l'approche détaillée dans la section précédente, un système augmenté est introduit.

L'amplitude de la saturation en vitesse à été choisie telle que $|\dot{\beta}| \leq \bar{\dot{\beta}} = 60°/0.2s$.

Les matrices de pondération dont la dimension a été adaptée au système augmenté sont choisies de la façon suivante : $Q = \text{diag}\{1, 0.1, 0.01, 0.01\}$, $R = 100$ et $\tilde{R} = 10$. En conservant initialement un indice de performance $\nu = 1$, le théorème 2.6 est ensuite utilisé pour calculer le correcteur dont la matrice de gain statique est donnée par :

$$K = [0.0976,\ 2.31,\ 0.157,\ -7.089].$$

Une fois encore, le rayon de la boule incluse dans la région d'attraction est extrêmement réduit avec $\alpha = 0.000043$. Ce résultat découle une fois de plus du conservatisme de la formulation polytopique et de la méthode employée.

La solution est alors évaluée en utilisant des simulations temporelles pour différentes vitesses telles que celles fournies Fig. 3.6. On constate une nouvelle fois la capacité à supprimer l'oscillation de flottement en présence de saturation en vitesse de l'actionneur.

3.5 Conclusion du chapitre

Dans ce Chapitre 3, l'ensemble d'équations développées dans le Chapitre 1 est adapté au problème spécifique du flottement de décrochage. En particulier, le problème est réduit au cas unidimensionnel d'une aile rigide en oscillation pure autour de son axe de tangage. Les non-linéarités présentes dans les équations aérodynamiques sont incluses dans une formulation polytopique grâce à des paramètres bornés et incertains. Cette formulation intéressante permet notamment d'appliquer les différents théorèmes développés dans le Chapitre 2. Des simulations numériques sont alors fournies afin d'illustrer l'applicabilité de chacun des théorèmes pour un système polytopique incertain en présence de saturation en position et en vitesse. Cependant, même si à chaque fois, le correcteur permet de supprimer les oscillations dues au phénomène de flottement, il apparaît que le rayon de la boule incluse dans le domaine de convergence est extrêmement faible, n'incluant pas les conditions initiales des exemples utilisés. Ceci illustre le conservatisme de la méthode employée.

Conclusion

Du fait des diverses non-linéarités souvent présentes dans les modèles aéroélastiques, le problème de contrôle de telles classes de systèmes complexes est bien souvent réduit à la linéarisation des équations afin d'appliquer des techniques classiques de l'automatique. L'objectif de ce travail était donc d'appliquer ces techniques de la théorie du contrôle à un système aéroélastique. En particulier, des non-linéarités comme la commutation de paramètres, termes bilinéaires ou incertitudes sont considérées, de même que des saturations, afin d'offrir une approche générale aux problèmes aéroélastiques. De plus, ce travail tend à être suffisamment général afin d'être étendu aux cas de l'*active flow control* tels que les actionneurs à air pulsé.

Contributions

Dans le Chapitre 1, un modèle aéroélastique est introduit et détaillé. La validité du modèle aérodynamique est démontrée sur une aile rigide NACA 0018 oscillante autour de son axe de tangage et à faible nombre de Reynolds, exhibant ainsi des phénomènes de séparation et de vorticité. Le modèle s'avère particulièrement efficace pour prédire l'hystérésis et les lâchers tourbillonnaires de bord d'attaque. Si une identification plus avancée aurait pu être réalisée pour des fréquences et des amplitudes plus larges, les paramètres obtenus permettent de valider le modèle et particulièrement sa capacité à capturer ces différents phénomènes lors de l'oscillation de l'aile. Cependant, comme dans de nombreux modèles, de nombreuses non-linéarités sont présentes, rendant délicat le problème de contrôle associé. Dans un deuxième chapitre, des résultats relatifs au contrôle linéaire quadratique sont présentés pour des systèmes LTI et étendus aux systèmes polytopiques aux paramètres incertains. En particulier, des saturations en position et en vitesse sont considérées. Utilisant une formulation LMI, les théorèmes permettent non seulement de fournir des méthodes de synthèse de correcteurs mais également de définir des régions d'attraction au sein desquelles la stabilité locale peut être garantie. La saturation en vitesse s'avère être une extension des saturations en position, en considérant un système augmenté du système initial. Dans le troisième

chapitre, la structure du modèle initial développé dans le Chapitre 1 est étudiée. En effet, le modèle proposé initialement présente des non-linéarités telles que la commutation de paramètres, termes bilinéaires ou incertitudes. De plus, les actionneurs présentent des saturations non négligeables qui doivent être prises en compte. Pour étudier ce système complexe, l'ensemble des équations est manipulé afin d'englober ces saturations dans un système polytopique. En particulier, les approches suivantes ont été employées pour adresser chacune des non-linéarités :

Termes bilinéaires : L'un des états du système s'avérait être borné mais non directement mesurable. Pour cette raison, celui-ci a été considéré comme un paramètre variable incertain.

Système à commutation : Suivant l'approche employée dans [54], l'ensemble des paramètres commutant entre deux ensembles de valeurs en fonction de l'état du système est maintenant considéré comme variant linéaire entre ces deux valeurs. Comme le signal de commutation n'est pas accessible avec précision, cet ensemble de paramètres variants et bornés est considéré comme incertain.

Incertitudes : Des incertitudes sur la vitesse de l'écoulement sont également considérées. La variation est supposée également bornée et forme ainsi un paramètre variant incertain.

Ces paramètres variants incertains et bornés permettent donc de former un polytope menant à une formulation multi-affine du système, ce qui permet d'appliquer les théorèmes développés dans le Chapitre 2.

Ces techniques permettent donc de résoudre avec succès le problème de flottement considéré. En particulier, les techniques de synthèse développées dans le Chapitre 2 permettent de synthétiser un correcteur en présence de saturation, en position comme en vitesse, et ce malgré les variations des paramètres incertains. Cependant, du fait de la formulation employée, un degré important de conservatisme est introduit. En effet, si les correcteurs donnent satisfaction dans les cas étudiés et les conditions de flottement, la garantie de stabilité ne peut plus être fournie par les théorèmes, aboutissant à des régions d'attractions restreintes. La relaxation des fonctions de coûts, mais également l'ajustement des fonctions de pondération intervenant dans les théorèmes devraient être considérés.

Perspectives

Comme mentionné précédemment, le modèle aérodynamique proposé dans le Chapitre 1 permet de modéliser de façon très satisfaisante l'hystérésis et les oscillations dues aux lâchers des nappes tourbillonnaires, pour les fréquences et les amplitudes considérées dans les expériences réalisées. Cependant, il serait intéressant de collecter un plus grand nombre d'expériences avec une variation plus large de ces paramètres. De même, les expériences pourraient être généralisées aux cas du tangage et du pompage afin de valider le modèle de façon plus large.

Une extension naturelle de ce travail consisterait à réaliser des expériences afin de tester les correcteurs synthétisés et simulés dans le Chapitre 3. Pour cela, il serait nécessaire de considérer un système en boucle fermée non plus en retour d'état mais en retour de sortie. Le développement d'observateurs pourrait alors être étudié. Dans ce cas, la formulation du Chapitre 3 pourrait être reconsidérée afin de réduire le conservatisme en diminuant le nombre de paramètres incertains. Une approche similaire a été employée dans [58], s'appuyant sur les travaux de Takagi-Sugeno.

Enfin, l'une des principales extensions qui est à l'origine de la motivation de cette thèse est d'étendre ces résultats à l'*active flow control*. Le modèle développé dans le Chapitre 1 a été réalisé dans la perspective de pouvoir s'étendre à l'AFC, notamment en permettant de reproduire l'hystérésis et le lâcher tourbillonnaire, tout en conservant un nombre de paramètres et d'états limités. L'AFC cherchant à contrôler cette vorticité, notamment en soufflant ou pulsant de l'air en bord d'attaque, ce modèle s'avère particulièrement adapté. Si les premiers travaux réalisés dans ce sens n'ont pu aboutir du fait d'un actionneur au débit trop réduit, les résultats obtenus restent encourageants et devraient pouvoir être poursuivis [27].

Bibliography

[1] Konstantinos Zikidis, Alexios Skondras, and Charisios Tokas. Low observable principles, stealth aircraft and anti-stealth technologies. *Journal of Computations & Modelling*, 4(1):129–165, 2014.

[2] Narendra Kumar and Sampat R. Vadera. Stealth materials and technology for airborne systems. In *Aerospace Materials and Material Technologies*, pages 519–537. Springer, 2017.

[3] David R Williams and Jürgen Seidel. Crossed-actuation AFC for lateral-directional control of an ICE-101/saccon ucav. In *8th AIAA Flow Control Conference*, page 3167, 2016.

[4] Lars Rundqwist and Karin Stahl-Gunnarsson. Phase compensation of rate limiters in unstable aircraft. In *Control Applications, 1996., Proceedings of the 1996 IEEE International Conference on*, pages 19–24. IEEE, 1996.

[5] Bei Lu et al. Linear parameter-varying control of an F-16 aircraft at high angle of attack. 2005.

[6] David R Williams, Xuanhong An, Simeon Iliev, Rudibert King, and Florian Reißner. Dynamic hysteresis control of lift on a pitching wing. *Experiments in Fluids*, 56(5):1–12, 2015.

[7] Shakir Jiffri, Sebastiano Fichera, John E Mottershead, and Andrea Da Ronch. Experimental nonlinear control for flutter suppression in a nonlinear aeroelastic system. *Journal of Guidance, Control, and Dynamics*, 2017.

[8] Arnaud Malher. *Amortisseurs passifs non linéaires pour le contrôle de l'instabilité de flottement*. PhD thesis, Paris Saclay, 2016.

[9] Michael Amitay and Ari Glezer. Controlled transients of flow reattachment over stalled airfoils. *International Journal of Heat and Fluid Flow*, 23(5):690–699, 2002.

[10] Yuehan Tan, Thomas M Crittenden, and Ari Glezer. Aerodynamic control of a dynamically pitching vr-12 airfoil using discrete pulsed actuation. In *54th AIAA Aerospace Sciences Meeting*, page 321, 2016.

[11] Stefan Vey, Christian N Nayeri, Christian O Paschereit, and David Greenblatt. Plasma flow control on low aspect ratio wings at low Reynolds numbers. *AIAA paper*, 1222:4–7, 2010.

[12] Casey Fagley, John Farnsworth, Chris Porter, Jürgen Seidel, Thomas McLaughlin, Jinik Lee, and Eunseok Lee. Open-loop dynamics of the asymmetric vortex wake behind a von Kármán ogive at high incidence. *International Journal of Flow Control*, 5(1):59–78, 2013.

[13] Chris Porter, Casey Fagley, John Farnsworth, Jürgen Seidel, and Thomas McLaughlin. Closed-loop flow control of a forebody at a high incidence angle. *AIAA Journal*, 52(7):1430–1440, 2014.

[14] Roeland De Breuker, Mostafa Abdalla, Attilio Milanese, and Pier Marzocca. Optimal control of aeroelastic systems using synthetic jet actuators. In *49th AIAA Structures, Structural Dynamics, and Materials Conference*, page 1726, 2008.

[15] Wesley Kerstens, Jens Pfeiffer, David Williams, Rudibert King, and Tim Colonius. Closed-loop control of lift for longitudinal gust suppression at low Reynolds numbers. *AIAA journal*, 49(8):1721–1728, 2011.

[16] David Greenblatt, Hanns Mueller-Vahl, David Williams, and Florian Reissner. Goman-Khrabrov model on pitching airfoils with flow control. In *8th AIAA Flow Control Conference*, page 4240, 2016.

[17] Hanns F Müller-Vahl, Christoph Strangfeld, Christian N Nayeri, Christian O Paschereit, and David Greenblatt. Control of thick airfoil, deep dynamic stall using steady blowing. *AIAA Journal*, 53(2):277–295, 2014.

[18] Hanns Friedrich Müller-Vahl, Christian Navid Nayeri, Christian Oliver Paschereit, and David Greenblatt. Dynamic stall control via adaptive blowing. *Renewable Energy*, 97:47–64, 2016.

[19] Avraham Seifert, A Darabi, and Israel Wyganski. Delay of airfoil stall by periodic excitation. *Journal of Aircraft*, 33(4):691–698, 1996.

[20] David Greenblatt and Israel J Wygnanski. The control of flow separation by periodic excitation. *Progress in Aerospace Sciences*, 36(7):487–545, 2000.

[21] S Scott Collis, Ronald D Joslin, Avi Seifert, and Vassilis Theofilis. Issues in active flow control: theory, control, simulation, and experiment. *Progress in Aerospace Sciences*, 40(4):237–289, 2004.

[22] Xuanhong An, David R Williams, Jeff Eldredge, and Tim Colonius. Modeling dynamic lift response to actuation. In *54th AIAA Aerospace Sciences Meeting*, 2016.

[23] Xuanhong An, Lou Grimaud, and David R Williams. Feedforward control of lift hysteresis during periodic and random pitching maneuvers. In *Active Flow and Combustion Control 2014*, pages 55–69. Springer, 2015.

[24] Maxime Feingesicht, Cédric Raibaudo, Andrey Polyakov, Franck Kerherve, and Jean-Pierre Richard. A bilinear input-output model with state-dependent delay for separated flow control. In *Control Conference (ECC), 2016 European*, pages 1679–1684. IEEE, 2016.

[25] Maxime Feingesicht, Andrey Polyakov, Franck Kerhervé, and Jean-Pierre Richard. Model-based feedforward optimal control applied to a turbulent separated flow. In *IFAC 2017-20th World Congress of the International Federation of Automatic Control*, page 6, 2017.

[26] Maxime Feingesicht, Andrey Polyakov, Franck Kerhervé, and Jean-Pierre Richard. Sliding mode control for turbulent flows. In *IFAC 2017-20th World Congress of the International Federation of Automatic Control*, page 8, 2017.

[27] Fabien Niel, Casey Fagley, Jürgen Seidel, and Thomas McLaughlin. Modeling of transient blowing actuation using pulse width modulation on a dynamically pitching NACA 0018 airfoil. In *35th AIAA Applied Aerodynamics Conference*, page 3564, 2017.

[28] Wanan Sheng, Rodderic Galbraith, and Frank Coton. A modified dynamic stall model for low Mach numbers. *Journal of Solar Energy Engineering*, 130(3):031013, 2008.

[29] Shao Song, Zhu Qinghua, Chenglin Zhang, and Ni Xianping. Airfoil aeroelastic flutter analysis based on modified leishman-beddoes model at low Mach number. *Chinese Journal of Aeronautics*, 24(5):550–557, 2011.

[30] Jeesoon Choi, Tim Colonius, and David R Williams. Surging and plunging oscillations of an airfoil at low Reynolds number. *Journal of Fluid Mechanics*, 763: 237–253, 2015.

[31] Chen Gang, Sun Jian, and Li Yueming. Active flutter suppression control law design method based on balanced proper orthogonal decomposition reduced order model. *Nonlinear Dynamics*, 70(1):1–12, 2012.

[32] Steven L Brunton and Clarence W Rowley. Empirical state-space representations for Theodorsen's lift model. *Journal of Fluids and Structures*, 38:174–186, 2013.

[33] Andrea Mannarino. *Nonlinear aeroservoelasticity: reduced order modeling and active control*. PhD thesis, 2016.

[34] Gang Chen, Jian Sun, and Yue-Ming Li. Adaptive reduced-order-model-based control-law design for active flutter suppression. *Journal of Aircraft*, 49(4):973–980, 2012.

[35] Thomas W Strganac, Jeonghwan Ko, David E Thompson, and Andrew J Kurdila. Identification and control of limit cycle oscillations in aeroelastic systems. *Journal of Guidance Control and Dynamics*, 23(6):1127–1133, 2000.

[36] Jean-Jacques E Slotine, Weiping Li, et al. *Applied nonlinear control*, volume 199. Prentice hall Englewood Cliffs, NJ, 1991.

[37] Sohrab Haghighat, Zhiwei Sun, Hugh HT Liu, and Junqiang Bai. Robust stall flutter suppression using $\mathcal{H}_2/\mathcal{H}_\infty$ control. In *ASME 2014 Dynamic Systems and Control Conference*. American Society of Mechanical Engineers, 2014.

[38] Hugo Lhachemi, David Saussie, and Guchuan Zhu. Flutter suppression for a two degree of freedom aeroelastic wing section: a structured h-infinity-based gain-scheduling approach with explicit hidden coupling terms handling. In *AIAA Guidance, Navigation, and Control Conference*, page 1735, 2017.

[39] Zhiwei Sun, Sohrab Haghighat, Hugh HT Liu, and Junqiang Bai. Time-domain modeling and control of a wing-section stall flutter. *Journal of Sound and Vibration*, 340:221–238, 2015.

[40] Wen Fan, Hugh HT Liu, and Raymond HS Kwong. Linear parameter-varying control of a wing-section stall flutter. In *ASME 2014 Dynamic Systems and Control Conference*, pages V001T01A003–V001T01A003. American Society of Mechanical Engineers, 2014.

[41] Zebb Prime, Ben Cazzolato, Con Doolan, and Thomas Strganac. Linear-parameter-varying control of an improved three-degree-of-freedom aeroelastic model. *Journal of Guidance, Control, and Dynamics*, 33(2):615–619, 2010.

[42] George Platanitis and Thomas W Strganac. Control of a nonlinear wing section using leading-and trailing-edge surfaces. *Journal of Guidance, Control, and Dynamics*, 27(1):52–58, 2004.

[43] Steven L Brunton and Bernd R Noack. Closed-loop turbulence control: Progress and challenges. *Applied Mechanics Reviews*, 67(5):050801, 2015.

[44] Jinwu Xiang, Yongju Yan, and Daochun Li. Recent advance in nonlinear aeroelastic analysis and control of the aircraft. *Chinese Journal of Aeronautics*, 27(1):12–22, 2014.

[45] Tomohiro Takagi and Michio Sugeno. Fuzzy identification of systems and its applications to modeling and control. *IEEE transactions on systems, man, and cybernetics*, (1):116–132, 1985.

[46] Thomas E Noll, John M Brown, Marla E Perez-Davis, Stephen D Ishmael, Geary C Tiffany, and Matthew Gaier. Investigation of the Helios prototype aircraft mishap. *Mishap Report, NASA Report*, 1, 2004.

[47] Mikhail Goman and Alexander Khrabrov. State-space representation of aerodynamic characteristics of an aircraft at high angles of attack. *Journal of Aircraft*, 31 (5):1109–1115, 1994.

[48] Van Khiem Truong. A 2-d dynamic stall model based on a Hopf bifurcation. In *European Rotorcraft Forum*. Associazione Italiana di Aeronautica ed Astronautica, 1993.

[49] Alexandre Seuret, Christophe Prieur, Sophie Tarbouriech, and Luca Zaccarian. Lq-based event-triggered controller co-design for saturated linear systems. *Automatica*, 74:47–54, 2016.

[50] Nailu Li, Mark J Balas, Hua Yang, and Wei Jiang. Flow control and stability analysis of rotating wind turbine blade system. *Journal of Guidance, Control, and Dynamics*, 2016.

[51] R Dat, CT Tran, and Didier Petot. Modèle phénomènologique de décrochage dynamique sur profil d'hélicoptère. *TP ONERA 1979-149*, 1979.

[52] Douglas D Bueno, Clayton R Marqui, Luiz Góes, and Paulo JP Gonçalvez. Aeroelastic stability analysis using linear matrix inequalities. *Journal of the Brazilian Society of Mechanical Sciences and Engineering*, 34(SPE2):545–551, 2012.

[53] Khiem Van Truong. Modeling aerodynamics, including dynamic stall, for comprehensive analysis of helicopter rotors. *Aerospace*, 4(2):21, 2017.

[54] Carlos Olalla, Ramon Leyva, Abdelali El Aroudi, and Isabelle Queinnec. Robust LQR control for pwm converters: an LMI approach. *IEEE Transactions on industrial electronics*, 56(7):2548–2558, 2009.

[55] Stephen Boyd, Laurent El Ghaoui, Eric Feron, and Venkataramanan Balakrishnan. *Linear matrix inequalities in system and control theory*. SIAM, 1994.

[56] Pascal Gahinet, Arkadii Nemirovskii, Alan J Laub, and Mahmoud Chilali. The LMI control toolbox. In *Decision and Control, 1994., Proceedings of the 33rd IEEE Conference on*, volume 3, pages 2038–2041. IEEE, 1994.

[57] Gary Balas, Richard Chiang, Andy Packard, and Michael Safonov. Robust control toolbox. *For Use with Matlab. User's Guide, Version*, 3, 2005.

[58] Víctor Costa da Silva Campos, Anh-Tu Nguyen, and Reinaldo Martinez Palhares. LMI-based adaptive control for uncertain polytopic systems. In *Decision and Control (CDC), 2016 IEEE 55th Conference on*, pages 3222–3227. IEEE, 2016.